

# **Neutronics and Thermal-Hydraulics Safety Related Investigations of an Innovative Boron- Free Core Integrated Within a Generic Small Modular Reactor**

Zur Erlangung des akademischen Grades  
**Doktor der Ingenieurwissenschaften**  
von der KIT-Fakultät für Maschinenbau  
des Karlsruher Instituts für Technologie (KIT)

Genehmigte

**Dissertation**

von

Yousef Ibrahim Alzaben

geboren in Riad, Saudi Arabien

Tag der mündlichen Prüfung: 28.10.2019

Hauptreferent: Prof. Dr.-Ing. Robert Stieglitz  
Karlsruhe Institut für Technologie

Korreferent: Prof. Dr.-Phys. César Queral  
Universidad Politécnica de Madrid



I hereby declare that the work in hand is from me independently and I have used nothing other than the given sources and aids and have marked passages included from other works, whether verbatim or in content, as such and that the work in hand complies with the recent relevant version of the statutes of the Karlsruhe Institute of Technology (KIT) in assurance of good scientific practice.

Karlsruhe, October 28, 2019

Yousef Alzaben



---

## ABSTRACT

The main objectives of the doctoral thesis can be sorted into two main areas: (i) Designing a boron-free core that can fit into a generic light-water SMR and fulfilling general regulatory requirements; and (ii) Investigating the behavior of the developed boron-free core integrated within a generic light-water SMR for selected design basis accidents. The assessment of the developed boron-free core is conducted through comparing neutron physical and thermal-hydraulics parameters (cold shutdown margin, inherent reactivity feedback coefficients, power distribution, fuel, and clad temperature) to acceptance criteria stipulated by many nuclear regulatory authorities based on accepted international norms. Designing an SMR-core without soluble boron in the coolant has many advantages and challenges.

The advantages offered by the boron-free-operation concept, on the one hand, are observed in reducing the moderator temperature coefficient; eliminating the boron dilution accident; and reducing the risk associated with the boric acid induced corrosion of the reactor pressure vessel and its internal components. The soluble-boron-free concept, on the other hand, imposes several core design challenges. Duty reactivity control in the developed core is provided by solely moving control rods which would cause local changes on the power distribution. Therefore, higher power peaking is expected. This may cause fuel rod failure (i.e. the first barrier against the release of radioactive material) especially under accidents leading to localized power increase such as control rod ejection accident. Although such a core design exhibits a highly negative moderator temperature coefficient that improves operational stability, it may have disadvantages during overcooling scenarios such as a steam line break accident.

To meet these technical challenges, the boron-free core design involved an extensive iterative process between the fuel assembly design and core/control rods arrangement until matching pre-imposed safety criteria. The way to address these challenges is to design optimized fuel assemblies which best fit the core arrangement. For example, core locations known to have high neutron density are loaded with fuel assembly with low enrichment (or higher neutron absorbing capability) in order to lower the power density at that location. As control rods are the only means to manage power maneuvering, therefore inserting a control rod at core location will decrease the neutron flux there, whereas an increase of the neutron flux will occur at another location. This fact is treated through a hybrid control rod design with axially different absorbing materials to flatten power distribution. Thus, a proper control rods design and control assembly arrangement is a vital issue to overcome this challenge alongside with a suitable burnable absorber loading in each fuel assembly.

The final optimized core design consists of 57 fuel assemblies composed of 17x17 square lattice arrays with an active length of 2 m, which fit into a generic Korean SMR design (i.e. System-integrated Modular Advanced Reactor (SMART)). The optimized core design is characterized by a

very high negative moderator temperature coefficient of (-76.0 pcm/°C) due to eliminating the soluble boron from the coolant. The predicted cold shutdown margin with single failure of the highest control rod worth is about (-3000 pcm) fulfilling the imposed safety criterion of (-1000 pcm) with a high margin, and thus proves a proper primary shutdown system design. The total power peaking of this core during normal operation (i.e. at hot full power and critical condition) is 2.7 being below the safety criterion of 3.3 with sufficient margin mainly due to having heterogeneous radial and axial core composition. The maximum fuel centerline and cladding temperatures during normal operation are 1053°C and 363°C, respectively, being far below acceptance limit.

Furthermore, the behavior of the optimized core design under control rod ejection accident is studied during standby (i.e. at hot zero power and critical condition) and normal operation. This investigation showed that the core design is robust against fuel and cladding failures thanks to its inherent safety features. The control rod ejection accident is analyzed using a coupled 3D spatial kinetics and subchannel thermal-hydraulic codes with two methodologies in describing the heat transfer coefficient in the gap region between the fuel pellet and cladding internal surface. The first methodology followed the conservative approach of having a constant value of the fuel-clad gap heat transfer coefficient. Whereas the second methodology relied on a more realistic estimation of the fuel-clad gap heat transfer coefficient by describing the physical phenomena occur within the gap region in a simplified manner. The outcome of these two studies showed that using the first approach does not necessarily always yield a conservative estimation of key safety parameters. Therefore, it is suggested to couple an advanced fuel behavior code to the 3D spatial neutrons kinetics and subchannel thermal-hydraulic codes particularly for evaluating the consequences of control rod ejection accident at the end-of-cycle.

Since high negative moderator temperature coefficient may lead to unfavorable consequences, the developed core has been integrated into the generic SMART-plant to study both the core and plant behavior in case of a steam line break accident. In addition, to evaluate the performance of the safety system responsible for removing the core residual heat passively without any human intervention and AC-power support. This investigation demonstrated a high safety margin against the core re-criticality and return-to-power after the reactor trip. Also, the analysis showed that the asymmetric cooling behavior normally expected following a steam line break accident is terminated at the core inlet because a complex flow mixing header assembly structure is placed at the downcomer within the reactor pressure vessel. These two findings suggest the elimination of the flow mixing header assembly structure that may result in reducing maintenance and inspection work within the reactor pressure vessel, and thus reducing operational cost.

## KURZFASSUNG

Die Hauptziele der Doktorarbeit lassen sich in zwei Hauptbereiche unterteilen: (i) Entwerfen eines borfreien Kerns, der in ein generisches Leichtwasser-SMR eingebaut werden kann und die allgemeinen behördlichen Anforderungen erfüllt; und (ii) Untersuchung des Verhaltens des entwickelten borfreien Kerns, der in ein generisches Leichtwasser-SMR integriert ist, unter ausgewählten Auslegungsstörfall-Bedingungen. Die Bewertung des entwickelten borfreien Kerns wird durchgeführt, indem die physikalischen und thermohydraulischen Parameter der Neutronen (Kaltabschaltgrenze, Rückkopplungskoeffizienten der inhärenten Reaktivitätskoeffizienten, Leistungsverteilung, Brennstoff- und Hüllrohrtemperatur) mit Akzeptanzkriterien verglichen werden, die von vielen Atomaufsichtsbehörden auf der Grundlage festgelegter und akzeptierter internationalen Normen. Die Konstruktion eines SMR-Kerns ohne aufgelöstes Bor im Kühlmittel hat viele Vorteile und Herausforderungen.

Die Vorteile des borfreien Betriebskonzeptes zeigen sich zum einen in der Reduzierung des Moderator- Temperaturkoeffizienten; Beseitigung eines Borverdünnungstörfallszenariums; und Reduzieren des Risikos, das mit der durch Borsäure induzierten Korrosion des Reaktor Druckbehälters und seiner inneren Teile verbunden ist. Das Bor freie Konzept bringt andererseits mehrere zentrale Auslegungsherausforderungen mit sich. Die Reaktivitätssteuerung im entwickelten Kern erfolgt ausschließlich durch Bewegen von Steuerstäben, was zu lokalen Änderungen der Leistungsverteilung führen könnte. Daher wird eine höhere Leistungsspitze erwartet. Dies kann ein Versagen des Brennstabs verursachen (d. H. Die erste Barriere gegen die Freisetzung von radioaktivem Material), insbesondere bei Unfällen, die zu einem lokalisierten Leistungsanstieg führen, wie z. B. einem Unfall durch Auswerfen des Steuerstabs. Ein stark negativer Moderator-Temperaturkoeffizient verbessert zwar die Betriebsstabilität, kann jedoch zu ungünstigen Konsequenzen bei Unfällen mit übermäßiger Kühlung des Kerns führen.

Um diesen technischen Herausforderungen zu begegnen, umfasste die Bor freie Kernkonstruktion einen umfangreichen iterativen Prozess zwischen der Brennelement-auslegung und der geeignete Anordnung der Kontrollstäbe im Kern, wobei die Erfüllung der auferlegten Sicherheitskriterien berücksichtigt wurde. Um diesen Herausforderungen zu begegnen, müssen optimierte Brennelemente entworfen werden, die am besten zur Kernanordnung passen. Beispielsweise werden Kernbereiche, von denen bekannt ist, dass sie eine hohe Neutronendichte aufweisen, mit Brennelementen mit geringer Anreicherung oder höheren Neutronenabsorption beladen, um das Leistungsprofil an dieser Stelle zu senken. Da Steuerstäbe die einzigen Mittel sind, um Leistungsänderungen vorzunehmen, wird durch Einsetzen eines Steuerstabs an einer Stelle einerseits der Neutronenfluss an dieser Stelle verringert, andererseits wird eine Erhöhung des Neutronenflusses an einer anderen Stelle auftreten. Diesem Umstand wird durch die Entwicklung eines Hybrid-Steuerstabdesigns mit axial unterschiedlichen absorbierenden Materialien begegnet, um die Leistungsverteilung zu glätten. Daher ist eine ordnungsgemäße Konstruktion der Steuerstäbe und die Anordnung der Steuerbaugruppen ein entscheidender Aspekt, um diese Herausforderung zusammen mit einer geeigneten Beladung der einzelnen Brennelemente mit brennbaren Absorbern zu bewältigen.

Das endgültige optimierte Kerndesign besteht aus 57 Brennelementen mit  $17 \times 17$  Brennstabpositionen und einer aktiven Länge von 2 m, die in ein generisches koreanisches SMR-Design (d. H. SMART) passen. Das optimierte Kerndesign zeichnet sich durch einen sehr hohen negativen Moderator-Temperaturkoeffizienten von  $(-76,0 \text{ pcm} / ^\circ \text{C})$  aus, da kein lösliche Bor im Kühlmittel vorgesehen ist. Die vorhergesagte Abschaltreaktivität bei einem einzelnen Ausfall des höchsten Steuerstabwerts beträgt ungefähr  $(-3000 \text{ pcm})$ , was die auferlegte Sicherheitsgrenze von  $(-$

1000 pcm) mit einer hohen Sicherheitsspanne erfüllt. Dies zeigt, dass das primäre Abschaltssystem ordnungsgemäß ausgelegt ist. Die Gesamtleistungsspitze des optimierten Kerns während des normalen Betriebs (d. H. bei heißer Volleistung und kritischem Zustand) beträgt 2,7, und liegt mit ausreichendem Margen unterhalb der Sicherheitsgrenze von 3,3. Dieser Befund beruht auf dem Entwurf eines heterogenen Kerns im Hinblick auf radiale und axiale Materialzusammensetzung. Die maximale Temperatur der Brennstoffsmittellinie und des Hüllrohrs während des normalen Betriebs beträgt 1053 ° C bzw. 363 ° C mit einer hohen Abstand gegenüber dem Schmelzpunkt des Brennstoffs und des Hüllrohrmaterials von 2840 ° C bzw. 1200 ° C.

Das Verhalten des optimierten Kerndesigns bei einem Unfall mit einem Auswurf des Steuerstabs wird während des Standby (d. H. bei heißer Nullleistung und kritischem Zustand) und des normalen Betriebs untersucht. Diese Untersuchung ergab, dass das Kerndesign dank seiner inhärenten Sicherheitsmerkmale robust gegen Brennstoff- und Hüllrohrversagen ist. Der Auswurfunfall des Steuerstabes wird unter Verwendung einer gekoppelten mehrdimensionalen ä 3D-Kinetik und thermohydraulischer Unterkanalcodes mit zwei Methoden zur Beschreibung des Wärmeübertragungskoeffizienten im Spaltbereich zwischen Brennstoffpellet und Hüllrohr analysiert. Die erste Methode folgte dem konservativen Ansatz, einen konstanten Wert für den Wärmeübertragungskoeffizienten des Brennstoff-Hüllrohr-Spaltes zu haben. Während die zweite Methode auf einer realistischeren Schätzung des Wärmedurchgangskoeffizienten des Brennstoff-Hüllrohr-Spaltes beruhte, indem die im Spaltbereich auftretenden physikalischen Phänomene auf vereinfachte Weise beschrieben wurden. Die Ergebnisse dieser beiden Studien zeigten, dass der erste Ansatz nicht immer notwendigerweise eine konservative Schätzung der wichtigsten Sicherheitsparameter ergeben. Daher wird empfohlen, einen erweiterten Brennstabmechanik-code mit den thermohydraulischen Codes für räumliche 3D-Kinetik und Unterkanal zu koppeln, um insbesondere die Folgen eines Unfalls mit Auswurf der Steuerstabes am Ende des Zyklus zu bewerten.

Aufgrund der Befürchtung, dass die hohe negative Moderator Temperatur zu nachteiligen Folgen führen könnte, wurde der entwickelte Kern in die generische SMART-Anlage integriert, um das Verhalten von Kern und Anlage nach einem Bruch der Dampfleitung zu untersuchen. Darüber hinaus ist die Effizienz des Sicherheitssystems zu bewerten, das für die passive Abfuhr der Nachzerfallswärme ohne menschliches Eingreifen und ohne Wechselstromunterstützung verantwortlich ist. Diese Untersuchung zeigte, dass der Reaktor eine hohe Sicherheitsmarge gegen Re-kritikalität und Leistungsanstieg nach der Reaktorabschaltung aufgrund der ausreichenden Abschaltreaktivität des Kerns. Das Ergebnis dieser Analyse zeigte, dass das asymmetrische Kühlverhalten, das normalerweise nach einem Dampfleitungsbruch zu erwarten ist, am Kerneinlass aufgrund des Vorhandenseins der Strömungsvermischungsvorrichtung im Reaktordruckbehälter aufgehoben wird. . Die hier erzielten Ergebnisse legen nahe, die auf die komplizierte Vermischungsvorrichtungen zu verzichten, und dadurch Wartungs- und Inspektionsarbeiten innerhalb des Reaktordruckbehälters sowie Betriebskosten zu senken. Hierzu sind weiterführenden Untersuchungen notwendig.

## ACKNOWLEDGMENTS

This doctoral thesis would not see the light without the support of many people. At first, I would like to express my gratitude to Prof. Dr-Ing. Stieglitz for his supervision, advice and continues feedbacks on the progress of this thesis. My deepest gratitude also goes to Dr. Sanchez-Espinoza, a friend and a technical advisor, for his guidance and support from the very early stage of this thesis. It is because of their endless encouragement, I have completed this work successfully.

A special thanks to Prof. Queral, a co-examiner, for his valuable comments that has greatly contributed to the success of this work. I wish also to thanks all staff members at the Institute of Neutron Physics and Reactor Technology (INR) of Karlsruhe Institute of Technology; especially Dr. Uwe Imke, the main developer of SUBCHANFLOW (SCF) code, for answering all my questions and clarifying many doubts related to SCF. In addition, thanks to all my colleagues at the reactor physics and dynamics group of INR that stood by me in difficult moments. I am also very grateful to the administrative support brought by the INR's secretaries, Mrs. Petra Klug and Mrs. Birgit Zagolla.

I am deeply and forever indebted to my parents for believing in me, their prayers, and encouragement throughout my entire life. Because of them this dream came to reality. I wish also to express my love and gratitude to my wife Sarah for her endless love, patience and encouragement during many ups and down periods throughout this study journey. In addition, a special thanks goes to my little princess Lina, because of her magical smile many long stressful days have turned into days full of joy and sweet moments. Also, a special thanks goes to all my brothers and sisters for their moral support and encouragements from the early starts of this doctoral study.

Last but not least, I wish to thanks King Abdulaziz City for Science and Technology (KACST) for their financial support during this study period.

Karlsruhe, October 28, 2019

Yousef Alzaben



---

## LIST OF PUBLICATIONS

### *Peer-reviewed Journal Papers*

- Y. Alzaben, V. H. Sanchez-Espinoza, R. Stieglitz, “Simulation of KSMR Core Zero Power Conditions Using The Monte Carlo Code Serpent”, *International Journal For Nuclear Power*, Vol. 64, pp. 103–105, Feb. 2019. ISSN: 1431-5254.
- Y. Alzaben, V. H. Sanchez-Espinoza, and R. Stieglitz, “Analysis of a steam line break accident of a generic SMART-plant with a boron-free core using the coupled code TRACE/PARCS,” *Nuclear Engineering and Design*, vol. 350, pp. 33–42, Aug. 2019. <https://doi.org/10.1016/j.nucengdes.2019.05.002>
- Y. Alzaben, V. H. Sanchez-Espinoza, and R. Stieglitz, “Core neutronics and safety characteristics of a boron-free core for Small Modular Reactors,” *Annals of Nuclear Energy*, vol. 132, pp. 70–81, Oct. 2019. <https://doi.org/10.1016/j.anucene.2019.04.017>
- Y. Alzaben, V. H. Sanchez-Espinoza, and R. Stieglitz, “Analysis of a control rod ejection accident in a boron-free Small Modular Reactor with coupled neutronics/thermal-hydraulics code,” *Annals of Nuclear Energy*, vol. 134, pp. 114–124, Dec. 2019. <https://doi.org/10.1016/j.anucene.2019.06.009>

### *Peer-reviewed Conference Papers*

- Y. Alzaben, V. Sanchez, R. Stieglitz, “Neutronics Safety-related Investigations of a Generic SMART Core with State-of-the-Art Tools”, in *NUTHOS-11: The 11<sup>th</sup> International Topical Meeting on Nuclear Reactor Thermal Hydraulics, Operation and Safety*; Gyeongju, Korea, October 9-13, 2016. Paper ID: N11A0254.
- Y. Alzaben, V. Sanchez, R. Stieglitz, “Extending Serpent2/Subchanflow Coupling For Depletion Calculation - Current Status and Challenges”, in *Proceeding of the PHYSOR 2018 conference*, Cancun, Mexico, April 22-26, 2018. Paper ID: 57
- Y. Alzaben, C. Ziegahn, V. Sanchez, “Extension of Serpent2/Subchanflow Coupling For Hexagonal Fuel Assemblies”, in *Proceeding of the PHYSOR 2018 conference*, Cancun, Mexico, April 22-26, 2018. Paper ID: 88
- L. Mercatali, Y. Alzaben, V.H. Sanchez-Espinoza, “Propagation of Nuclear Data Uncertainties in PWR Pin-Cell Burnup Calculations via Stochastic Sampling”, in *ICONE26: 26<sup>th</sup> International Conference on Nuclear Engineering*, London, England, July 22-26, 2018. Paper ID: ICONE26-81711. ISBN: 978-0-7918-5145-6.
- V.H. Sanchez-Espinoza, V. M. Marin, Y. Alzaben, G. Jimenez, and R. Stieglitz, “Integral SMART Plant Model Development using the System Thermal-Hydraulic Code TRACE for Transient Analysis,” in *NUTHOS-12: The 12<sup>th</sup> International Topical Meeting on Nuclear Reactor Thermal Hydraulics, Operation and Safety*, Qingdao, China, October 14-18, 2018. Paper ID: 574



## TABLE OF CONTENTS

<b>ABSTRACT</b> .....	<b>V</b>
<b>KURZFASSUNG</b> .....	<b>VII</b>
<b>ACKNOWLEDGMENTS</b> .....	<b>IX</b>
<b>LIST OF PUBLICATIONS</b> .....	<b>XI</b>
<b>CHAPTER 1: INTRODUCTION</b> .....	<b>17</b>
1.1 Thesis Motivation.....	17
1.2 State-of-the-art of Light-water Small Modular Reactors .....	19
1.3 Description of the System Integrated Modular Advanced Reactor .....	22
1.4 Objectives and Scope of This Thesis .....	25
1.5 The Safety-Based Core Optimization Approach.....	26
1.6 Structure of the Thesis .....	27
<b>CHAPTER 2: REACTOR ANALYSIS FUNDAMENTALS</b> .....	<b>29</b>
2.1 Multi-physics and Multi-scale Concepts .....	29
2.2 Reactor Physics .....	30
2.2.1 Deterministic reactor physics solution approach .....	31
2.2.2 Stochastic reactor physics solution approach .....	33
2.2.3 Neutron multiplication and criticality .....	33
2.2.4 Reactor power anomalies .....	34
2.2.5 Reactivity control mechanisms.....	35
2.2.6 Reactivity feedback coefficients.....	36
2.3 Thermal-Hydraulics.....	37
2.3.1 Hydraulic analysis.....	37
2.3.2 Thermal analysis .....	38
2.3.3 Boiling crisis prediction .....	39
2.4 Reactor Safety .....	40
2.4.1 Defense-in-depth principle.....	41
2.4.2 Relevant initiating events for the SMART .....	42
2.4.3 Acceptance criteria .....	43
<b>CHAPTER 3: SIMULATION TOOLS</b> .....	<b>49</b>
3.1 Reactor Physics Analysis Tools.....	49
3.1.1 The Monte Carlo code SERPENT .....	49
3.1.2 The reactor core simulator PARCS.....	50
3.2 Thermal-Hydraulics Analysis Tools .....	51
3.2.1 The reactor core sub-channel code SUBCHANFLOW .....	51
3.2.2 The reactor system analysis code TRACE .....	52
<b>CHAPTER 4: OPTIMAL NEUTRONICS AND THERMAL-HYDRAULICS CORE CHARACTERISTICS</b> .....	<b>55</b>
4.1 Fuel Assemblies and Core Description .....	55
4.2 Global and Local Core Neutronics Characteristics .....	58
4.2.1 HFP excess reactivity, CSDM, reactivity feedback coefficients and $\beta_{\text{eff}}$ .....	58

4.2.2	Axial offset, radial and axial power peaking factors.....	58
4.3	Global and Local Core Thermal-Hydraulics Characteristics.....	61
4.3.1	Core average heat-up and pressure drop .....	61
4.3.2	Coolant enthalpy-rise factor .....	62
4.3.3	Centerline fuel and cladding wall-averaged temperatures .....	62
<b>CHAPTER 5: VERIFICATION OF THE CORE ANALYSIS METHODOLOGY .....</b>		<b>65</b>
5.1	Multi-group Cross-Section Generation Methodology.....	65
5.2	Verification Approach of the Cross-Section Generation Methodology .....	66
5.2.1	Verification of the core eigenvalue.....	67
5.2.2	Verification of the core power distribution .....	67
<b>CHAPTER 6: ANALYSIS OF A CONTROL ROD EJECTION ACCIDENT IN THE BORON-FREE CORE .....</b>		<b>69</b>
6.1	Description of the Accident and Assumptions.....	69
6.2	Analysis of the REA with PARCS/SCF .....	70
6.2.1	Initial and boundary conditions .....	70
6.2.2	Analysis of a REA at HZP condition - from global perspective.....	71
6.2.3	Analysis of a REA at HZP condition - from local perspective.....	74
6.2.4	Fuel-cladding gap heat transfer coefficient and gap width behavior .....	78
6.3	Summary and Perspective.....	79
<b>CHAPTER 7: ANALYSIS OF A STEAM LINE BREAK ACCIDENT OF A GENERIC SMART-PLANT WITH THE BORON-FREE CORE .....</b>		<b>81</b>
7.1	Description of the Accident and Assumptions.....	81
7.2	Analysis of the SLB-Accident with TRACE/PARCS.....	82
7.2.1	Initial and boundary conditions .....	82
7.2.2	Accident progression .....	82
7.3	Total Loss of the Ultimate Heat Sink Following the SLB-Accident .....	90
7.4	Summary and Perspective.....	92
<b>CHAPTER 8: SUMMARY AND CONCLUSIONS .....</b>		<b>93</b>
<b>CHAPTER 9: OUTLOOK .....</b>		<b>97</b>
<b>REFERENCES .....</b>		<b>100</b>
<b>APPENDIX-A: NEUTRONICS AND THERMAL-HYDRAULICS CORE MODELLING .....</b>		<b>109</b>
<b>APPENDIX-B: SMART SYSTEM THERMAL-HYDRAULICS MODELING USING TRACE .....</b>		<b>113</b>

---

## LIST OF ACRONYMS AND ABBREVIATIONS

AOO	Anticipated Operational Occurrences
ARO	All Control Rods Out
ATWS	Anticipated Transient Without SCRAM
BOL	Beginning-of- Life
BWR	Boiling Water Reactor
CHF	Critical Heat Flux
CR	Control Rod
CSDM	Cold Shutdown Margin
CVCS	Control Volume Control System
CZP	Cold Zero Power
DNBR	Departure from Nucleate Boiling Ratio
FA	Fuel Assembly
FIV	Feedwater Isolation Valve
FMHA	Flow Mixing Header Assembly
HFP	Hot Full Power
HZP	Hot Zero Power
IAEA	International Atomic Energy Agency
LWR	Light Water Reactor
MSIV	Main Steam Isolation Valve
MTC	Moderator Temperature Coefficient
NPP	Nuclear Power Plant
PRHRS	Passive Residual Heat Removal System
PSIS	Passive Safety Injection System
PWR	Pressurized Water Reactor
REA	Control Rod Ejection Accident
RPV	Reactor Pressure Vessel
SBF	Soluble Boron Free
SG	Steam Generator
SLB	Steam Line Break
SMART	System Integrated Modular Advanced Reactor
SMR	Small Modular Reactor
SRV	Safety Relief Valve



## CHAPTER 1: INTRODUCTION

### 1.1 Thesis Motivation

Nowadays, nuclear power supplies 11% of the world's installed electrical capacity (World Nuclear Association, 2019a). Nuclear reactor vendors worldwide are seeking to advance their designs with proven technological means and new safety approaches (e.g. passive safety systems) for reducing capital costs and improving safety performance. In the near future, nuclear power plants (NPPs) will be of evolutionary design. In the long-term, revolutionary designs could find its way to promote a new era of nuclear power generations.

Two major challenges facing today's NPP projects are its high capital costs and long construction time, which limit its spread over some parts of the world. Cost breakdown for various power generation technologies is presented in Fig. 1.1 (IAEA, 2018a).

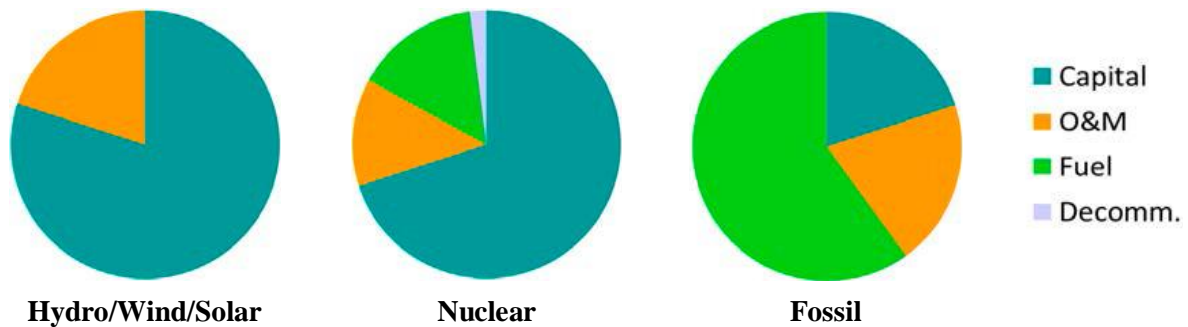


**Fig. 1.1: Illustrative cost breakdown for various power generation technologies (IAEA, 2018a)**  
(Note: O&M stands for operation and maintenance)

The global trend in NPP projects shows a clear increase in its construction period as illustrated in Fig. 1.2. In the past decade, nine countries completed the construction of 53 reactors within an average construction time of about ten years (Schneider and Froggatt, 2018).

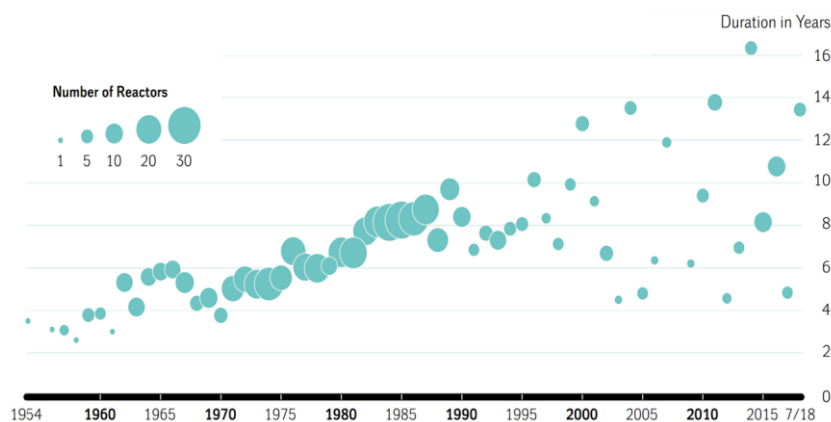


**Fig. 1.2: Average annual construction time in the world from 1954 to 2018 (Schneider and Froggatt, 2018)**

(Note: Vertical axis represents construction duration in years. Horizontal axis represents the year in which an NPP is connected to the grid)

Many nuclear reactors built in the early generation were small\*. Then, with evolving technology and due to the increasing demand for electricity, gigawatt-scale reactors were developed with the concept that large reactors have a smaller unit cost per unit of generated electricity.

As capital costs and construction time increased with large new NPP projects around the globe, attention is turning again to smaller alternatives, the so-called small modular reactors (SMRs). SMRs are defined according to the (World Nuclear Association, 2019b) as “*nuclear reactors generally 300MW<sub>e</sub> equivalent or less, designed with modular technology using module factory fabrication, pursuing economies of series production and short construction times*”.

In regard to modularity in design, (Morgan, 1993) has compared the nuclear industry with the aviation industry since both industries operate within highly regulated regimes and share an overall high standard in safety and reliability. He pointed out that if an aircraft was made and certified one at a time, similar to nuclear reactors, then “*many travellers would find the level of safety unacceptable and air travel would be much more expensive, pilots and mechanics would have to be specially trained to operate each aircraft, many replacement parts would have to be custom made, and every time an aircraft experienced a problem, engineers and managers would be unsure how to extrapolate the lessons to other aircrafts*”. Therefore, with the current approach in the nuclear industry, there is no way to mass produce gigawatt-scale reactors in the way that Boeing 747s and Airbus A380s are built. However, by adopting a smaller design capable to be mass produced in a factory with high levels of quality control and conveyed to its final location, the nuclear industry might begin to look more like the aviation industry. Because individual reactors would be smaller, the capital cost and, hence, the financial risks of buying one would be lower.

This line of argument has led the nuclear community to be more interested in the development of SMRs that would incorporate passive safety systems, and use modular construction techniques. Also, the smaller size might allow customers to buy capacity in an incremental way that suits their energy demand and financial profile. SMRs could also facilitate the deployment of nuclear power in locations for which large reactors are ill-suited and permit novel approaches to siting that are infeasible for large reactors. For example, underground construction is a feature advertised by light water SMR vendors (e.g. Westinghouse SMR (IAEA, 2018b), NuScale (NuScale Power, 2012), SMR-160 (Oneid, 2012), mPower (Halfinger and Haggerty, 2012)). In addition, SMRs could be deployed within a mixture of energy portfolio in a decentralized energy system, the so-called micro-grid concept. Together with other clean energy sources, SMRs could help in de-carbonizing an energy sector.

Integral SMRs, in general, are based on the concept of integrating steam generators, reactor coolant pumps, pressurizer, and reactor core within the reactor pressure vessel (RPV). Thus, analyzing

---

\* The world's first nuclear power plant that generated electricity for commercial use was a small reactor (5 MW<sub>e</sub>) built in the Soviet Union in 1954 (IAEA, 2018a).

such complex systems operated at different conditions is of great interest in the nuclear scientific community. Specifically, in the case of postulated design basis accidents. The knowledge of the temporal evolution of postulated accidents is mandatory to assess the safety features of any reactor system.

Many light-water SMRs vendors claim that these new reactor concepts are characterized by an enhanced safety margin in comparison to conventional LWRs. The state-of-the-art of the technological and safety developments of different light water SMR concepts is discussed hereafter.

## 1.2 State-of-the-art of Light-water Small Modular Reactors

The integral reactor concept is not new to the nuclear community; this concept was first demonstrated in the “Otto Hahn” ship<sup>†</sup> in 1968 (Halfinger and Haggerty, 2012) that had a core operated at a rated thermal power of 38 MW<sub>th</sub> and cooled by non-borated light water. The concept of soluble boron free (SBF) operation is not new as well. In 1989, a study conducted by Combustion Engineering for the Electric Power Research Institute (EPRI) questioning the technological visibility of eliminating soluble boron in large PWRs which they came to the following conclusion: “A significant result of this study is the realization that the feasibility of a soluble boron free design improves as the core power and size are reduced, primarily because of the intrinsic xenon stability of small PWRs. Further, current thinking on small PWRs generally tends towards lower average power density than existing large PWRs, allowing the former to more easily accommodate the higher relative power peaking expected in any soluble boron free design” (Electric Power Research Institute (EPRI), 1989). Therefore, this study suggested that the SBF operation is more feasible to small and low power density reactor cores, as in the SMRs. However, designing a reactor core with the SBF concept may lead to a complex core design with higher power peaking factors. Consequently, this may result under accidental conditions in fuel rod failures. Therefore, there is a need to discuss deeply the drawbacks as well as the advantages offered by the SBF concept to investigate the technological visibility of the SBF core design.

The advantages of having the SBF concept is observed in reducing (more negative) the moderator temperature coefficient (MTC). Thus, improved operation flexibility and stability is gained, on the one hand. During overcooling accidents (e.g. steam line break), on the other hand, a high positive reactivity insertion may occur due to the high negative MTC. By eliminating the soluble boron from the coolant, the risk associated with the boric acid induced corrosion of the RPV and its internal parts is eliminated. Moreover, the absence of the soluble boron in the primary coolant loop leads to a reduction of radioactive waste volumes. According to (Ecomatrix, 2009), 90% of tritium produced in a typical PWR primary-coolant is due to the neutron activation with the soluble boron. Therefore,

---

<sup>†</sup> The Otto Hahn reactor vessel was equipped with a reactor core, three canned reactor coolant pumps, and a helical steam generator located in the outer annulus of the reactor vessel.

eliminating the soluble boron from the primary-coolant will drastically reduce decommissioning processes since tritium is known to be very mobile radioactive nuclide (IAEA, 1981). Consequently, these advantages will reduce the requirements for the maintenance of the chemical volume control system (CVCS)<sup>‡</sup>.

Although these benefits from eliminating soluble boron are appealing, they come with a list of challenges for an SBF core design. Duty reactivity control in a boron-free core is solely provided by control rod movement immediately translating to local changes of the power distribution; therefore, higher power peaking is expected. Operating a reactor core with high power peaking, and thus high linear heat generation rate would enhance the risk of fuel rod failure. This situation becomes even more serious under events that lead to highly localized power generation such as in the case of control rod ejection events. In boron operated PWRs, the CVCS supposed to inject soluble boron into the reactor coolant to assure for a safe shutdown condition, are acting as a secondary shutdown system. Simplifying the CVCS by eliminating the soluble boron from the coolant seems to remove a diverse and redundant shutdown system. However, installing an emergency boration system may be a viable solution. For instance, the GE Hitachi Advanced Boiling Water Reactor (ABWR) is equipped with a Standby Liquid Control (SLC) system that is capable to inject soluble boron to maintain the reactor in a safe sub-critical state at room temperature (around 20°C) and without the help of control blade insertion (GE, 2011). The SLC system is installed for ABWR to mitigate the consequences of anticipated transients without scram (ATWS) events.

These challenges associated with the SBF concepts led many light water SMR designers to neglect their benefits, whereas other vendors favored their offered advantages. Table 1.1 lists several light water SMRs features that were identified as promising for near term commercialization according to the SMR outlook report (Strategic Insights, 2015) along with AP1000 features as a basis for comparison between large modern PWRs and SMRs.

All these SMR concepts listed in Table 1.1 claimed that their designs are providing a higher safety margin against postulated events in comparison to conventional large PWRs. This thesis is targeting at analyzing this claim by the example of the System Integrated Modular Advanced Reactor (SMART) design.

---

<sup>‡</sup> The chemical volume control system (CVCS) objective is to purify the reactor coolant and maintain favorable chemical conditions (pH level) that limit corrosion by the addition of corrosion-inhibiting chemicals. In addition, CVCS is responsible of adjusting boron concentration in the reactor coolant through the use of number of large tanks, heat exchangers, pumps, piping, valves and control systems (Manno and Golay, 1985).

**Table 1.1: Summary of key nuclear design parameters for a range of promising light water SMRs (Land-based) and a modern large PWR (Strategic Insights, 2015) (IAEA, 2018b) (IAEA, 2011)**

Reactor Name (vendor)	AP1000 (Westinghouse)	Westinghouse SMR (Westinghouse)	mPower (Babcock and Wilcox)	SMR-160 (Holtec)	NuScale (NuScale Power)	SMART (KAERI)	CAREM (CNEA & INVAP)	ACP100 (CNNC)
Power Thermal ( $MW_{th}$ ) Electrical ( $MW_e$ )	3400 1150	800 225	575 195	525 160	160 50	330 100	100 30	385 125
No. of fuel assemblies in the core	157	89	69	N/A	37	57	61	57
Active fuel height (m)	4.3	2.4	2.4	3.7	2.0	2.0	1.4	2.15
Reactivity control mechanism	Control rods Soluble boron	Control rods Soluble boron	Control rods only	Control rods only	Control rods Soluble boron	Control rods Soluble boron	Control rods only	Control rods Soluble boron
Average core power density ( $MW_{th}/m^3$ )	110	82	76	N/A	47	62.6	N/A	69
Cooling Mode	Forced	Forced	Forced	Natural	Natural	Forced	Natural	Forced
Reactor Pressure (MPa)	15.5	15.5	14.8	15.5	12.8	15	12.25	15
Core Outlet/Inlet Temperature ( $^{\circ}C$ )	325 280	324 294	319 291	316 196	314 258	323 295.7	326 284	320 287

### 1.3 Description of the System Integrated Modular Advanced Reactor

The System-integrated Modular Advanced Reactor (SMART) (Park, 2011) is an advanced small-sized integral pressurized water reactor developed by Korea Atomic Energy Research Institute (KAERI). The SMART's reactor core, pressurizer, steam generators (SGs), and reactor coolant pumps are all integrated into a single RPV (see Fig. 1.3). This feature enabled large-sized pipe connection to be removed; thus, eliminating the possibility of large scale pipe breaks associated with loss of coolant accidents. The SMART RPV houses four canned-motor pumps and eight helical-coiled SGs. The SGs in SMART are placed above the reactor core in order to provide enough coolant density gradients for establishing natural circulation inside the RPV in case of an accident. The working principle of the helical-coiled SGs is different from the U-tube design used in conventional PWRs. In the helical-coiled SGs, the primary coolant flows downward outside the helical-coiled tubes, whereas the secondary coolant flows upward inside the helical-coiled tubes, which is the opposite of U-tube SGs. Also, the coolant volume inside the helical-coiled tubes (i.e. coolant inventory of the SG's secondary-side) is much smaller than in U-tube SGs. Therefore, the thermal-hydraulic performance differs from using U-tube SG designs.

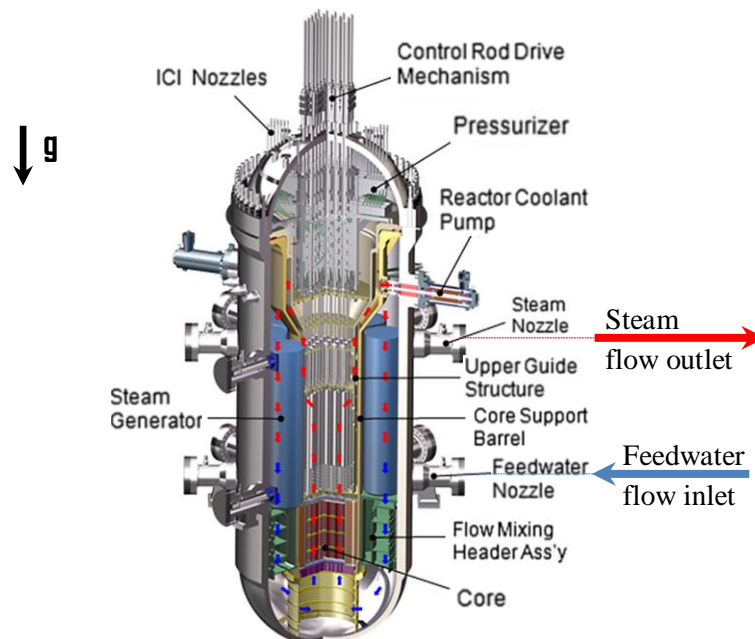


**Fig. 1.3: An overview of SMART's reactor pressure vessel and its internal components (Park, 2011)**

The reactor core of SMART is designed to provide a thermal power of 330 MW<sub>th</sub> with 57 fuel assemblies (FAs) that have an active length of 2 m (almost half of conventional PWRs) with slightly enriched uranium oxide (UO<sub>2</sub>) of less than 5 wt%. Soluble boron and 25 rod cluster control assemblies are used to control core excess reactivity during operation and bring the core into a safe shutdown state. In order to reduce boron concentration during the SMART normal operation at the beginning-of-

life, SMART FAs are loaded with a number of lumped burnable absorbers made of Gadolinia ( $Gd_2O_3$ ) mixed with the  $UO_2$  (Park, 2011). The general data of the SMART-plant is summarized in Table 1.2.

**Table 1.2: General SMART's data (Park, 2011) (Choi, 2015) (Kim et al., 2016) (Chung et al., 2015)**

<b>General plant data (Primary-side)</b>	
Rated reactor thermal power ( $MW_{th}$ )	330
Gross plant electric output ( $MW_e$ )	100
Reactor pressure vessel inner diameter (m)	5.3
Reactor pressure vessel total height (m)	15.5
Number of steam generators	8
Steam generators type	Helical-coiled
Cooling mode	Forced circulation
Number of reactor coolant pumps	4
Rated primary flow rate (kg/s)	2090
Operating pressure (MPa)	15
<b>General plant data (Secondary-side)</b>	
Feedwater flow rate (kg/s)	160.8
Feedwater pressure (MPa)	6.03
Steam generator inlet temperature ( $^{\circ}C$ )	200.0
Steam pressure (MPa)	5.2
Steam generator outlet temperature ( $^{\circ}C$ )	> 296.4
<b>Core data</b>	
Average core power density ( $MW/m^3$ )	62.6
Equivalent core diameter (m)	1.832
Reactivity control	Control rods and soluble boron
Core inlet mass flow rate (kg/s)	2006.4
Core inlet temperature ( $^{\circ}C$ )	295.7
Core outlet temperature ( $^{\circ}C$ )	323.0
<b>Fuel assembly data</b>	
Number of fuel assemblies	57
Lattice geometry	Square with 17x17 array
Active fuel height (m)	2.0
Fuel material	$UO_2$
Cladding material	Zircaloy-4
Moderator/Coolant material	Light water
Burnable absorber material	$Gd_2O_3-UO_2$
<b>Control rod data</b>	
Number of control rods	25
Absorber material	Ag-In-Cd

The SMART plant is equipped with different safety systems to assure that the main safety functions are maintained such as core sub-criticality and core coolability in the short and long term. There are two SMART designs available from KAERI that have the same RPV with all its internal structures and differs in some of safety systems. The first design has both passive and active safety systems that has already obtained the standard design approval from Korean regulatory body in 2012 (Keung Koo Kim et al., 2014). The second design is based on fully passive systems (Bae, 2018). In this work, all performed analysis is based on the second design. Fig. 1.4 illustrates an overview of the containment and associated safety systems of the passive SMART design.

**CPRSS:** *Containment Pressure and Radioactivity Suppression System.*

**PRHRS:** *Passive Residual Heat Removal System.*

**PSIS:** *Passive Safety Injection System.*

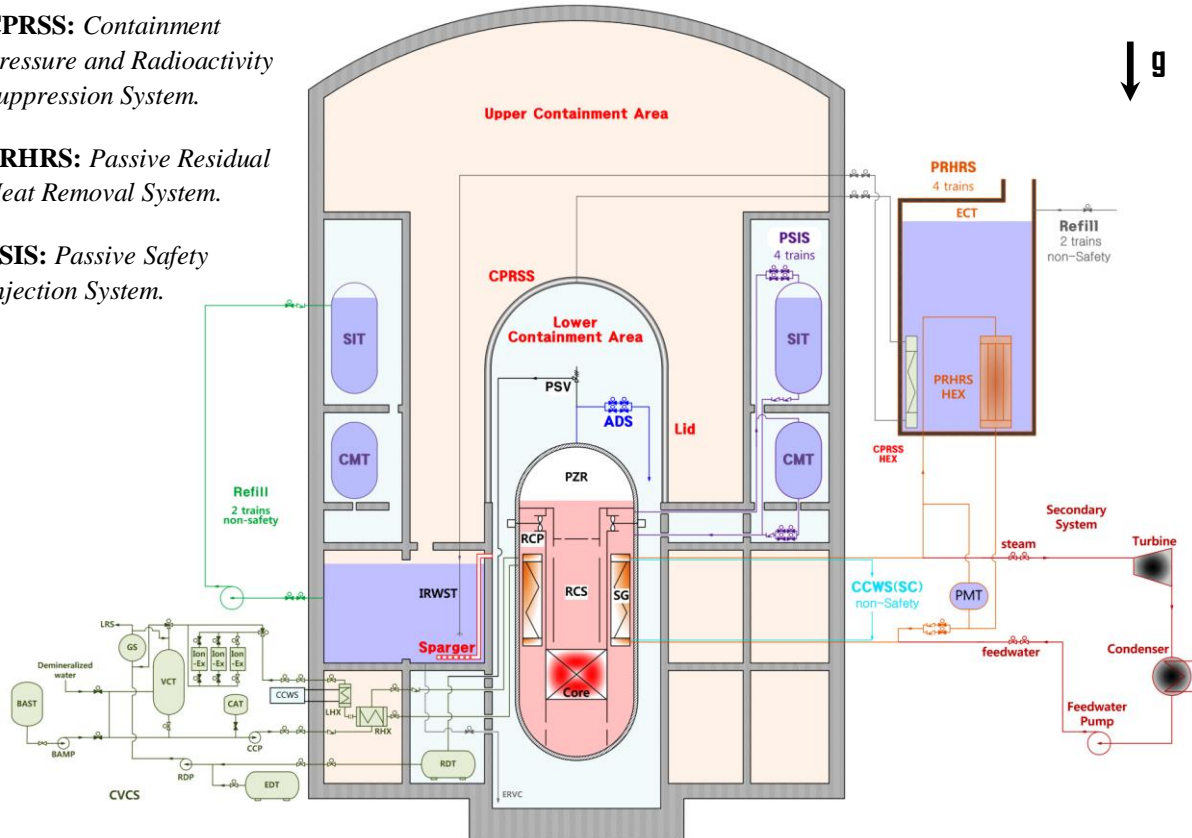


**Fig. 1.4:** An overview of the SMART containment and associated safety systems (Bae, 2018)

One peculiar safety system for the long term core coolability is the passive residual heat removal system (PRHRS). This system is responsible for removing core decay heat through natural circulation in case of an emergency condition. The PRHRS consists of four independent trains with a 50% capacity for each train. Each train has a heat exchanger submerged in an emergency cooldown tank (ECT), a makeup tank, valves, and pipes. The ECT is located outside the containment building in a higher level than the helical-coiled SGs to facilitate the establishment of natural circulation within the secondary-side. A schematic of PRHRS and its connection to the secondary-side is shown in Fig. 1.5. During normal operation, the PRHRS is deactivated through closing all isolation valves connected to the secondary-side. In an accidental condition, the main steam isolation valves (MSIVs) and feedwater isolation valves (FIVs) are closed allowing the generated steam from helical-coiled SGs to flow into the submerged heat exchangers within the ECT. Then, the heat is transferred from the steam to the water of the ECT through condensation.

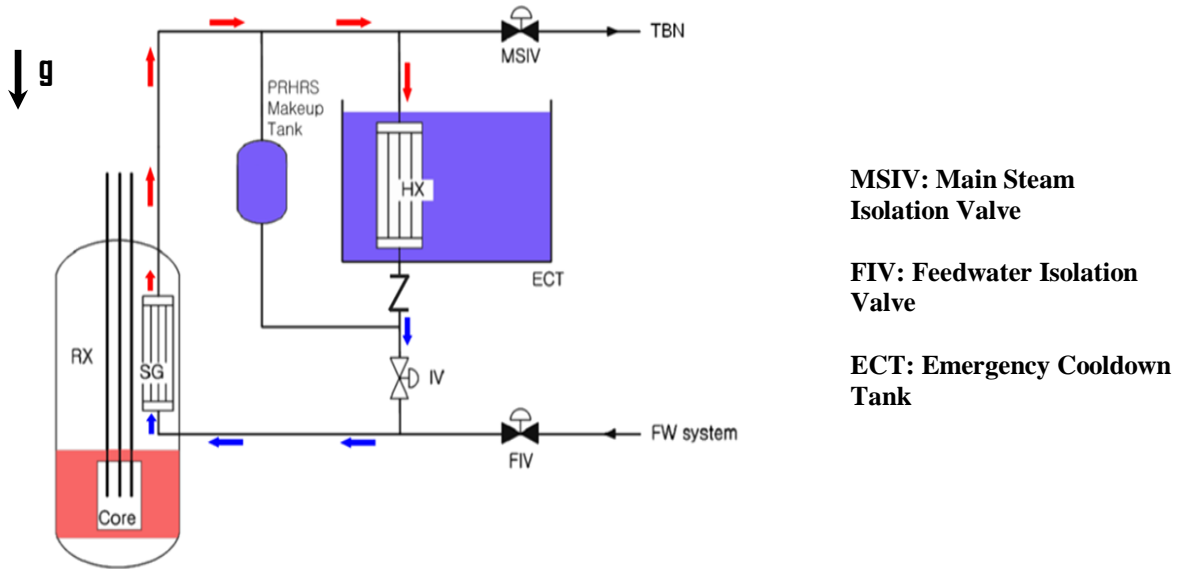


**Fig. 1.5: A schematic of the passive residual heat removal system and its connections to the SG's secondary-side (Park, 2011)**

## 1.4 Objectives and Scope of This Thesis

The main objectives of the present doctoral thesis are (i) the neutronic and thermal-hydraulic design of a boron-free core with inherent safety features that can fit within the SMART-plant (i.e. inside the reactor pressure vessel); and (ii) the analysis of the behavior of the boron-free core integrated within the SMART-plant under selected design basis accidents. The development and optimization of a boron-free core require an iterative process considering many competing parameters in order to obtain an optimal core design. These competing parameters are listed below:

- **Reactor shutdown systems:** To reach a safe sub-critical shutdown core state, control rods with high absorption materials are required. However, operating a reactor core with high absorber rods may not be adequate since it may lead to high power peaking.
- **Neutron economy:** Extensive use of control rods and also burnable poisons to compensate for core excess reactivity and managing power maneuvering causes a harder neutron spectrum\*. On the one hand, a harder spectrum is beneficial to reduce the initial fuel enrichment due to generating more plutonium in the core. On the other hand, a harder spectrum yields higher neutron fluence on the inner wall of the RPV; thus, reducing its lifetime.
- **Neutronic safety:** Due to the elimination of soluble boron from the reactor coolant, a deeper control rods insertion is needed to achieve core criticality during normal operation. This deeper control rods insertion skews the axial power distribution towards the core bottom, where the

\* A greater proportion of the neutrons will be at higher energies since thermal neutrons will be captured by the absorbing materials.

coolant temperature is lower than at the core exit. Therefore, a high power peaking at the core bottom is expected leading to an uneven fuel burnup.

- **Thermal-hydraulic safety:** High power peaking within the core requires an adequate cooling to safely remove heat generated at those fuel pins with high power peaking. However, the SMR-core to be developed has to be placed within the SMART RPV without any changes to its cooling features (i.e. the rating of the reactor coolant pumps).

These above mentioned challenges are tackled through an iterative process via a safety-based approach to reach an optimized core design. Further, the safety performance of the optimized boron-free core is investigated for two design basis accidents: (i) control rod ejection accident; and (ii) steam line break accident with single and multiple failure consequences.

The scope of the present investigations is limited to safety analysis at the beginning-of-life of the first core to demonstrate the principle feasibility of an SBF concept. The evaluation of core behavior during normal operation and accidental conditions at the end-of-life requires additionally a fuel cycle analysis and a development of control rod insertion strategy during fuel depletion, which is out-of-scope of the current doctoral thesis.

## 1.5 The Safety-Based Core Optimization Approach

The development of an optimized core design with enhanced inherent safety features (i.e. due to the high negative MTC as a consequence of removing the soluble boron from the coolant) is a challenging problem with many degree of freedom (large search space). The core design variables of this large search space problem can be classified under the following categories:

### (A) Geometrical search variables:

1. Fuel assembly dimension (assembly array size, total and active height, assembly pitch, pin pitch, pellet radius, clad inner/outer radius, and guide/instrumentation tube inner/outer radius).
2. Fuel assembly configuration (number of fuel rods, guide/instrumentation tubes and burnable absorbers (if any) in each fuel assembly).
3. Core dimension (total number of fuel assemblies in the core).
4. Core configuration (locations of fuel assemblies in the core).

### (B) Material search variables:

1. Fuel material (fuel pellet initial composition, enrichment, and density).
2. Cladding material (composition and density).
3. Burnable absorbers (composition and density).
4. Control rods (composition and density).

**(C) Thermal-hydraulics search variables:**

1. Core thermal power.
2. Core coolant inlet flow rate.
3. Core inlet temperature.
4. Core exit pressure.

To reduce the number of free variables of this large search space problem, the accumulated industrial experience in designing LWRs is adopted along with some constraints coming from the SMART design. The fuel assembly dimension is based on the well-proven 17x17 PWR fuel assembly design except for the active length. The active length and the total number of fuel assemblies are fixed to fit the SMART RPV. All thermal-hydraulics boundary conditions are the same as in the SMART-core. The optimal core design is then achieved in an iterative process, which is terminated when the pre-defined acceptance criteria are satisfied. Fig. 1.6 shows the safety-based core optimization process.

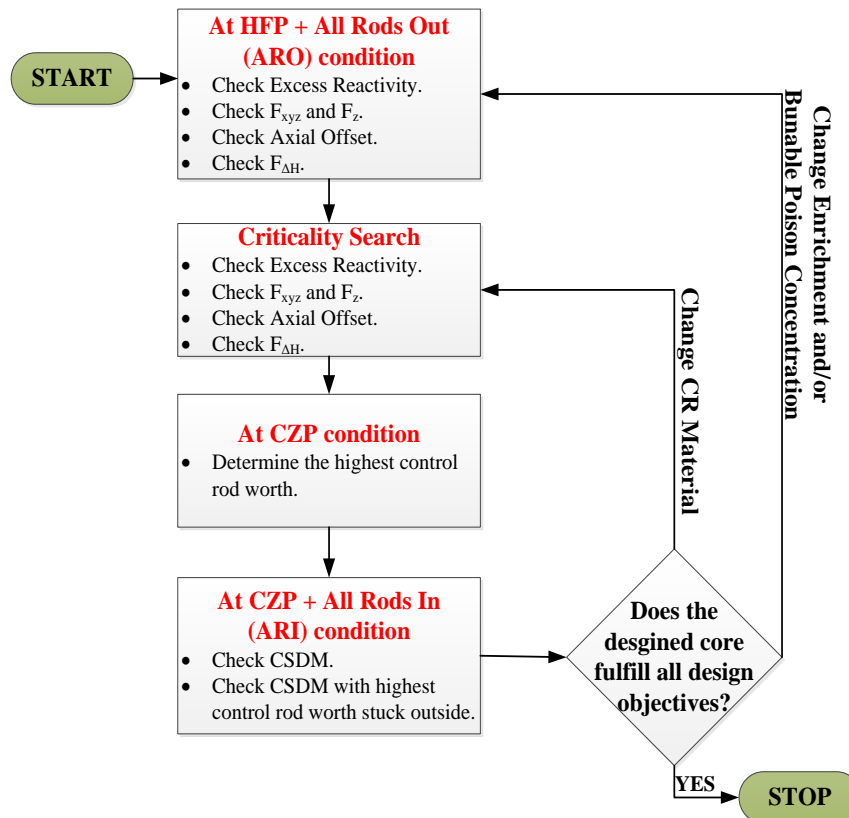


**Fig. 1.6: The Safety-based core optimization process**

## 1.6 Structure of the Thesis

This doctoral thesis is organized into nine chapters. Following the introduction, chapter 2 explores the background physics for performing reactor analysis in terms of reactor physics, thermal-hydraulics and reactor safety. Chapter 3 presents the capability of the simulation tools used to develop a boron-free core and study its safety performance when integrated within the SMART plant. In chapter 4, the

features of the developed boron-free core are highlighted from both neutronics and thermal-hydraulics perspective. Chapter 5 then describes the design verification process of the developed core along with a comparison with the obtained results against a high-fidelity solution. After that, chapter 6 discusses the developed boron-free core behavior under control rod ejection accidents from a safety perspective. Later on, chapter 7 continues on analyzing the safety performance of the developed core integrated within the SMART-plant under the steam line break accident in two scenarios: (i) safety systems are not affected following the accident; and (ii) failure of the PRHRS leading to the loss of the ultimate heat sink. Finally, the major outcomes of the thesis are summarized in chapter 8, and the recommendation for future research directions are highlighted in chapter 9.

## CHAPTER 2: REACTOR ANALYSIS FUNDAMENTALS

In this chapter, the theoretical background of this dissertation is highlighted. First, the multi-physics and multi-scale definitions are introduced. Then, reactor physics concepts (e.g. multiplication factor) and calculation approaches are described. Hydraulic and thermal analysis is then presented. Finally, the defense-in-depth principle is demonstrated along with some relevant postulated initiating events for the SMART plant.

### 2.1 Multi-physics and Multi-scale Concepts

In an operating nuclear reactor, various physical phenomena are interrelated at different scales that challenge the safety assessment. Reactor analysts during the early days of the nuclear era relied on different computer codes that were developed to describe each physical phenomenon separately (e.g. neutron physics, thermal-hydraulics, structural mechanics, fuel performance, coolant chemistry, etc.). Such an approach required many assumptions and simplifications associated to perform a credible safety assessment of a reactor system. As a result, a conservative safety analysis with large safety margins is obtained to account for the “unknown” information.

At present, the rapid progress in computational power; the knowledge gain from continuous research; and the need to improve the economics and operational flexibility of nuclear reactors keeping high safety standards motivated the concept of coupling different physics domains in order to relax assumptions made earlier in the decoupled analysis, and reduce conservatism of legacy codes. Such an approach is known as the multi-physics approach.

Multi-physics simulations that take into account the coupling between neutronic and thermal-hydraulic phenomena are of great importance in reactor safety and design, in which the nuclear scientific community devoted special attention to improving their efficiency, accuracy, and robustness. In this regard, coupled neutronics and thermal-hydraulics codes for the reactor core analysis, on the one hand, were developed such as COBAYA3/CTF (Jiménez Escalante, 2010), DYN3D/FLICA4 (Gómez Torres, 2011), DYNSUB (Gómez Torres, 2011), COBAYA3/SUBCHANFLOW (Calleja et al., 2014), PARCS/CTF (Ramos et al., 2017), COBAYA4/CTF (García-Herranz et al., 2017), DYN3D/CTF (Périn and Velkov, 2017), and PARCS/SUBCHANFLOW (Basualdo et al., 2017) to improve the prediction accuracy of the core behavior taking into account the local feedbacks (at nodal level) between undergoing core physical processes. On the other hand, coupled neutronics and system thermal-hydraulics codes were developed, for instance, RELAP5/PARCS (Barber et al., 1998), RELAP5/PANBOX (Jackson et al., 1999), TRAC-M/PARCS (Miller and Downar, 1999), TRAC/NEM (Beam et al., 1999), CATHARE-CRONOS2-FLICA (Mignot et al., 2004), ATHLET-QUABOX/CUBBOX (Langenbuch and Velkov, 2005), TRACE/S3K (Nikitin et al., 2010), DYN3D/ATHLET (Kozmenkov et al., 2015), TRACE/PARCS (U.S. NRC, 2013) and TRADYN

(Gonzalez-Vargas et al., 2018) to evaluate the behavior of nuclear power plants under postulated design basis accidents with strong space-time dependence in the core.

The multi-scale concept is related to the description of a certain physical phenomenon occurring at different spatial scales and how they are interrelated. For example, in a nuclear reactor, the reactor pressure vessel's radius is in the order of several meters, the fuel rod diameter is in the order of few centimeters, and the size of the bubbles in the coolant flowing within these structures is in the order of millimeters. The fluid flowing in the nuclear reactor core is governed by the same physical laws, however, the hypotheses used in different scales are chosen in agreement with the effects that must be reproduced at a given scale.

The degree of spatial refinement of numerical codes is known to be strongly related to the computing power available. The wider scales have been explored and used for several years, in which methods have been verified and validated. Due to the advancement in computational power and novel measurement techniques, recent developments have moved in the direction of understanding phenomena taking place at smaller scales. In the reactor physics field, nodal codes are developed to solve for the eigenvalue and eigenfunction (i.e. neutron flux) using the multi-group diffusion or the simplified P3 (SP3) equations at fuel assembly level (Bell and Glasstone, 1970), where information at fuel pin level is lost. To recover that information, the pin power reconstruction methodology was introduced (Koebeke and Hetzelt, 1985), improved (Rempe et al., 1989), and adopted in many nodal reactor dynamic codes. This spatial refinement allowed reactor analyst to access local safety information such as maximum fuel pin and cladding temperature.

In the following sections, concepts introduced throughout this dissertation related to neutron physics, thermal-hydraulics, and reactor safety will be discussed.

## 2.2 Reactor Physics

The design of a nuclear reactor requires the prediction of how neutrons are distributed within the reactor core. As neutrons move within the reactor core, they undergo several interactions with matter e.g. capture, fission or scattering. The neutron interaction probabilities are known as “cross-section”. Microscopic cross-section data (e.g. absorption, fission, scattering, etc.) are unique for each material (nuclides) and energy-dependent, where the energy-dependency for some energy ranges is still not completely known so far.

The neutron transport phenomenon in the reactor core is governed by the linearized form of the Boltzmann transport equation, which is a statistical formulation for the description of atoms and molecules transport in a media, known as neutron transport equation<sup>\*</sup>. The linearization of the

---

<sup>\*</sup> The reader is advised to refer to (Bell and Glasstone, 1970) for the mathematical derivation of the neutron transport equation.

Boltzmann transport equation is actually originating from the fact that neutron-to-neutron interaction is negligible. For example, in an operating LWR, the neutron density in the core is in the order of  $10^{14}$  per  $\text{cm}^3$ , whereas the number of atoms per  $\text{cm}^3$  is about  $10^{24}$ . This example illustrates that a neutron is heavily surrounded by atoms; thus, neutron-to-nucleus interaction is by far more likely than neutron-to-neutron interaction.

The neutron transport equation is very complex to be solved because the neutron interacting with matter (under different reactions) depends on six dimensions: position (3 dimensions), energy, angle and time. In reactor physics, many methodologies were developed aiming to solve the neutron transport equation with certain approximations. Two big branches are then distinguished in dealing with the neutron transport equation: deterministic and stochastic (Monte Carlo) methods, which will be briefly introduced in the next subsections alongside with the most relevant terminologies used throughout this thesis.

### 2.2.1 Deterministic reactor physics solution approach

Several deterministic methodologies have been developed to approximate the neutron transport equation including collision probability (CP) method, spherical harmonics ( $P_N$ ) method, discrete ordinates ( $S_N$ ) method, method of characteristics (MOC), and neutron diffusion method. Recently, the MOC has been used for providing full core direct transport solution. However, the computational burden of this approach is still very high, and thus, limiting its utilization for routinely industrial applications (e.g. fuel reshuffling, core optimization, etc.). The current deterministic approach used by the nuclear industry is based on the “two-step” core calculation.

In the first step, one or few fuel assemblies (FAs) are modeled with fine spatial and energy discretization, normally each cell in the fuel assembly is explicitly modeled with around hundreds of cross-section energy-groups. These FAs are commonly represented in a 2D-model with reflective outer boundary condition. The FA is then homogenized, and the multi-group cross-sections are collapsed into a few-group structure. For thermal reactors (e.g. LWRs) two energy-groups are normally used. To account for the thermal-hydraulic feedback and reactor operation conditions on the cross-section data, this step is repeated in so-called branch calculations, for various fuel and moderator temperatures, boron concentration, control rod positions (in/out), and burnup status. These branches are then combined in a cross-section data library for each FA type in the core in multi-dimensional look-up tables or fitting functions.

In the second step, the libraries generated from the first step are then loaded into a core simulator. Nowadays, the most common core simulators are based on the nodal diffusion method, in which coarse meshes are used to represent a fuel assembly. Fig. 2.1 presents the “two-step” computational procedure for deterministic reactor physics calculations.

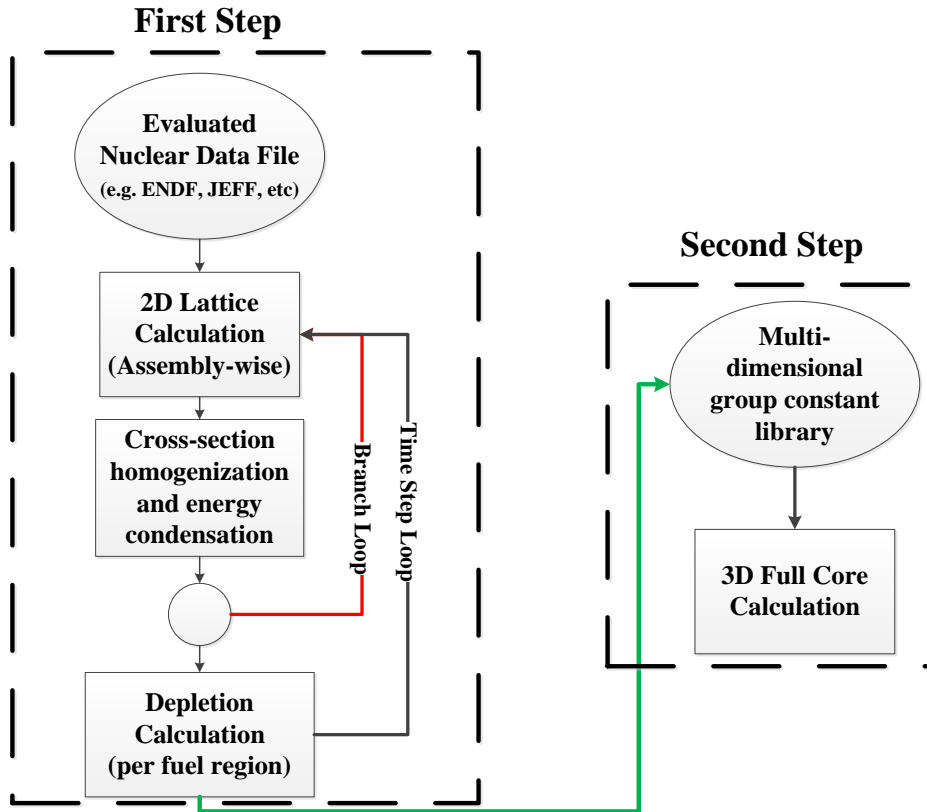


**Fig. 2.1: Two-step computational procedure for deterministic reactor physics calculations**

From a theoretical perspective, the validity of the diffusion equation is limited by the angular distribution of neutrons to be at most linearly anisotropic. This validity breaks down near regions of high neutron absorption (such as control rods or burnable poison pins) or near highly scattering regions with little absorption (such as water rods or reflectors). Nevertheless, the diffusion equation is employed in many commercial core simulators used by the nuclear industry as it can predict quantities of interest (e.g. power distribution) fairly accurately. The key issue behind that is through providing “*equivalent*” homogenized cross sections to the core simulator through the so-called homogenization correction methods.

Two homogenization correction methods have been developed to recover the deficiency of the neutron diffusion theory: the Generalized Equivalence Theory (GET) (Smith, 1986), and the Super homogenization (SPH) method (Herbert, 1981). The GET adds another degree of freedom to the diffusion equation to allow the conservation of neutron flux or currents at a node boundary through defining a new parameter called discontinuity factor (DF). DF is defined as the ratio of heterogeneous to homogenous neutron flux at a surface of interest (e.g. fuel assembly outer surface). The SPH method introduces a new homogenization parameter called SPH factor to correct the homogenized cross sections in order to reproduce the reaction rates from the heterogeneous calculation. The SPH factor is defined as the ratio of the heterogeneous to homogenous volume-averaged neutron flux. The

SPH method involves an iterative process to assure the convergence of the homogenous reaction rates to the heterogeneous ones.

### 2.2.2 Stochastic reactor physics solution approach

In addition to these deterministic treatments of the neutron transport equation, stochastic (Monte Carlo) techniques can be also applied to find the neutron flux distribution within a reactor core. In general, Monte Carlo (MC) methods provide an exact solution to a variety of mathematical problems by performing statistical sampling experiments. In neutron transport calculations, the applicability of the MC method arises from the fact that the macroscopic cross-sections are interpreted as a probability of interaction per unit distance traveled by a neutron (Bell and Glasstone, 1970). Thus, in the MC method, a neutron path is followed from the moment of birth (e.g. by fission) until the disappearance from the system (either by absorption or leakage), the so-called neutron history. To provide statistically significant MC solution, a large number of neutron histories is normally required. A well-known drawback of MC methods is the slow convergence of the statistical uncertainty in a region-of-interest with the number of particles scored in that region. Namely, a statistical uncertainty decreases as particle scores increases in an inverse-square-root relationship. For example, ten times decrease of statistical uncertainty in a parameter-of-interest requires a hundred times more of neutron histories. Therefore, more CPU times are required. To solve this slow convergence problem, variance reduction techniques have been developed over the past years. In general, the MC approach is considered superior to the deterministic one because a higher degree of accurate geometrical representation can be achieved by MC methods. In addition, MC methods can use directly continues (point-wise) energy nuclear data and does not rely on self-shielding approximations compared to deterministic codes. Traditionally, MC codes are used to provide a reference solution for the deterministic reactor physics calculation approach.

### 2.2.3 Neutron multiplication and criticality

To sustain a fission chain reaction, one or more neutrons produced from a fission event must survive to produce another fission event. The neutron multiplication factor is introduced to indicate the degree of sustainability of a fission chain reaction. It is defined as the total number of fission neutron produced, on average, by one neutron from a previous fission event. This quantity is normally referred to the effective multiplication factor ( $k_{\text{eff}}$ ) and is formulated by the following six-factor formula:

$$k_{eff} = \eta \cdot f \cdot \varepsilon \cdot p \cdot P_{FNL} \cdot P_{TNL} \equiv k_{\infty} \cdot P_{FNL} \cdot P_{TNL} \quad (2.1)$$

The reproduction factor ( $\eta$ ) is defined as the number of neutrons emitted by fission for one neutron absorption in the fuel. This factor is directly related to the fissile content of the fuel (e.g. uranium enrichment). The thermal utilization factor ( $f$ ) is defined as the probability that a thermal neutron will be absorbed in a fissile nuclide instead of being absorbed in another nuclide. The fast

fission factor ( $\epsilon$ ) is defined as the ratio of total fission neutron produced to the number of neutrons formed as a result of thermal fissions. This factor accounts for the additional fission caused by fast neutrons. The resonance escape probability ( $p$ ) is defined as the probability that a neutron will cross the resonance capture region to the thermal region without getting absorbed. The aforementioned factors does not account for the neutron leakages from the reactor core. To account for neutron leakages, the two factors ( $P_{FNL}$ ) and ( $P_{TNL}$ ) are introduced: The ( $P_{FNL}$ ) accounts for the probability that a fast neutron will not leak-out of the system, whereas the ( $P_{TNL}$ ) accounts for the probability that a thermal neutron will not leak-out of the system. These two non-leakage factors depend on the geometry of the system under consideration.

These definitions of the six-factor formula are only used as a mean for expressing the results obtained from detailed multi-group calculations (e.g. diffusion equation), and of understanding their physical significance. Nowadays, core simulators predict the effective multiplication factor (or eigenvalue) by solving the multi-group diffusion equation and not by solving the six-factor formula (Bell and Glasstone, 1970). A reactor state is denoted as sub-critical, critical, or super-critical if the  $k_{eff}$  is below, equal, or above unity, respectively. Another common way of representing the  $k_{eff}$  is called reactivity ( $\rho$ ), which is defined as:

$$\rho = \frac{k_{eff} - 1}{k_{eff}} \quad (2.2)$$

A reactor core reactivity ( $\rho$ ) is commonly expressed in units of pcm (1 pcm =  $10^{-5}$ ). In the reactor kinetics theory, reactivity is sometimes normalized to the effective delayed neutron fraction ( $\beta_{eff}$ ) and expressed in dollar unit (\$). The significance of expressing reactivity in (\$) allowed reactor physicist to compare the dynamics response of different reactors, regardless of their core material loading. Nuclear reactors are operated with  $k_{eff}$  of unity (or  $\rho$  equal to zero) to sustain the fission chain reaction (i.e. with constant power in steady state).

## 2.2.4 Reactor power anomalies

During reactor operation, fission products are continuously produced by the fission process itself and consumed by either neutron absorption to form another nuclide (burnout) or radioactive decay. Two of the most concerned fission products to reactor physicists are Xenon-135 ( $Xe^{135}$ ) and Samarium-149 ( $Sm^{149}$ ). These two nuclides have a large neutron absorption cross-section and are called neutron poisons. These neutron poisons may halt the fission chain reaction, if not properly managed.  $Xe^{135}$  is 95% of the times are produced from the decay of iodine-135 ( $I^{135}$ ) and the rest as a direct fission product, whereas it is consumed by neutron absorption to form  $Xe^{136}$  or simply decay to  $Cs^{135}$ . The  $I^{135}$  is produced from the decay of tellurium-135 ( $Te^{135}$ ), a direct fission product, which has a half-life of 11 seconds. Hence,  $I^{135}$  is normally assumed to be produced directly from fission, and therefore, directly proportional to neutron flux (Lamarsh and Baratta, 2001).

A reactor power anomalies arising from, for example, control rod movement or misalignment causes an imbalance in the fission rates within that location, hence, alternating the  $I^{135}$  buildup and  $Xe^{135}$  consumption. Under steady state core operation (i.e.  $Xe^{135}$  concentration is in equilibrium, and total core power is constant): an increase of neutron flux in a specific core location, causes the  $Xe^{135}$  concentration to reduce due to burnout which then allows the flux to increase further. In contrast, a decrease of neutron flux in a specific core location causes an increase to the  $Xe^{135}$  concentration due to the decay of  $I^{135}$ , and therefore, further decreases of the neutron flux at that location. This process is reversed such that in the high-flux region, neutron flux decreases as soon as the  $I^{135}$  levels buildup sufficiently, and vice versa. This pattern is repeated, which is called Xenon oscillations, with periods of the order of about 15 hours. Reactor operators normally prevent this power anomaly by controlling the amount of axial power offset (or simply axial offset). Axial offset (AO) is defined as the difference between the core power in the top-half and in the bottom-half normalized to the total core power, as written in equation (2.3).

$$\text{Axial offset} = \frac{\text{Core Power in the Top half} - \text{Core Power in the Bottom half}}{\text{Total Core Power}} * 100 \quad (2.3)$$

Compliance with the AO limits, normally defined within technical specification, prevent a high top or bottom skewed axial power distribution and minimize the potential for Xenon oscillations.

### 2.2.5 Reactivity control mechanisms

Normally nuclear reactors are designed with core reactivity above zero (or  $k_{\text{eff}}$  greater than unity) to account for the negative reactivity inserted by  $Xe^{135}$  and  $Sm^{149}$  buildups, and fuel depletion. This extra reactivity is called core excess reactivity. In order to maintain core criticality, mechanical or chemical shim control system is designed to compensate for core excess reactivity.

Control rods (mechanical shim) are composed of strong neutron absorber materials. Various alloys such as silver, indium and cadmium (Ag-In-Cd), hafnium, or boron carbide ( $B_4C$ ) are the most used material combinations nowadays in thermal reactors under operation (some fast reactors use control rods made of  $B_4C$  with enriched B-10 to values close to 90%).

Chemical shims are another form to reduce core excess reactivity which is soluble-based compounds that are homogeneously mixed with a moderator. The most common chemical shim in commercial PWRs is boric acid ( $H_3BO_3$ ). By varying the concentration of boric acid in the moderator, core reactivity is varied as well. The changing of boron concentration in the coolant is a slow process. Thus, the chemical shim is always used in conjunction with mechanical control rods in a nuclear reactor, as control rods provide fast reactivity compensation. Having a chemical shim dissolved in the reactor coolant substantially reduces the number of control rods required in the core. Furthermore,

since the chemical shims are uniformly distributed throughout the reactor core, changes in its concentration can be achieved without disturbing the power distribution in the core.

Despite of these two external means to compensate the core excess reactivity, burnable poisons are another form to manage core reactivity. These burnable poisons consist of nuclides with large absorption cross-sections which are converted into nuclides with low absorption cross-sections as a result of neutron absorption. Burnable poisons normally are classified into two types: discrete and integral. A number of materials have been utilized for burnable poisons in LWRs. For example, Pyrex glass is used as a discrete burnable poison material which contains about 12% of boron oxide ( $B_2O_3$ ). Also, another example of a discrete burnable poison is the wet annular burnable absorber (WABA) which has a burnable absorber material made of boron carbide ( $B_4C$ ) contained in an alumina matrix ( $Al_2O_3$ ), used in AP1000 design (Franceschini et al., 2015). Examples of integral burnable poisons includes gadolinia ( $Gd_2O_3$ ) or erbia ( $Er_2O_3$ ) mixed directly with  $UO_2$  fuel, used in many advanced LWR designs (Lamarsh and Baratta, 2001). Another example of an integral burnable poison is formed by applying a thin uniform coating of zirconium diboride ( $ZrB_2$ ) on the outer surface of  $UO_2$  fuel pellets (Franceschini et al., 2015).

### 2.2.6 Reactivity feedback coefficients

Reactivity feedback coefficients describe the change of core reactivity due to changes in a thermal-hydraulic parameter (such as fuel temperature, coolant density, and coolant temperature) or a reactor core state (such as changes in boron concentration and core power level). These feedback coefficients characterize the dynamic behavior of a reactor core and are normally considered as the inherent safety core parameters. For a safe and stable reactor operation, reactor cores are designed with negative feedback coefficients. For a boron-free pressurized SMR cooled by light water, the important reactivity feedback coefficients are: reactivity coefficient of fuel temperature, moderator temperature, and core power level.

Fuel temperature reactivity feedback coefficient, or Doppler coefficient, is defined as the ratio of core reactivity difference per unit change in fuel temperature. An increase in the fuel temperature enhances the thermal motion of nuclei in the fuel material, leading to a broadening of the resonances in the microscopic cross-sections (Doppler Effect). The broadening of cross-sections resonances causes a reduction in the resonance escape probability (see equation (2.1)), and hence, the core reactivity. Main contributors to a negative Doppler coefficient are the capture resonances in fertile fuel nuclide (e.g.  $U^{238}$  and  $Pu^{240}$ ). Typically, the Doppler coefficient in LWRs is in the range of -5 pcm/K to -2 pcm/K. The Doppler coefficient is very important in limiting fast transients (e.g. control rod ejection accident), which could cause a prompt super-critical reactivity insertion associated with an exponential power growth.

Moderator temperature reactivity feedback coefficient, or simply moderator temperature coefficient (MTC), is defined as the core reactivity change per a unit change in moderator temperature. In PWRs, the MTC definition is slightly changed to encapsulate both effects of moderator temperature and density. Namely, the changes in moderator temperature inherently correspond to changes in the moderator density. As the moderator temperature increase, the moderator expands causing a reduction in moderating atoms (e.g. water molecules) and its density. As a result, this leads to hardening the neutron spectrum, causing a shift to higher energies, and consequently higher resonance absorption. This phenomenon lowers the resonance escape probability, therefore, inserts a negative reactivity into the core. Usually, the MTC<sup>†</sup> in PWRs ranges from 0 pcm/K to -80 pcm/K.

Power reactivity feedback coefficient is defined as the change in core reactivity per percent change in the reactor power. It is normally expressed in units of (pcm/% power). The power reactivity feedback coefficient combines all the previous feedback coefficients and is commonly measured during reactor commissioning due to the fact that the moderator and fuel temperatures effect cannot be separated. In PWRs, the power coefficient can range from -20 pcm/% to -30 pcm/%.

## 2.3 Thermal-Hydraulics

Thermal-hydraulics analysis is crucial for a nuclear reactor design due to not only the strong interaction between the neutron populations and thermal-hydraulics condition in the reactor core, but also the determination of plant performance and safety assessment. The thermal-hydraulics analysis can be subdivided into two parts: hydraulic and thermal analysis.

The hydraulic analysis focuses on determining the coolant flow regime, which is vital for predicting the heat transfer coefficient from a fuel cladding to the coolant, and pressure losses. The thermal analysis pays attention to the temperature distribution in the fuel pellet, fuel-clad gap, cladding, and coolant.

In the next subsections, the most important aspects related to this thesis of both hydraulic and thermal analysis is covered, whereas the description of the underlying theory can be found in (Todreas and Kazimi, 1993) and (Todreas and Kazimi, 2001).

### 2.3.1 Hydraulic analysis

Hydraulic analysis of nuclear reactors focuses on determining pressure drop across individual components and describing fluid motion. Knowledge of the pressure drop is very important not only in normal reactor operation, but especially for the analysis and assessment of accidental situations. In normal reactor operation, the power generated in the core must be safely removed from the core by the

---

<sup>†</sup> In some PWR designs, MTC could be slightly positive at the beginning-of-cycle during start-up due to the large amount of boron concentration in the coolant.

coolant mass flow. Reactor coolant pumps are designed so that they provide the necessary coolant mass flow rate in a steady-state condition. The pressure build-up across the pumps equals the total pressure loss across the entire cooling system. Hence, the knowledge of the precise total pressure drop in a system is required for selecting a proper pump. The pressure drop has four components: static head, acceleration, friction, and local losses. The pressure drop due to the static head is caused by gravity forces between different heights. The acceleration pressure drop is caused by changes in flow velocity as a result of a change in coolant density. The pressure drop due to friction is caused by shear stress on the wall. The last component of the pressure drop is due to local losses caused by a change in cross-sectional flow area or flow direction (e.g. presence of spacer grids in the core). Knowing pressure drop is significant as well in accidental conditions, for example, onset or collapse of natural circulation flow in the entire system or subsystem.

The description of fluid motion is very important to understand heat transfer mechanisms and structural behavior. The flow pattern is usually characterized by the dimensionless Reynolds number ( $Re$ ).  $Re$  is defined as the ratio between inertial and viscous forces. When the viscous forces are dominant, the flow becomes laminar and when the inertia forces are dominant, the flow becomes turbulent. Knowing the nature of the flow regime has a direct impact on the reactor thermal analysis.

### 2.3.2 Thermal analysis

The thermal analysis of water-cooled reactors needs to study heat transfer phenomena, in which mainly originating from fuel elements, in order to predict temperature distributions within fuel pins and reactor structures. An accurate prediction is necessary since acceptance criteria of safety analysis are defined by means of limiting values of thermal parameters (e.g. maximum fuel temperature). Predicting temperature distribution within the fuel pellet, fuel-cladding gap, fuel cladding and coolant is a challenging problem.

The heat transfer within the fuel pellet is governed by heat conduction that depends on the material properties: thermal conductivity and specific heat capacity. These two thermal properties are a function of temperature and fuel burnup. As fuel pellet get irradiated in the reactor core, its composition and structure changes due to fission gas release leading to swelling and cracking of the fuel pellet. Limiting the fuel temperature from reaching the melting point is one of the safety parameters normally imposed on a nuclear reactor. The melting point of  $UO_2$  pellet (fuel material used nowadays in LWRs) is  $2840^\circ C$  for fresh fuel and decreases by approximately  $3^\circ C$  for every 1 MWd/kgHM burnup (Carbajo et al., 2001).

The heat transfer through the fuel-cladding gap is governed by heat conduction and heat radiation. The heat conduction occurs through filled gap gas and regions of solid-to-solid contact that might arise due to irradiation induced fuel swelling. The heat radiation becomes effective at a high temperature

between the fuel pellet outer-surface and cladding inner-surface. Traditionally, the rate of radiation exchange between hot surfaces is ignored for reactor analysis during normal operation; however, it should be accounted for accidental scenarios resulting in a loss of coolant media (e.g. in loss of coolant accident). The effective fuel-cladding gap heat transfer coefficient, in general, ranges between a few thousand and more than ten thousand  $W/(m^2.K)$  depending on the fuel irradiation status, fuel and cladding fabrication (wall roughness), and temperature.

In the fuel cladding, the heat transfer can be described by heat conduction mechanism, where normally a linear temperature drop in the radial direction can be assumed due to not only the absence of heat generation source, but also the high thermal conductivity of metals such as Zircaloy. Cladding integrity is very crucial from a safety perspective since it represents the second barrier to confine fission products. From a thermal analysis perspective, limits are imposed on the peak cladding temperature of 1200 °C for Zircaloy-4, an embrittlement criterion, (Westinghouse Electric Corporation, 2005).

The transfer of heat from the cladding surface to the coolant can be described by heat convection which strongly depends on the flow regime and channel geometry. In practice, heat transfer coefficients are determined by empirical correlations that are formulated as a function of geometry, pressure, void content, and mass flow rate.

### 2.3.3 Boiling crisis prediction

When the heat flux (i.e. from the outer cladding surface to the coolant) exceeds a threshold limit, a vapor film is formed that drastically reduces wall heat transfer to the liquid. Thus, the heat transfer is deteriorated and the cladding temperature rapidly increases which may cause cladding failure. This phenomenon is known as the boiling crisis, and the heat flux threshold limit is called critical heat flux (CHF). The boiling crisis phenomenon takes place mainly under two main conditions: (i) under subcooled and low quality-region, which is called “Departure from Nucleate Boiling (DNB)”<sup>‡</sup>; and (ii) at a high-quality region, which is called “dryout”.

The DNB phenomenon, the first kind of boiling crisis, is common for PWRs where the nucleate boiling mechanism at the heated cladding surface changes completely. The nucleate boiling process is very efficient since it enhances the heat removal from cladding surface through a very high heat transfer coefficients and with an only small temperature difference between the cladding outer wall and coolant. Although the nucleate boiling process is beneficial from heat removal point-of-view, no PWRs operate in that condition<sup>‡</sup>. This is because operating a nuclear reactor near that condition could lead to the boiling crisis. Therefore, the prediction of the transition to the boiling crisis is of high relevance for safety. The Departure from Nucleate Boiling Ratio (DNBR) is normally used as an

---

<sup>‡</sup> Sometimes in PWRs subcooled boiling can be found in few channels; however the bulk coolant temperature must be below saturation temperature.

indication of the boiling crisis phenomenon, which is defined as the ratio of the CHF ( $q''_{cr}$ ) at a specific location to the operating local heat flux ( $q''_{local}$ ) at that location, as expressed in equation (2.4).

$$\text{DNBR} = \frac{q''_{cr}}{q''_{local}} \quad (2.4)$$

In any PWR design, the minimum DNBR must be kept greater than unity (plus CHF correlation limit) during normal operation and anticipated operational occurrences (AOOs). A huge amount of experiments have been performed to clarify the physics of the phenomenon itself and also to characterize the CHF heat transfer mechanism. The results of such experiments helped to establish CHF correlations and look-up tables valid for the corresponding predictions. In general, CHF correlation is a function of coolant mass flux, steam quality, coolant enthalpy (inlet and saturated), system pressure, geometry, spacer grid type, and surface condition (i.e. through surface tension).

Generally, the CHF decreases with increasing coolant enthalpy (i.e. towards core exit) (Tong and Weisman, 1996); therefore the minimal value of DNBR is usually near the coolant channel exit. Hence, reducing maximum coolant enthalpy adds an additional margin against DNB. The enthalpy-rise hot channel factor ( $F_{\Delta H}$ ) relates the maximum enthalpy rise to the average enthalpy rise in a reactor core (see equation (2.5)). This factor is typically minimized in a core design to limit local heat flux from approaching the CHF.

$$F_{\Delta H} = \frac{\max[h_{exit} - h_{inlet}]}{\frac{1}{N_{FA}} \sum_{i=1}^{N_{FA}} [h_{exit}(i) - h_{inlet}(i)]} \quad (2.5)$$

In which  $h_{inlet}$  and  $h_{exit}$  denote the coolant enthalpy at channel inlet and exit, respectively, and  $N_{FA}$  refers to the total number of fuel assemblies in a reactor core.

The second kind of boiling crisis is typical of BWRs that occurs in high-quality regions. The mechanism leading to the boiling crisis in BWRs is different than the one in PWRs. Under two-phase annular flow the liquid film evaporates completely leading to the so-called dryout. Therefore, the heat transfer from the cladding surface into the coolant is deteriorated.

## 2.4 Reactor Safety

Safety analyses focus on ensuring a nuclear reactor (structures, systems, and components) always operate within operational margins consistent with the “defense-in-depth” principle imposed by a national regulatory authority. According to the IAEA Safety Fundamentals (IAEA, 2006): “*a nuclear facility must be designed, constructed, commissioned, operated and decommissioned with the constant objective to ensure the protection of the workers, public and the environment against the harmful effects of the ionizing radiation*”. Thus, safety functions (either as engineering structures, systems, and components or human actions) are defined in a nuclear facility with an objective to provide preventive

and/or mitigative measures to avoid or minimize any radiological risk. Fundamental safety functions can be classified under the following categories: (i) control of core reactivity; (ii) coolability of a reactor core; (iii) confinement of radioactive material; and (iv) limit radioactive substances emissions and the radiological exposure. A robust nuclear reactor design and the implementation of the “defense-in-depth” principle are required to fulfillment of these safety functions.

The “defense-in-depth” principle, relevant postulated initiating events for the SMART, and acceptance criteria are discussed in the following subsections.

### **2.4.1 Defense-in-depth principle**

The defense-in-depth (DiD) principle consists in a hierarchical deployment of different levels of equipment and procedures to maintain the effectiveness of multi-physical barriers placed between radioactive materials and workers, the public or the environment, in normal operation, anticipated operational occurrences and, accidental conditions (IAEA, 1996). The DiD principle centered on two strategies: first, to prevent accidents and second, if prevention fails, to mitigate their potential consequences and prevent any evolution to more serious conditions. Accident prevention is definitely the first priority. The elements of DiD concept are twofold: multi-physical barriers and successive level of protection. The multi-physical barriers, in general, are placed to ensure the confinement of radioactive material. Their specification may vary depending on a reactor design (or in general a nuclear installation) and the possible deviation from normal operation. For example, in typical LWRs, the multi-physical barriers are the fuel matrix, fuel cladding, reactor coolant system pressure boundary, and containment system. The successive level of protection of the DiD principle is presented in Table 2.1, as proposed by the (Western European Nuclear Regulators Association, 2013) following learned lessons from TEPCO Fukushima Dai-ichi accident.

**Table 2.1: The successive level of the DiD as proposed by WENRA (Western European Nuclear Regulators Association, 2013)**  
(Different colors indicate an event frequency)

DiD level	Plant condition	Objective	Essential means	Radiological consequences
1	Normal operation	Prevention of abnormal operation and failures	Conservative design and high-quality construction	No off-site radiological impact (bounded by regulatory operating limits for discharge)
2	Anticipated operational occurrences (AOO)	Control of abnormal operation and failures	Control and limiting systems and other surveillance features	
3a	Postulated single initiating event with single failure	Control of accident to limit radiological releases and prevent escalation to core melt conditions	Reactor protection system, safety systems, accident procedures	No off-site radiological impact or only minor radiological impact
3b	Postulated single initiating event with multiple failures		Additional safety features, accident procedures	
4	Postulated core melt accidents	Control of accidents with core melt to limit offsite releases	Complementary safety features to mitigate core melt, accidents management with core melt (severe accidents)	The off-site radiological impact may imply limited protective measures in area and time
5*	Significant release	Mitigation of radiological consequences	Off-site emergency response	Off-site radiological impact necessitating protective measures

**Green:** Expected during a lifetime of a plant

**Yellow:** Rare & unlikely events

**Red:** Extremely rare events

\* Level 5 of DiD is used for emergency preparedness planning purposes.

### 2.4.2 Relevant initiating events for the SMART

The SMART plant under consideration has several initiating events categorized on the basis of their probability of occurrences (i.e. event frequency). Table 2.2 shows the SMART's event categories, and a representative event in each category selected in terms of producing a higher bounding and most limiting event with respect to safety, according to (Bae, 2018).

**Table 2.2: Representative initiating events of the SMART plant (Bae, 2018)**

DiD level	Event Category	Representative Event
2	Decrease in Reactor Coolant System Flow Rate	Total Loss of Reactor Coolant Flow
2	Increase in Reactor Coolant Inventory	Pressurizer Level Control System Malfunction
3a	Decrease in Reactor Coolant Inventory	Small Break LOCA
3a	Reactivity and Power Distribution Anomalies	Control Rod Assembly Ejection
3a	Increase in Heat Removal by the Secondary System	Main Steam Line Break
3a	Decrease in Heat Removal by the Secondary System	Feedwater Line Break

Generally, reactor transients are about imbalances between heat production and removal. The transients could be caused by reactivity insertions that lead to excessive power production, or heat transport system failures that hinder heat removal. In this thesis, the control rod ejection (REA) and steam line break (SLB) accidents are selected for analyzing the developed boron-free core integrated within the SMART plant. The rationale for selecting these two accidents is that the REA represents a very fast transient such that no possible safety system can cope with its sequences and only the inherent safety core features can provide preventive actions. Whereas the SLB accident represents a slow transient in which safety systems such as the passive residual heat removal system are designed to prevent the reactor from proceeding into a subsequent DiD level.

Therefore, the acceptance criteria from safety perspective of these two accidents are discussed in detail in the next section alongside with the acceptance criteria imposed on DiD level 1 and level 2 (i.e. during normal operation and AOO).

### 2.4.3 Acceptance criteria

#### DiD level 1 and level 2 acceptance criteria

During normal reactor operation and AOO fuel rods failures are not allowed to prevent any radiological releases to workers, public or environment. The acceptance criteria during these two plant conditions are:

- 1) Control rods system should provide enough shutdown margins at Cold Zero Power<sup>§</sup> (CZP) condition with single failure criterion of the highest control rod worth. The limit of cold shutdown margin (CSDM) with single failure criteria according to (KTA, 2012) is 1000 pcm.
- 2) Fuel temperature should be below the melting temperature of the fuel material.
- 3) Boiling crisis should be avoided, which results in fuel cladding overheat and failure. The minimum DNBR is checked to avoid the boiling crisis phenomenon.
- 4) Cladding strain should be less than 1%. A cladding strain equal to or more than 1% means the cladding lost its ability to recover elastically. This is minimized by limiting the (i) internal fission gas pressure (i.e. between the fuel pellet and cladding), and (ii) average cladding temperature to be less than 450°C (Westinghouse Electric Corporation, 2005).
- 5) Total power peaking factor shall not exceed the acceptance criterion. The acceptance criterion is actually imposed on the linear power in order not to result in cladding failures. The

---

<sup>§</sup> Cold Zero Power (CZP) is defined as the highest core reactivity situation where a reactor core is at atmospheric pressure and temperature, and free xenon. Sometimes is called cold shutdown condition.

maximum allowed linear power according to (Westinghouse Electric Corporation, 2005) for a typical fuel rod design (UO<sub>2</sub> pellet encapsulated with Zircaloy-4 cladding) is 41.5 kW/m<sup>\*\*</sup>. Therefore, the limit of the total power peaking factor ( $F_{xyz}^{limit}$ ) for the developed boron-free core is 3.3, which is calculated according to equation (2.6).

$$F_{xyz}^{limit} = \frac{q'_{max}}{q'_{avg} * f} \quad (2.6)$$

In which  $q'_{max}$  and  $q'_{avg}$  of equation (2.6) refer to the maximum allowed and core averaged linear power, and  $f$  indicates the total uncertainty that is due to measurement and manufacturing uncertainties (i.e. equal to 1.05\*1.03 (Westinghouse Electric Corporation, 2005)).

### **REA acceptance criteria**

To understand the basis of REA acceptance criteria, fuel and cladding failure modes have to be discussed. Following a control rod ejection, a positive reactivity is inserted that promptly increases core power. Consequently, this might lead to an immediate pellet deformation due to thermal expansion. At a higher fuel burnup, the pellet deformation is enhanced due to the expansion of the accumulated fission gases within the fuel matrix leading to crack formation and growth. This result in a pellet-cladding gap narrowing or even gap closure and finally to a cladding ruptures. This phenomenon is known as pellet-cladding mechanical interaction (PCMI). It is more likely to occur at low or near zero power and high fuel burnup because as the fuel depletes, the delayed neutron fraction ( $\beta_{eff}$ ) tends to decrease and Doppler feedback coefficient tends to be less negative. These two factors result in high power pulse amplitude, and consequently a strong fuel enthalpy increase. In extreme cases, if the energy released from the fuel pellet is very high, the fuel pellets may melt. The fuel melting associated with a cladding failure would lead to a violent fuel-coolant thermal interaction causing a rapid steam formation and pressure pulses in the coolant. Such pulses might result in a loss of fuel assemblies' structural integrity and damage of the reactor pressure vessel internals. Therefore, impair the core cooling capability (Rudling et al., 2016).

---

\*\* This value actually comes from the analyses of loss of coolant accident (LOCA) consequences. According to (Westinghouse Electric Corporation, 2005): “LOCA could cause fuel swelling and clad burst. This could impede the flow of water from the Emergency Core Cooling System (ECCS), which refills the reactor pressure vessel and refloods the core after the initial LOCA blowdown. Delaying or impeding ECCS flow could cause more damage than originally calculated. Since the potential for rod burst could not be eliminated, the only alternative was to reduce the peak allowed linear power for normal operation. Therefore, the assumed LOCA would start with a lower peak power.” There are also additional limiting factors related to axial power profile that generally originated from the consequences of LB-LOCA (eliminated in the SMART design) and SB-LOCA. These axial limiting factors strongly depend on the location of safety system injection (e.g. from upper core and/or downcomer injection) and break location following an SB-LOCA, in which there determinations are out-of-scope of current investigation.

At the beginning-of-life (BOL) or low fuel burnup, the dominant failure mode is basically due to prolonged high cladding temperature that results from the continuous vapor film formation at the cladding-to-coolant interface which effectively insulates the cladding from the coolant (Rudling et al., 2016). Therefore, it leads to cladding failure. Such a phenomenon is avoided when the local heat flux is far from the DNB point. This failure mode is called high-temperature failure mode and is most probably happened following the REA at intermediate power levels up to full power conditions. Another mode of high-temperature failure (Rudling et al., 2016) may occur as well by thermal shock during the re-wetting phase (post-DNB) of the overheated heavily oxidized cladding. For Zr-4 cladding, cladding temperature above 700°C (Rudling et al., 2016) found to suffer from rapid oxidation from both the UO<sub>2</sub>-metal reaction on the inside surface and the water-metal reaction on the outside surface. Oxygen absorbed during the oxidation process deteriorates the cladding mechanical properties. Consequently, thermal stresses that arise under quenching (re-wetting) may be sufficient to fracture the fuel cladding.

Since the REA is classified as a level 3a on the DiD scale, fuel rod failure might happen provided that the on-site and off-site dose consequences remain within acceptable limits. Hence, the main safety concerns in REAs can be summarized as a loss of (i) long-term coolable geometry; and (ii) integrity of the reactor pressure vessel.

To ensure that the long-term core cooling is not impaired, US-NRC (Clifford, 2015) defined the following coolability limits:

1. *Peak radial average fuel enthalpy must remain below 230 cal/g (963 kJ/kg).*
2. *A limited amount of fuel melting is acceptable provided it is restricted to (a) fuel centerline region and (b) less than 10% of any pellet volume. For the outer 90% of the pellet volume, peak fuel temperature must remain below incipient fuel melting conditions.*
3. *Mechanical energy generated as a result of (1) non-molten fuel-to-coolant interaction and (2) fuel rod burst must be addressed with respect to reactor pressure boundary, reactor internals, and fuel assembly structural integrity.*
4. *No loss of coolable geometry due to (1) fuel pellet and cladding fragmentation and dispersal and (2) fuel rod ballooning.*

According to the latest revised studies conducted by US-NRC (Clifford, 2015) about RIA regulation guidelines, the number of failed fuel rods should not be underestimated for a conservative radiological source term evaluation. Fuel cladding failure threshold can be divided into three categories:

- For zero power RIA scenarios: the fuel cladding failure threshold (Fig. 2.2) depends on the peak radial average fuel enthalpy and the pressure difference across cladding wall (i.e. internal rod pressure minus reactor pressure).

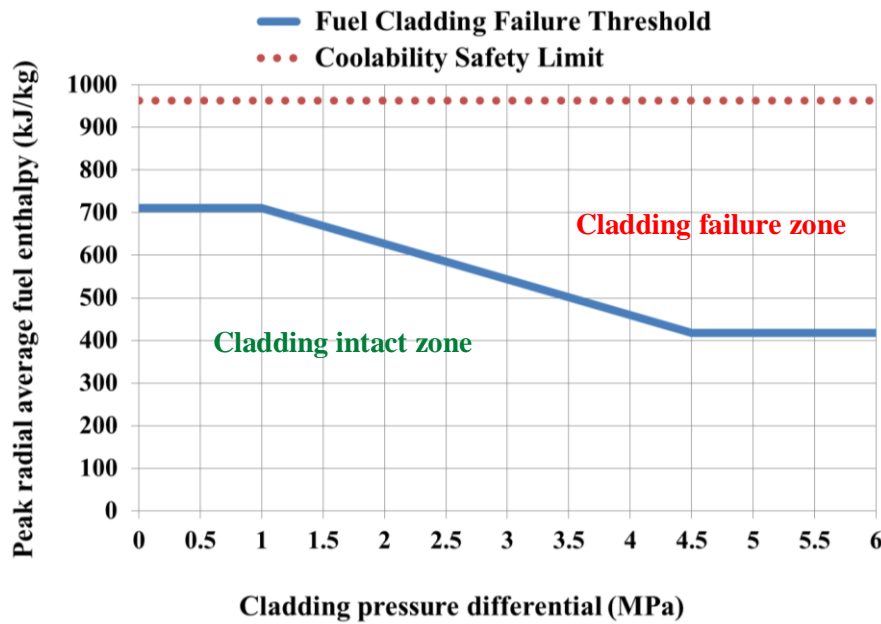


**Fig. 2.2: REA revised cladding failure threshold and fuel coolability limit, (Clifford, 2015), expressed by the peak radial average fuel enthalpy as a function of pressure difference over the fuel cladding.**

- For intermediate and full power RIA scenarios: fuel cladding failure is presumed if local heat flux exceeds DNB acceptance criterion. Since the determination of a DNBR acceptance criterion requires prior knowledge of a CHF correlation suited for the specific fuel assembly design and the reactor operating conditions, it is out-of-scope of the current study. Instead here, the maximum cladding temperature is used as an indication of fuel cladding failure.
- Failure thresholds due to pellet-cladding mechanical interaction (PCMI): this type of fuel cladding failure mode depends on the peak radial average fuel enthalpy rise and the amount of excess hydrogen uptake in the cladding<sup>††</sup>. There is two limits exist for this type of fuel cladding failure that depends on the thermal treatment of a cladding material during manufacturing; either Fully Recrystallized (RXA) or Stress Relief Annealed (SRA). Fig. 2.3 illustrates the limiting peak radial average fuel enthalpy rise as a function of the amount of excess cladding hydrogen for the two types of thermal treatments applicable to PWRs<sup>‡‡</sup>.

<sup>††</sup> The hydrogen produced during cladding oxidation ( $Zr + 2H_2O \rightarrow ZrO_2 + 2H_2$ ) precipitates as zirconium hydrides when it exceeds the hydrogen solubility limit in the cladding. Here, the term “*excess hydrogen*” refers to the amount of hydrogen above the solubility limit or precipitated hydrogen (Clifford, 2015).

<sup>‡‡</sup> Please note that these limiting peak radial average fuel enthalpy rise are not applicable to BWRs, in which there are different values for BWRs that can be found in (Clifford, 2015).

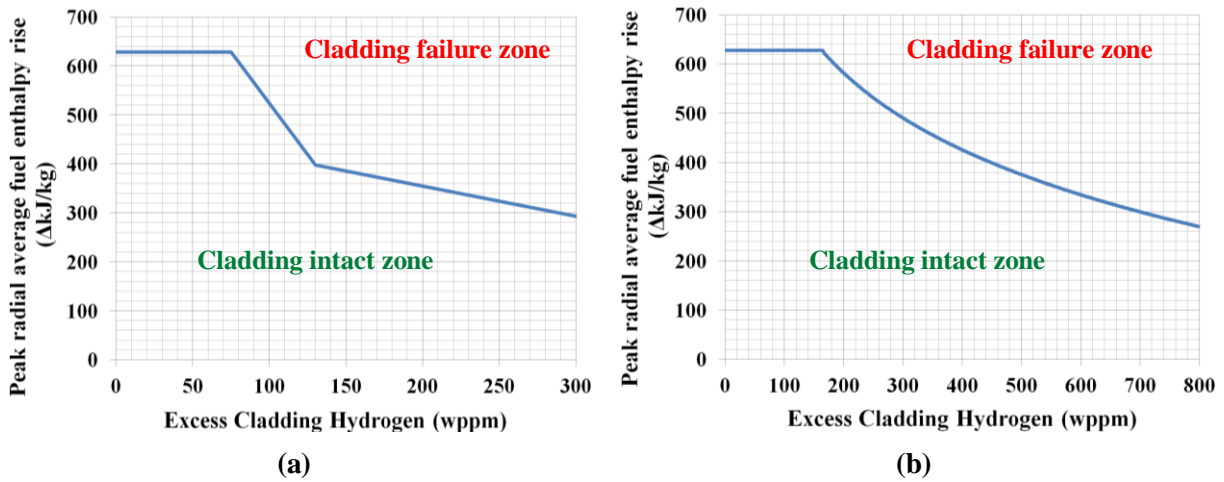


**Fig. 2.3: REA revised PCMI cladding failure threshold for (a) RXA and (b) SRA thermally treated cladding material, (Clifford, 2015); expressed by the peak radial average fuel enthalpy rise as a function of the amount of excess cladding hydrogen.**

### SLB acceptance criteria

As for the safety acceptance criteria of SLB accidents, the return-to-power and return-to-criticality following a reactor trip are the main safety concern in analyzing SLB accidents. Even after the reactor has been successfully shut down, the decay heat from the of fission products is sufficient to cause core melting. Thus, in order to prevent SLB accidents consequences from the next DiD level (level 4), long-term coolability of the core structures are to be ensured. More information about SLB accident and its consequences are discussed in chapter 7.



## CHAPTER 3: SIMULATION TOOLS

The general framework utilized in this thesis for developing and analyzing a boron-free core integrated into a generic SMART-plant is based on advanced simulation tools. The interaction between these tools to create the multi-physics framework is illustrated in Fig. 3.1.

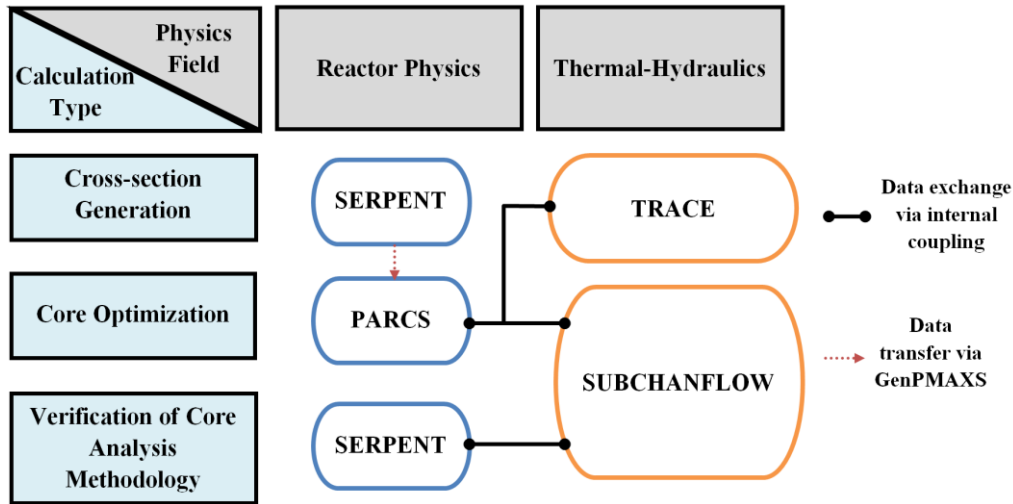


**Fig. 3.1: The multi-physics framework used for developing and analyzing the boron-free core integrated within a generic SMART-plant**

A short description of the capabilities and limitations of each simulation tools are given in the following subsections.

### 3.1 Reactor Physics Analysis Tools

Fuel assembly neutronics optimization studies and few-group cross-section generation for reactor core simulators are traditionally performed by lattice-physics deterministic codes (e.g. CASMO (Rhodes et al., 2013), HELIOS (Casal et al., 1991), SCALE/TRITON (Jessee and DeHart, 2018), SCALE/POLARIS (Jessee et al., 2014)). Moreover, the use of Monte Carlo methods for the few-group cross-section generation is rapidly increasing. In this work, the Monte Carlo code SERPENT (Leppänen et al., 2015) is used as a lattice-physics code and also as a reference solution for the reactor core simulator. Core loading and control banks pattern optimization as well as core dynamics behavior are conducted by the reactor core simulator PARCS (Downar et al., 2017). Selected features of these two codes, based on the work performed in this thesis, are summarized hereafter.

#### 3.1.1 The Monte Carlo code SERPENT

SERPENT is a multi-purpose three-dimensional code developed by VTT that performs stochastic modeling of the interactions of neutrons and photons using the Monte Carlo (MC) method. It uses continuous energy rather than multi-group energy microscopic cross-sections, and therefore it does not rely on an approximate self-shielding treatment in resonance regions. Unlike deterministic codes, MC

has a flexible geometrical capability which allows a high degree of accuracy to model complex geometries.

SERPENT has been widely used nowadays as a lattice-physics code for generating the needed data for core simulators; including homogenized few-group macroscopic cross-sections (e.g. transport, fission, absorption), scattering matrices, diffusion coefficients, kinetics parameters (e.g. delayed neutron fractions and decay constants), assembly discontinuity factors (ADF) and energy group-wise form-functions for the pin power reconstruction. SERPENT-generated data for core simulators have been verified and validated by many institutions. The SERPENT-DYN3D code sequence is verified against HELIOS-DYN3D and SERPENT full core for a typical 193-fuel assemblies PWRs (Fridman and Leppänen, 2011). The SERPENT-PARCS code sequence is verified against HELIOS-PARCS and SERPENT full core for a small PWR-like mini-core of nine fuel assemblies (Baiocco et al., 2017). The SERPENT-ARES code sequence is validated for the MIT BEAVRS benchmark at HZP-initial core condition (Leppänen et al., 2014) and HFP fuel cycle 1 condition (Leppänen and Mattila, 2016).

SERPENT has the capability to represent  $S(\alpha, \beta)$  thermal scattering data for  $^1\text{H}$  at any selected temperature through the use of linear interpolation between  $S(\alpha, \beta)$  thermal scattering data (Viitanen and Leppänen, 2016). Also, it treats point-wise cross-section temperature-dependent data by using Doppler-broadening pre-processor that is similar to the one used in NJOY (Viitanen and Leppänen, 2011). Both features enable the estimation of the thermal-hydraulic feedback on nuclear cross-sections. SERPENT version 2.1.29 is used throughout all performed simulations in this thesis. The coupled code SERPENT2/SUBCHANFLOW (Daeubler et al., 2015) is used in this work for verifying the core analysis methodology, which is described in details later in Chapter 5.

### 3.1.2 The reactor core simulator PARCS

PARCS is a 3D spatial kinetics core simulator used to simulate the neutronics core behavior under steady-state and time-dependent conditions. It solves the multi-group neutron diffusion or low-order transport equation ( $SP_3$ ) in Cartesian and hexagonal geometries. Numerous spatial kinetics solvers have been incorporated into PARCS, including the analytic nodal method (ANM), nodal expansion method (NEM) and hybrid ANM/NEM for orthogonal geometries; and triangular polynomial expansion method (TPEN) for non-orthogonal geometries.

Since safety criteria are imposed at the fuel pin level, PARCS has the capability to predict the pin power information through the use of pin power reconstruction (de-homogenization) methodology. A limitation in the development of that method (i.e. pin power reconstruction) is the assumption of smooth axial variations of the neutron flux such that the radial and axial dependences of the intra-nodal fluxes are assumed to be separable in space. This limitation, unfortunately, restricts the application of the pin power reconstruction method in cases with reactor cores that have strong axial

heterogeneities. An additional limitation to the pin power reconstruction is the fact that the thermal-hydraulics feedback is treated at the nodal level since cross-section data is generated by homogenizing completely a fuel assembly. Alternatively, a pin-by-pin cross-section generation is suggested to overcome the shortcoming of the pin power reconstruction. However, the pin-by-pin cross-section generation and the treatment of homogenization corrections at the pin level are beyond the scope of this thesis.

PARCS is capable as well to calculate decay heat either by a user-defined group-wise decay heat precursor yield fractions and decay constants or by selecting the default 6 groups ANL option. The default option, which is developed for UO<sub>2</sub> fuel as in the boron-free core, is used in the present work.

In this work, the hybrid ANM/NEM kernel is selected to assure a robust and fast neutronic core simulation. The nodal neutronics parameters needed by PARCS are generated in this work using SERPENT. Afterward, they are transferred to PARCS Macroscopic XS (PMAXS) format via the GenPMAXS (Xu and Downar, 2006) code. The coupled code PARCS/SUBCHANFLOW (Basualdo et al., 2017) has been used to study the impact of control rod ejection accident on the safety performance of the developed boron-free core.

## 3.2 Thermal-Hydraulics Analysis Tools

Core thermal-hydraulics and safety evaluation such as core heat-up, pressure drop, maximum fuel and cladding temperature, and minimum departure from nucleate boiling ratio (MDNBR) are determined through the use of the sub-channel thermal-hydraulic code SUBCHANFLOW (Sánchez et al., 2010). SMART-plant dynamics and the interaction of safety systems on the reactor core behavior under selected design-basis accidents such as steam line break are carried-out using the system analysis code TRACE (U.S. NRC, 2013). Description of both codes' selected features is highlighted in the following subsections.

### 3.2.1 The reactor core sub-channel code SUBCHANFLOW

SUBCHANFLOW (SCF) is a thermal-hydraulics sub-channel code developed at the Institute for Neutron Physics and Reactor Technology of Karlsruhe Institute of Technology to simulate LWRs and advanced reactor systems. The code can handle core geometries having rectangular or hexagonal fuel bundles at both sub-channel and fuel-assembly level. Single and two-phase flow conditions can be described by a set of three mixture balance equations for mass, momentum, and energy in the axial direction as well as an additional lateral momentum equation. A fully-implicit method is used to solve steady-state and transient problems. Coolant properties and state functions are implemented for water and steam using the IAPWS-97 formulation (Wagner et al., 2000). Thermo-physical property functions for liquid metals (sodium, lead, and lead-bismuth) and gaseous (helium, and air) are available as well. The heat conduction in fuel pins is solved by means of a standard finite volume

method. The heat transfer coefficient between fuel pin and reactor coolant is determined using empirical correlations depending on the heat transfer mode of the axial flow regimes. Void fraction, pressure drop, wall friction, and turbulent mixing are also calculated using constitutive relations.

SCF has been verified and validated against various benchmarks, including the NUPEC PWR Subchannel and Bundle Tests (PSBT) (Berkhan et al., 2011) (Imke and Sanchez, 2012), and BWR Full-Size Fine-Mesh Bundle Test (BFBT) post-test analysis for steady state (Imke et al., 2010) and transient (Jaeger et al., 2013). SCF has been coupled with different neutronics codes such as DYN SUB (Gomez-Torres et al., 2012), MCNP-SUBCHANFLOW (Ivanov et al., 2013), SERPENT-SUBCHANFLOW (Daeubler et al., 2015), COBAYA3-SUBCHANFLOW (Calleja et al., 2014), and PARCS-SUBCHANFLOW-TRANSURANUS (Basualdo et al., 2017).

Due to the complications behind the physics of the two-phase phenomena to describe precisely the boiling transition like the onset of- and departure from nucleate boiling, SCF relies on a number of empirical correlations to determine the critical heat flux (CHF) such as Modified Barnett – Babcock-Wilcox, Biasi, OKB, W-3, Levitan, and EPRI CHF correlations. These correlations have been developed based on common geometry and thermal-hydraulics conditions existing in LWRs. However, the geometry and flow condition of the fuel bundles loaded in the developed boron-free core is not covered by these CHF-correlations, and thus, an extrapolation is not recommended. Due to that limitation, the prediction of MDNBR will not be used as an indication for cladding failure; instead, the maximum cladding temperature will be used (see chapter 2.4.3).

### **3.2.2 The reactor system analysis code TRACE**

TRACE is a thermal-hydraulics code developed by the U.S. Nuclear Regulatory Commission (NRC) to simulate operational transients and design-basis accidents in PWRs and BWRs. It combines the capabilities of the four NRC legacy codes (TRAC-P, TRAC-B, RELAP5, and RAMONA) into a single modernized computational tool. TRACE solves the conservation of mass, momentum, and energy for two-phase flows using finite volume methods. TRACE can model 1D and 3D geometries on coarse computational meshes over which the problem variables are averaged. Namely, TRACE lacks the capability to capture in details fluid dynamics phenomena at a localized level such as the radial velocity profile across a pipe.

The 3D modeling features such as CARTESIAN and CYLINDRICAL VESSELS components in TRACE allows a simplified flow modeling in complex geometries. This type of modeling feature is being used to capture for instance coolant mixing behavior resulting from a steam line break accident. TRACE is tightly coupled to the reactor core simulator PARCS via a general interface (GI) and with the use of explicit coupling for time advancement. The TRACE/PARCS is normally used to simulate transients that have strong spatial dependence where the point kinetics method fails in capturing these

---

phenomena. Data exchanged in TRACE/PARCS is mesh-based, where mesh mapping between TRACE and PARCS is defined by an external file written according to the MAPTAB format (U.S.NRC, 2017). The MAPTAB format has two methods for mapping hydraulic/heat structure (TRACE) meshes to neutronics nodes (PARCS). In this work, the legacy explicit weight method is being used over the automated weight method. This is because the developed core is modeled by using a TRACE CARTESIAN VESSEL component and the MAPTAB automated weight method is not yet capable of handling this type of component. In this work, TRACE version 5.0 patch 4 is used to model the full SMART-plant integrated with the developed boron-free core.



## CHAPTER 4: OPTIMAL NEUTRONICS AND THERMAL-HYDRAULICS CORE CHARACTERISTICS

The scientific challenge of designing a core integrated within a generic water-cooled SMR-plant (e.g. SMART) is in fulfilling the imposed safety requirements while taking profit of the advantages offered by the boron-free concept. For this purpose, the optimization approach described earlier in subsection 1.5 has been followed. An optimal core design has been developed in an iterative process. In this chapter, the description of the optimized core and its features from both neutronics and thermal-hydraulics perspective are described in details.

### 4.1 Fuel Assemblies and Core Description

The basic fuel assembly (FA) design is based on the well-proven PWR technologies of 17x17 fuel rod arrays with 24 guide tubes and a central instrumentation tube. Since the developed core does not use soluble boron for reactivity control during normal operation, FAs are designed with fixed burnable poison rods. Each FA has either 20 or 24 burnable poison rods (See Fig. 4.1A and Fig. 4.1B) depending on their location in the core. These burnable poison rods are designed with an objective of reducing (i) the HFP excess reactivity at the BOL, and (ii) the power peaking in the core. The burnable absorber (BA) material used in the burnable poison rods is  $\text{Al}_2\text{O}_3$  mixed with  $\text{B}_4\text{C}$ . This type of material is currently in use at the operating PWR Watts Bar Nuclear Plant - Unit 2 (Godfrey et al., 2017). The fuel rods design is based on a typical PWR fuel rod design of less than 5% enriched  $\text{UO}_2$  pellets encapsulated with Zr-4 cladding.

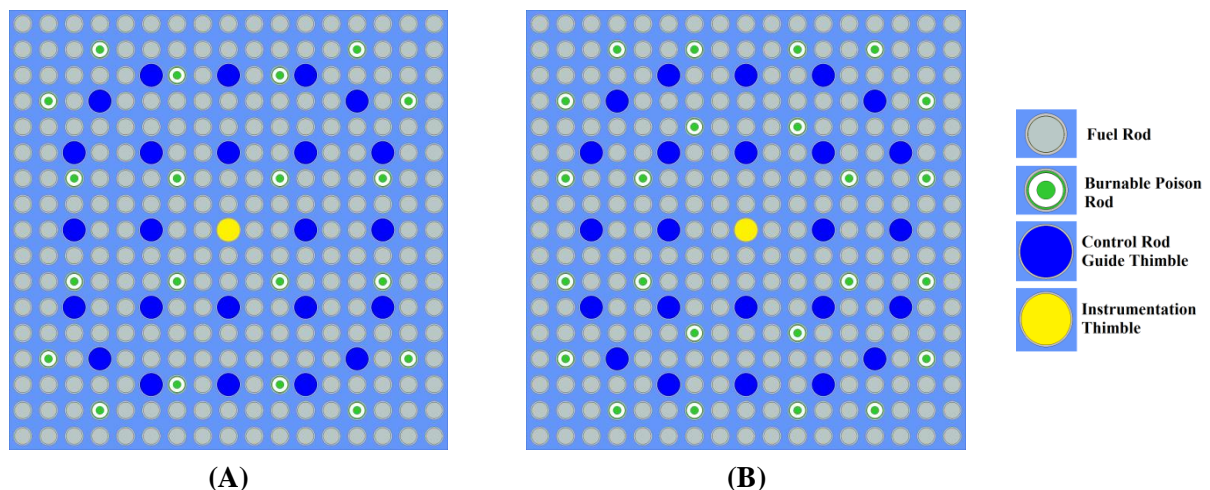


**Fig. 4.1: Fuel assembly layout with (A) 20 burnable poison rods, and (B) 24 burnable poison rods (This figure is generated from SERPENT)**

To reduce the radial and axial power peaking factors, 6 FA-types are designed with radially and axially varying enrichment and burnable poison loadings. To fulfill design objectives, the central FA in the core has the lowest enrichment, and peripheral FAs have no burnable absorbers. Instead, they have dummy rods filled only with  $\text{Al}_2\text{O}_3$ . Fig. 4.2 reveals the final optimized core design with the

radial and axial loading pattern. Table 4.1 shows the details information of each FA type presented in the final optimized core design.

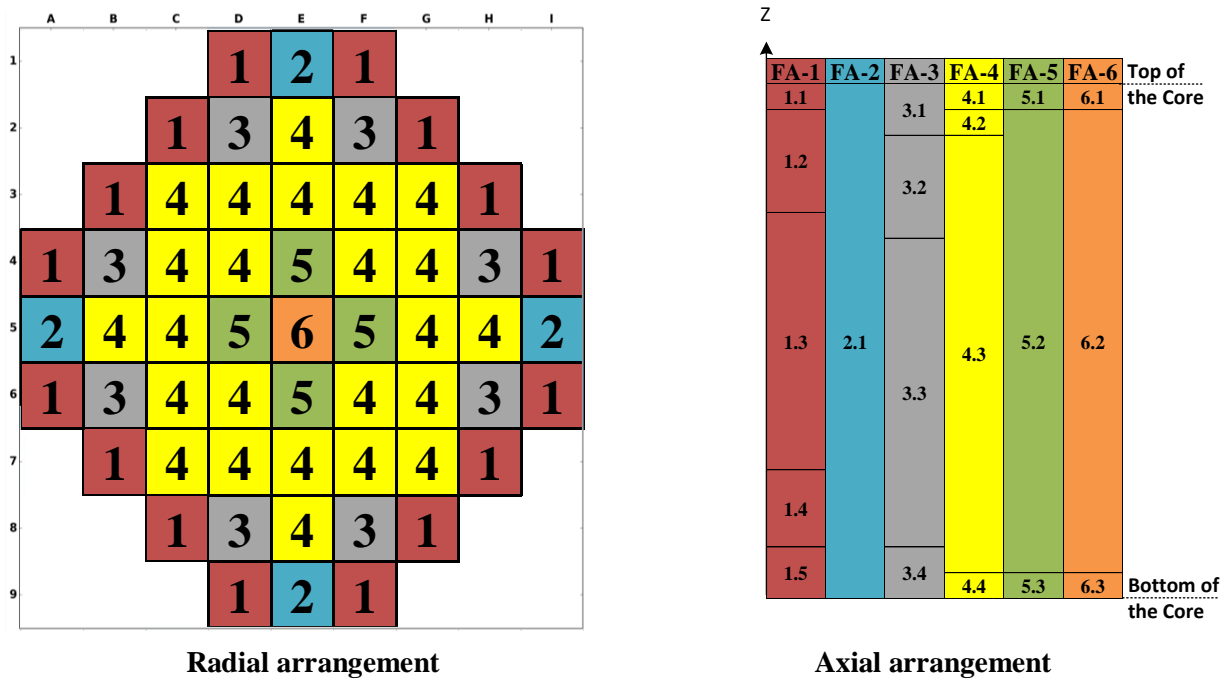
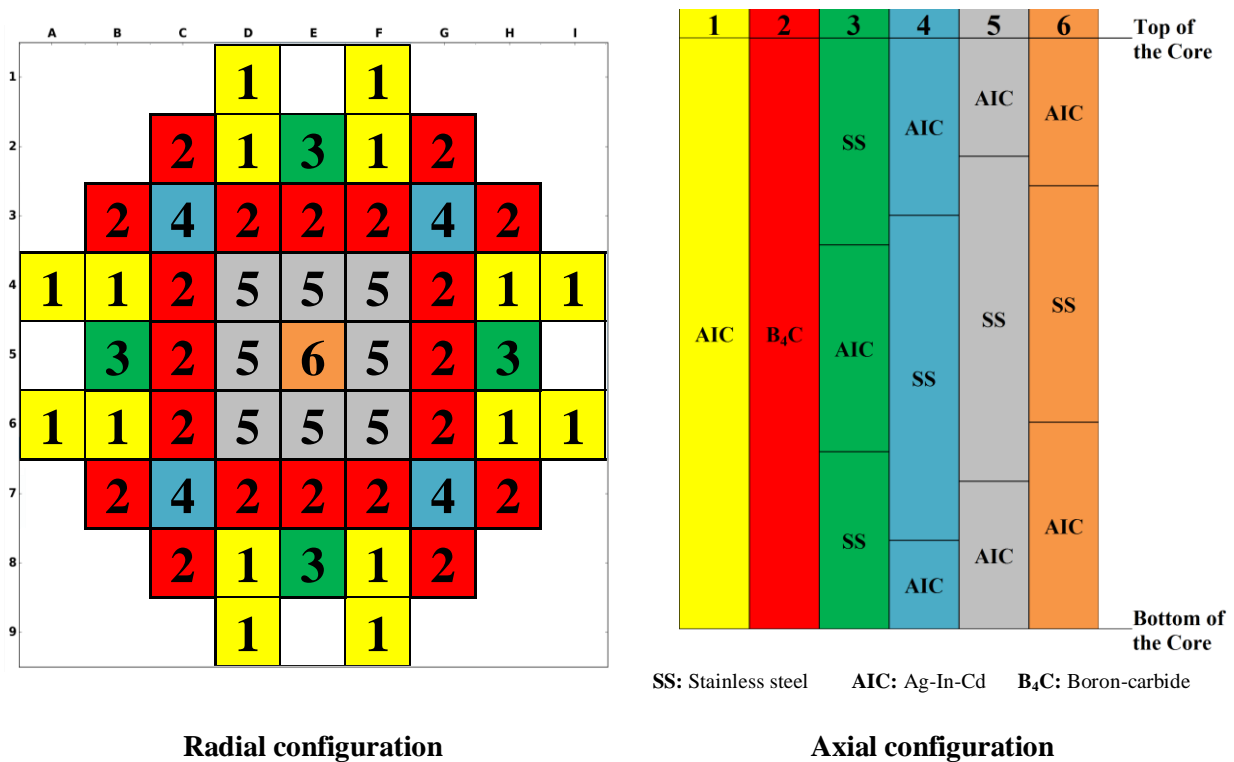


Fig. 4.2: Optimized core loading pattern

Table 4.1: Types and features of fuel assemblies in the core

FA Type	No. of Burnable Poison Rods	No. of FAs in the core	FA Axial Index	Fuel Enrichment (wt% of U <sup>235</sup> )	BA Inner Region Loading (wt% of B <sub>4</sub> C)	BA Outer Region Loading (wt% of B <sub>4</sub> C)
1	20	16	1.1	3.4	0.0	0.0
			1.2	3.2		
			1.3	3.0		
			1.4	3.2		
			1.5	2.0		
2	20	4	2.1	2.0	0.0	0.0
			3.1	2.5		
			3.2	2.0		
			3.3	4.2		
3	20	8	3.3	4.2	16	14
			3.4	2.0		
			4.1	2.5		
			4.2	3.0		
4	24	24	4.3	4.0	25	12
			4.4	2.0		
			5.1	2.5		
			5.2	3.8		
5	24	4	5.3	2.0	0.0	0.0
			6.1	2.5		
			6.2	3.0		
6	24	1	6.3	2.0	0.0	0.0

The control rods are designed and arranged to have three main functionalities: (i) rapid negative reactivity insertion as a mean of providing enough shutdown margins, (ii) coarse, and (iii) fine reactivity adjustment for power maneuvering and transient compensation. The selected absorber materials for the control rod design are  $B_4C$ , Ag-In-Cd, and stainless steel. These three absorber materials are chosen because of their accumulated operating experience in the nuclear industry. The control rods configuration that satisfies the three main functionalities is shown in Fig. 4.3.



**Fig. 4.3: Control rods configurations. CR- 1, 3, 4, 5, and 6 belong to the regulating banks, whereas CR-2 belongs to the safety shutdown bank. “White boxes” mean there is no CR at that position.**

The developed core has 53 rodded fuel assemblies arranged into two banks: regulating and safety shutdown banks. The regulating banks consist of 33 rodded fuel assemblies: 16 Ag-In-Cd control rods for coarse reactivity control and 17 hybrids control rods made from both Ag-In-Cd and stainless steel for fine reactivity control and axial power shaping. The safety shutdown banks consist of 20 control rods made of  $B_4C$  in fully extracted position during normal operation, and its goal is to provide enough and fast shutdown mechanism.

The details of the core modeling from both neutronics and thermal-hydraulics aspects using PARCS/SCF can be found at Appendix-A. The BOL detailed neutronics and thermal-hydraulics characteristics of the optimized core are given hereafter.

## 4.2 Global and Local Core Neutronics Characteristics

Global neutronics characteristics of the core such as excess reactivity, cold shutdown margin (CSDM), inherent safety reactivity feedback coefficients; effective delayed neutron fraction ( $\beta_{\text{eff}}$ ) and local parameters as the axial and radial power distributions are discussed in the following subsections.

### 4.2.1 HFP excess reactivity, CSDM, reactivity feedback coefficients and $\beta_{\text{eff}}$

The hot full power (HFP) excess reactivity is the reactivity amount needed to operate the reactor core at nominal full power condition and overcome Xenon and Samarium reactivity worth during power maneuvering.

After many iterations of the core optimization, it was found that a reduced HFP excess reactivity is needed for reaching enough CSDM. The CSDM is defined as the amount of negative reactivity needed to keep the core in a safe cold shutdown condition. This negative reactivity is provided by an adequate design of control rods. It is analytically determined by fully inserting all control rods except for the highest control rod worth stuck out of the core at 300 K, atmospheric pressure, and Xenon-free condition.

The reactivity feedback coefficient is the difference between two reactivity states due to a change in a parameter of interest. Fuel and moderator temperature, and power reactivity feedback coefficient are calculated for the optimized core. Table 4.2 presents the HFP excess reactivity, CSDM, reactivity feedback coefficients and effective delayed neutron fraction ( $\beta_{\text{eff}}$ ) as predicted by the coupled code PARCS/SCF.

**Table 4.2: Core global neutronics features**

<b>Parameters</b>	<b>Value</b>
<b>HFP excess reactivity (pcm)</b>	3530
<b>Cold shutdown margin with single failure criteria (pcm)</b>	-2960
<b>Fuel temperature coefficient (pcm/K)</b>	-2.0
<b>Moderator temperature coefficient (pcm/K)</b>	-76.0
<b>Power reactivity feedback coefficient (pcm/%)</b>	-15.0
<b>Effective delayed neutron fraction, <math>\beta_{\text{eff}}</math> (pcm)</b>	687

It can be noticed that all reactivity feedback coefficients are negative and thus satisfying core safety design objectives. The moderator temperature coefficient is found to be highly negative due to the absence of soluble boron in the moderator. Moreover, the CSDM is also found to be fulfilling the imposed safety criterion of -1000 pcm.

### 4.2.2 Axial offset, radial and axial power peaking factors

The axial offset is always desired to be as close to zero as reasonably achievable. A high axial offset is unfavorable because it leads to uneven core burning. As of that, some of the regulating

control rods are fully inserted during normal full power operation to flatten axial power distribution - on the one hand - and excess reactivity control - on the other hand. In this work, the axial offset at HFP and criticality condition is found to be -4%.

The control rods configuration that results in the lowest possible axial offset and power peaking factor, and maintained core criticality at HFP condition is presented in Fig. 4.4.

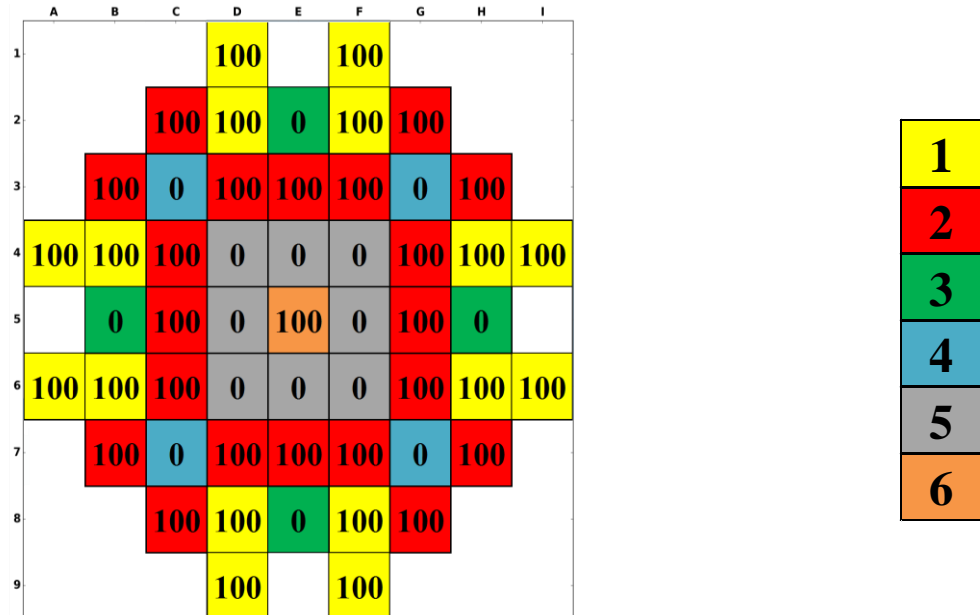


**Fig. 4.4: HFP control rods critical position.**  
**100% means CR is fully extracted, and 0% means CR is fully inserted.**  
**“White boxes” mean there is no CR at that position**  
**(CRs numbers are explained in Fig. 4.3)**

The radial power peaking factor is defined as the highest axially-integrated radial power normalized to the average core power. The axial power peaking factor represents the highest radially-integrated axial power normalized to the average core power. To determine the hottest fuel rod in the core, a coarse mesh (i.e. node-wise and channel-wise) calculation was first performed with PARCS/SCF until reaching a converged kinetic and thermal-hydraulic solution. With the pin power reconstruction capability in PARCS, the local pin power data are passed to SCF with a 3D pin-by-pin and sub-channel-wise model of the full core. Fig. 4.5 shows the calculated axially-integrated radial pin power distribution (normalized to the core-averaged power) of the optimized core at HFP critical condition as predicted by the coupled code PARCS/SCF. From Fig. 4.5, it can be observed that the radial power peaking is shifted to the core-periphery, rather than the central region, due to the low enrichment zone in the core center. In addition, some hot spots are observed in some FAs corners that suggest for a further optimization work at the FA level such as reducing corner fuel pins enrichment or adding thin coating layer of burnable absorber material e.g.  $ZrB_2$  to these corner fuel pins.

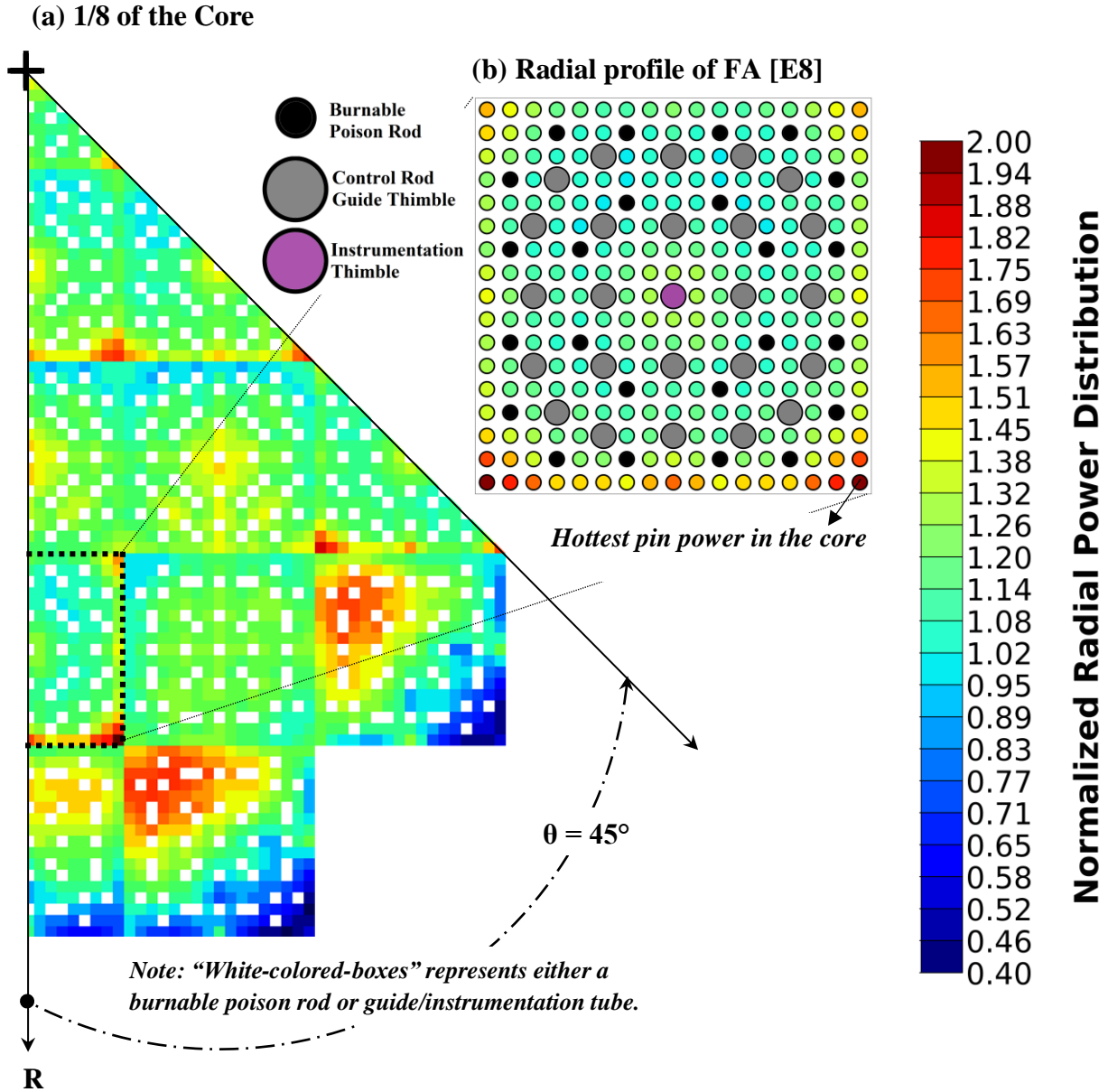


**Fig. 4.5:** Calculated (a) axially-integrated radial normalized pin power distribution for an eighth of the core at HFP condition with CRs at a critical position; (b) hottest fuel rod in the core found at fuel assembly located at E8, as predicted by the coupled code PARCS/SCF.

Fig. 4.6 shows the radially-integrated axial power distribution of the optimized core at HFP critical condition as predicted by the coupled code PARCS/SCF. A slight shift of the axial power profile towards the core bottom can be observed in Fig. 4.6. This is due to the fact that at HFP condition, the moderator density is higher in the core bottom than the top of the core. Hence, better neutron moderation is expected at the core bottom.

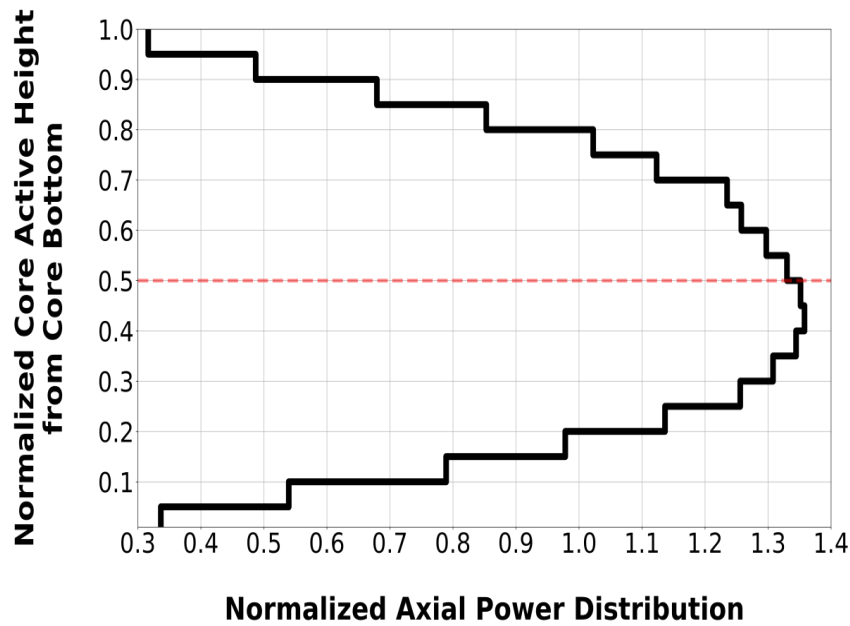


**Fig. 4.6: Calculated radially-integrated axial normalized power distribution at HFP condition with CRs at a critical position, as predicted by the coupled code PARCS/SCF.**

Observing Fig. 4.5 and Fig. 4.6 one can calculate the total power peaking factor ( $F_{xyz}$ ) by multiplying the radial and axial power peaking factor (i.e.  $1.98 \times 1.36 = 2.7$ ). This finding shows that the total power peaking factor is below the defined safety criterion (i.e. 3.3) with sufficient margin.

### 4.3 Global and Local Core Thermal-Hydraulics Characteristics

In order to assess the thermal-hydraulic design of the developed core, simulation at the HFP condition is performed using the coupled code PARCS/SCF. The developed core is optimized so that all objectives are met. Global thermal-hydraulics parameters such as core heat-up and pressure drop; and local parameters such as coolant enthalpy rise factor, maximum centerline fuel and cladding wall-averaged temperatures are discussed in the following subsections.

#### 4.3.1 Core average heat-up and pressure drop

The average core heat-up in the core is  $28^\circ\text{C}$ , which is the difference between the coolant inlet and average outlet temperatures. The pressure drop in the core is 28 kPa, which is related to (a) hydrostatic (gravitational) pressure losses; (b) frictional pressure losses; and (c) local losses (e.g. due to the existence of spacer grids). The calculated core pressure drop is normally much lower than in a typical PWR. This is attributed to both the small core height and the lower coolant flow rate in comparison to a typical PWR. This low core pressure drop facilitates the establishment of natural circulation under accidental conditions, which is a key feature to remove the residual heat out of the core.

### 4.3.2 Coolant enthalpy-rise factor

The coolant enthalpy-rise factor is defined as the ratio of the maximum to core average coolant enthalpy rise. It is generally understood that the heat flux that causes departure from nucleate boiling (DNB) decreases as the coolant enthalpy increases. Thus, by minimizing this factor, an increased safety margin against DNB is obtained. The coolant enthalpy-rise factor of the developed core is 1.3 at the HFP and critical condition. In other words, the maximum total FA power is only 30% higher than the average one in the core.

### 4.3.3 Centerline fuel and cladding wall-averaged temperatures

Local safety information such as the maximum centerline fuel and cladding wall-averaged temperatures are calculated to demonstrate that the imposed safety criteria are not exceeded during normal operation. Using the coupled code PARCS/SCF with the pin power reconstruction capability, the maximum pin-wise centerline fuel and cladding wall-averaged temperatures are 1053°C and 363°C, respectively, of the optimized core at HFP and critical condition. At that condition, the maximum sub-channel coolant temperature (at the core exit) is 335 °C. This detailed analysis proves that the fuel rods in the core are far away from the fuel melting threshold of 2840°C and cladding degradation of 1200°C. Fig. 4.7 and Fig. 4.8 show the centerline fuel and cladding wall-averaged temperatures distribution, respectively, of the optimized core at the axial plane where the maximum values are located. In addition, these two figures demonstrate the location of the hottest fuel pin in the core and its axial temperature distribution. It can be noticed from Fig. 4.7 a decrease in the axial centerline fuel temperature around the core center. This decrease is caused by the complete insertion of control rod type 3 (see Fig. 4.3 and Fig. 4.4), in which the control rod type 3 has around the middle of its axial composition a strong absorber material (i.e. Ag-In-Cd) compared to the other parts (i.e. stainless steel). Similar observation can be seen from Fig. 4.8 for the axial cladding wall-averaged temperature distribution.

A sensitivity study is conducted to check the importance of coolant flow mixing on predicting local safety information. It is found that the maximum pin-wise centerline fuel, cladding wall-averaged, and coolant temperatures are lowered only by a half degree Celsius in the case of no coolant flow mixing occurs between the sub-channels (i.e. with parallel channel way of modeling). This outcome shows that the coolant flow mixing effect is negligible during normal operation condition. Nonetheless, coolant mixing can be significant in cases with unsymmetrical flow rate, core inlet temperature or highly localized pin power conditions such as in control rod ejection, steam line break accidents, etc.

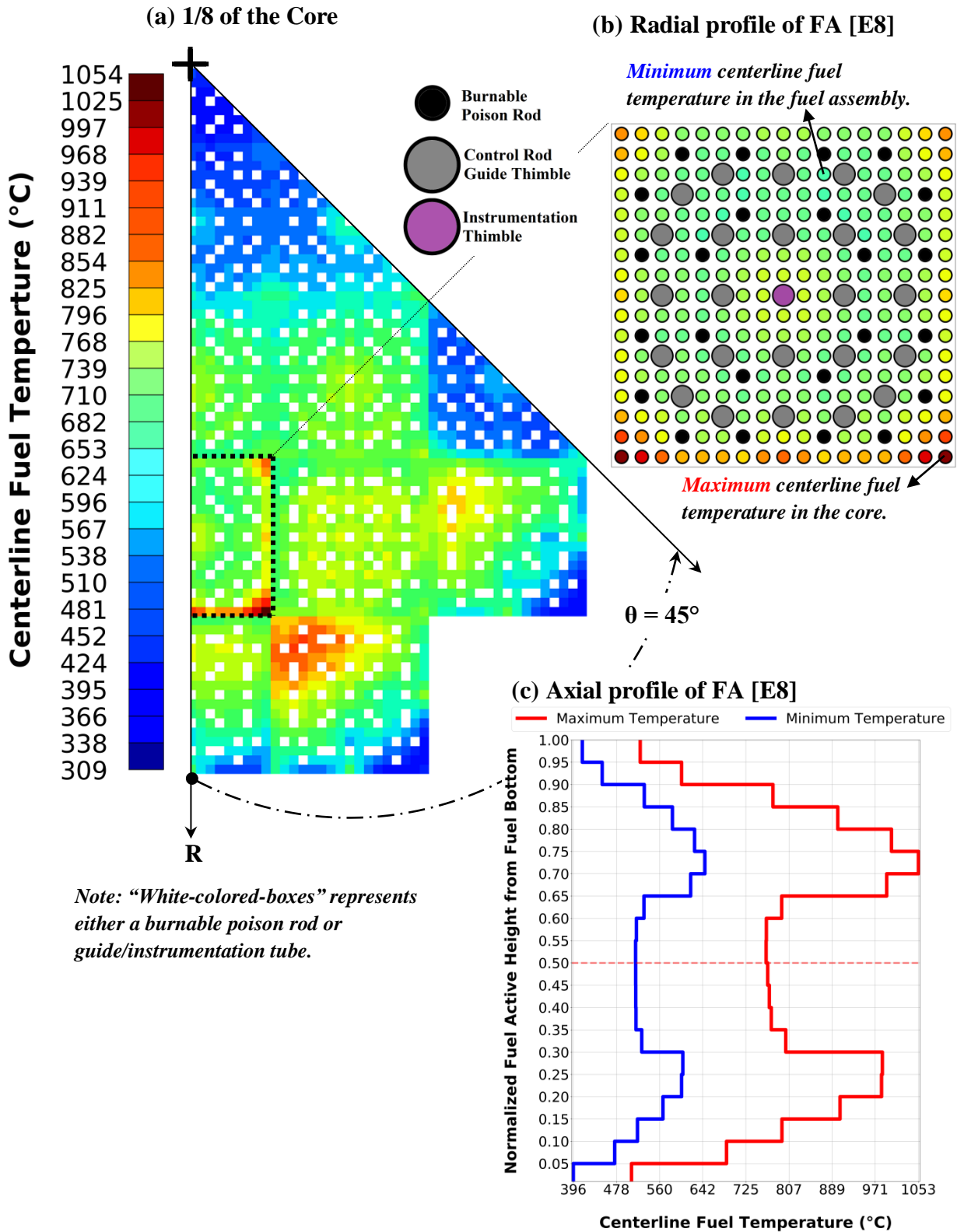


Fig. 4.7: Calculated (a) pin-wise radial centerline fuel temperature distribution for an eighth of the core at HFP condition with CRs at a critical position; (b) pin-wise centerline fuel temperature in the hottest FA located at E8 position; (c) axial profile of the pin-wise centerline fuel temperature as a function of the normalized fuel active height, as predicted by the coupled code PARCS/SCF.

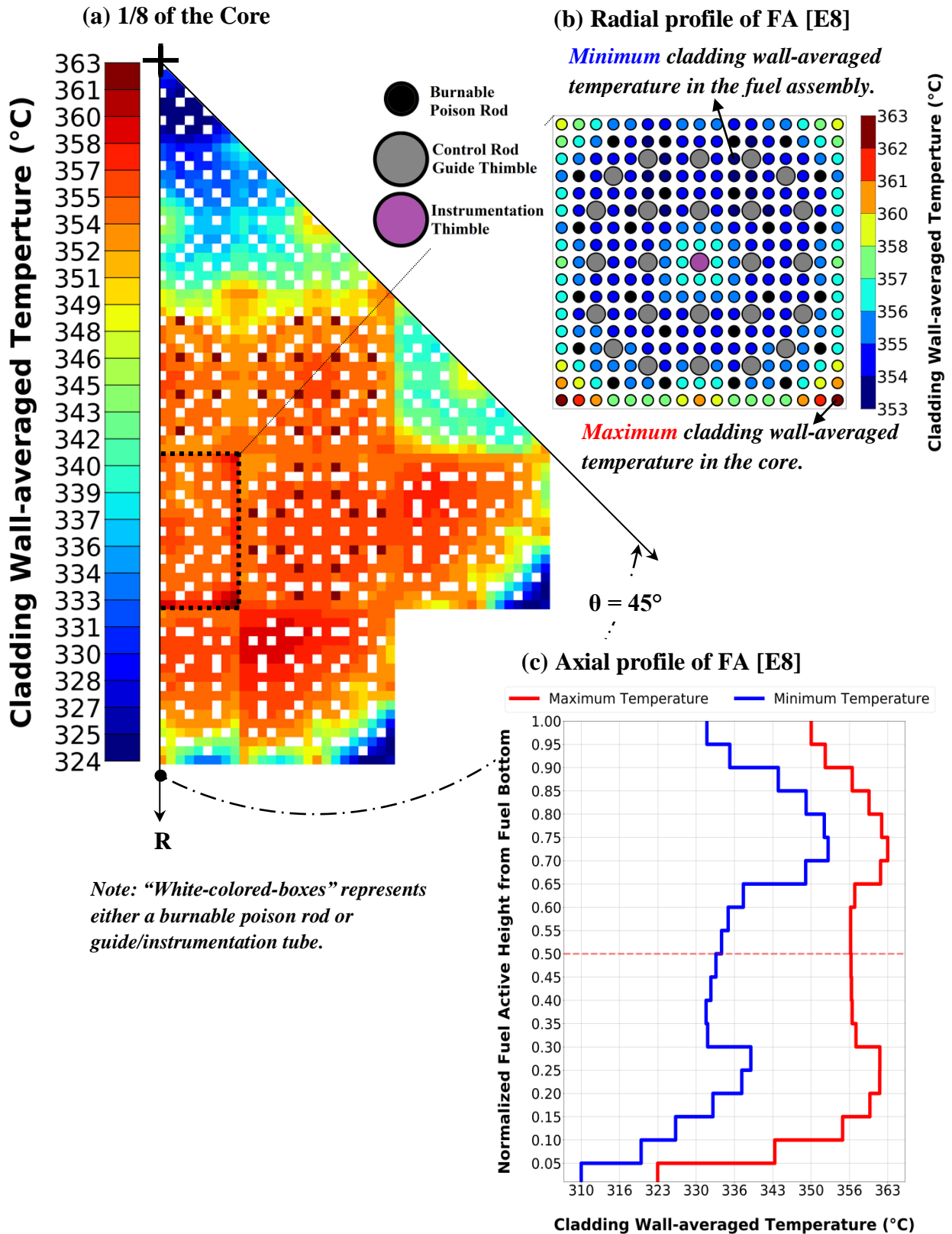


Fig. 4.8: Calculated (a) pin-wise radial cladding wall-averaged temperature distribution for an eighth of the core at HFP condition with CRs at a critical position; (b) pin-wise cladding wall-averaged temperature in the hottest FA located at E8 position; (c) axial profile of the pin-wise cladding wall-averaged temperature as a function of the normalized fuel active height, as predicted by the coupled code PARCS/SCF.

## CHAPTER 5: VERIFICATION OF THE CORE ANALYSIS METHODOLOGY

Since neither operational SMR data nor relevant experimental data are published in the open-literature to validate core analysis tools, a code-to-code comparison approach is used in this work. The predictions of the 3D diffusion code PARCS are compared to the Monte Carlo code SERPENT at the HZP condition. At the HFP condition, the predictions of the coupled code PARCS/SCF are compared against the coupled code SERPENT/SCF solution. This verification process allows assessing the quality of the results obtained by PARCS and PARCS/SCF with respect to the core characteristics. At first, the multi-group cross-section generation methodology is described. Then, the adopted verification approach and the main results are discussed.

### 5.1 Multi-group Cross-Section Generation Methodology

Multi-group constants are one of the key elements to determine the accuracy of neutronics core simulators such as PARCS. Here, SERPENT is used to generate nodal group constants in the core. For each fuel assembly (FA) type in the core, 2D models are developed using SERPENT accounting for the different material composition as a function of the active core height. These 2D models represent FA slices in a detailed manner, i.e. all pins are modeled explicitly. Then, spatial homogenization and energy-group condensation are carried-out for each FA-2D model using reflective boundary condition and two-group structure with a cutoff energy at 0.625 eV. For each model, group constants are generated for different branch variations originating from varying fuel temperature (from 26.85°C to 1826.85°C) and moderator temperature (from 26.85°C to 341.85°C), and CR position (In and out). The complete branch structure and details of the FA modeling are described in Appendix-A.

As the generation of nodal data in 2D models is carried out in an isolated manner without taking into account the neighboring fuel assemblies in the full core model, additional correction factors are introduced. These factors (or treatments) are applied to the cross-section homogenization and energy-condensation procedures.

For the homogenization correction, two famous methods exist in the literature: Generalized Equivalence Theory (GET) (Smith, 1986) and Super-homogenization (SPH) method (Herbert, 1981). The former method introduces the concept of discontinuity factors (DFs) for a better approximation of the neutron flux at the boundaries. The latter method introduces a homogenization (SPH) factor to modify the homogenized cross-sections in order to exactly reproduce the reaction rate from the heterogeneous solution. In this work, the GET approach is adopted.

For the energy-condensation correction, different methods have been developed over the years to correct the neutron spectrum used to collapse micro-energy group structure to macro-energy group structure (i.e. 2-group structure) in order to preserve neutron leakage. One of the most famous methods

is the B1 leakage-correction method (Stamm'ler and Abbate, 1983) used by many reactor physicists. Recently, Smith (Smith, 2017) revealed subtle details behind CASMO/SIMULATE treatment of cross-section generation. In which he concluded that the “*B1 spectrum calculations should not be used in commercial LWR analysis*”, instead the P1 spectrum correction methodology is encouraged, which is used in CASMO since 1985. By deeply analyzing the diffusion equation, one could conclude that the leakage-term is associated with the diffusion coefficient. Recently, a Monte-Carlo-based methodology has been developed to find the diffusion coefficient and transport cross-section by relying on the migration area concept\*. That methodology is called cumulative migration method and is first introduced by (Liu et al., 2018) in OpenMC (Romano et al., 2015). Afterwards, this method is adopted in SERPENT. In this work, the calculated diffusion coefficient and transport cross-section in a two-group structure is based on the cumulative migration method.

## 5.2 Verification Approach of the Cross-Section Generation Methodology

The “*solution verification*” concept (Oberkampf and Roy, 2010) is adopted in this work that has a goal of (a) assuring the correctness and consistency of the input and output data for a problem of interest; and (b) estimating the numerical accuracy due to solving a discrete equations of partial differential equations (PDEs). This concept is applied here to quantify the discrepancies between the low-fidelity core simulator PARCS and the high-fidelity solution SERPENT. These discrepancies arise from the modeling approximations, such as the use of diffusion theory, cross-section generation (i.e. multi-group and homogenization approximations), numerical discretization, etc. In this framework, it is assumed that the SERPENT solution represents the best solution for the physics of the neutron transport inside the reactor core, and can therefore be considered as a “quasi-exact” solution.

The cross-verification of PARCS against SERPENT solution is conducted for the (a) effective multiplication factor ( $K_{\text{eff}}$ ); and (b) nodal power distribution at HZP and HFP under ARO condition. The cross-verification at HFP condition is performed with both codes (i.e. PARCS and SERPENT) coupled to the thermal-hydraulics code SUBCHANFLOW.

The judgment criteria of a representative PARCS solution is based on whether the discrepancies found between PARCS and SERPENT fall within the propagated nuclear data uncertainties. According to (Avramova et al., 2015), the typical 1-sigma uncertainty due to nuclear data in  $K_{\text{eff}}$  and power distribution of LWRs is 500 pcm and 5%, respectively. These criteria are adopted here since the developed core is based on LWRs proven technology.

The verification outcomes between PARCS and SERPENT at the HFP condition are highlighted hereafter, whereas the results at the HZP condition could be found in (Alzaben et al., 2019a).

---

\* Migration area is defined as one-sixth of the square of the average distance travelled by a neutron from its birth point (as a fast neutron) to an absorption location (as a thermal neutron).

### 5.2.1 Verification of the core eigenvalue

The absolute difference in the effective multiplication factor obtained between the coupled codes PARCS/SCF and SERPENT/SCF at the HFP and ARO conditions is found to be 7 pcm. This value falls within 2 standard deviations of the SERPENT's eigenvalue. Therefore, it can be concluded that the PARCS/SCF obtained eigenvalue for the full core agrees well with the SERPENT/SCF solution within the 500 pcm judgment criterion.

### 5.2.2 Verification of the core power distribution

The axially-integrated normalized radial power distribution obtained by the coupled code PARCS/SCF and the relative percentage difference with respect to the coupled code SERPENT/SCF solution at HFP and ARO conditions is shown in Fig. 5.1. One can note that the maximum relative difference between the two coupled codes is 2.2% and is located at the core borders where there is a strong thermal flux distortion because of the fuel-reflector node interface. However, that maximum relative difference in the axially-integrated radial power distribution is still within the imposed 5% judgment criterion.

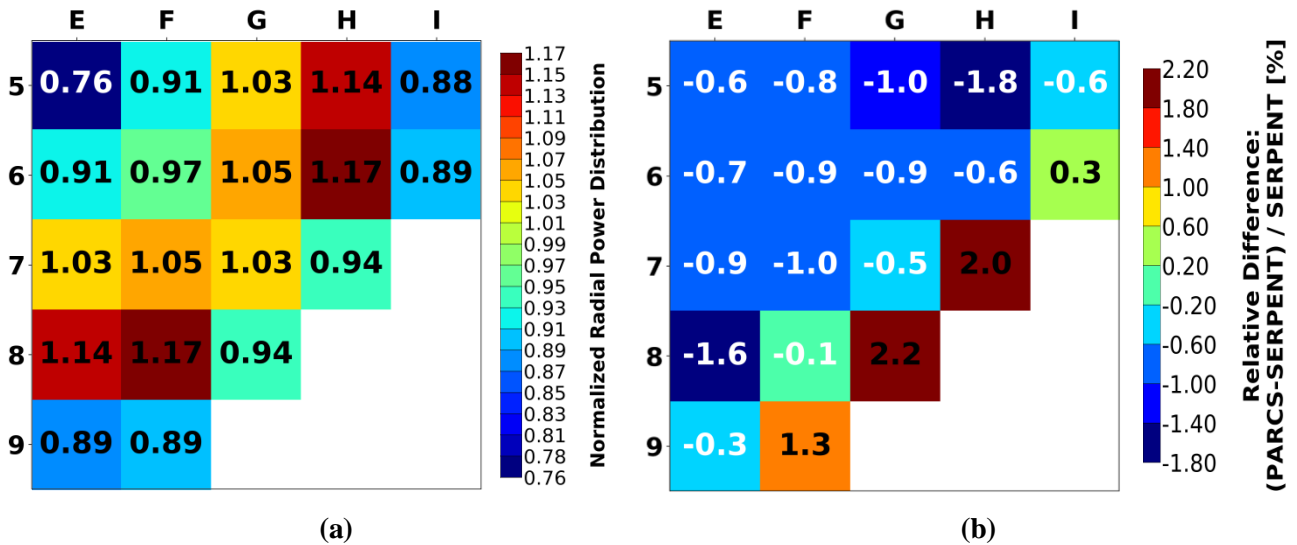


**Fig. 5.1: (a) Calculated axially-integrated normalized radial nodal power distribution for a quarter of the core at HFP and ARO conditions as predicted by the coupled code PARCS/SCF; (b) Spatial distribution of the relative percentage difference in the axially-integrated radial nodal normalized power distribution with respect to the solution of coupled code SERPENT/SCF.**

Fig. 5.2 and Fig. 5.3 present the power distribution relative difference on a node-to-node basis for the 3D core model between the coupled codes PARCS/SCF and SERPENT/SCF at HFP and ARO conditions. It can be observed that some fuel nodes near the top and bottom axial reflectors have a relative power difference higher than the 5% imposed criterion due to the strong axial flux distortion at the fuel-reflector interface. However, these nodes represent only 1% of the total fuel nodes in the core and have low nodal powers.

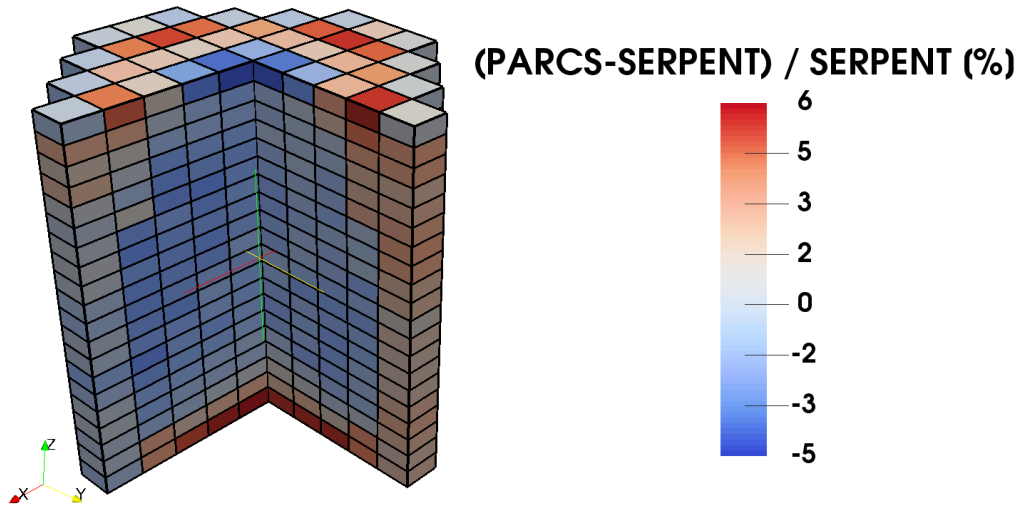


**Fig. 5.2: 3D spatial distribution of the relative percentage difference in the nodal normalized power between PARCS/SCF and SERPENT/SCF at HFP and ARO conditions.**

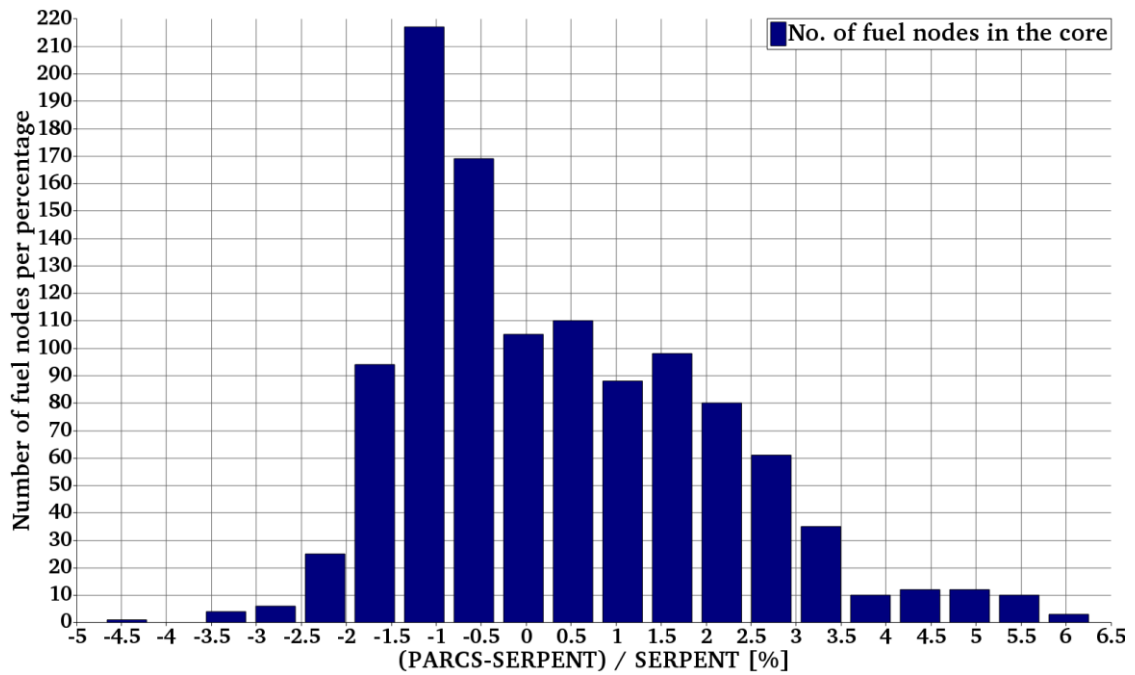


**Fig. 5.3: Histogram distribution of the relative difference in the nodal normalized power between PARCS/SCF and SERPENT/SCF at HFP and ARO conditions. (Note: the total number of bins represents the total number of fuel nodes in the entire core)**

Hence, it can be concluded that predictions obtained with the low-fidelity coupled PARCS/SCF model are a representative to the high-fidelity SERPENT/SCF solution within the propagated nuclear data uncertainties.

## **CHAPTER 6: ANALYSIS OF A CONTROL ROD EJECTION ACCIDENT IN THE BORON-FREE CORE**

The control rod ejection accident (REA) is a design basis event that occurs due to a mechanical failure of the control rod drive mechanism (CRDM) housing such that the pressure difference between the primary-system and containment is the driving force that ejects a control rod assembly entirely out of the reactor core (OECD/NEA, 2010). Therefore, a positive reactivity is inserted causing a sudden core power excursion associated with a rapid fuel temperature rise promoting fuel pellet thermal expansion. If the ejected control rod worth is greater than prompt-critical (1\$), the power will grow exponentially. The huge power increase will lead to a significant energy deposition in the fuel, even though the power surge is limited by the negative fuel Doppler feedback and delayed neutron effects. In this chapter, the assessment of the behavior of the boron-free core following the REA is studied and the main results are discussed.

### **6.1 Description of the Accident and Assumptions**

The REA (IAEA, 2003) event leads to a rapid reactivity insertion, as a consequence of an ejected control rod in a very short time that may challenge the fuel-cladding integrity.

In Gen-II PWR design, according to (OECD/NEA, 2010), the worst possible REA scenario happens when the highest control rod worth is totally ejected within 0.1 seconds from the Hot Zero Power (HZP) condition. This is because most of the excess reactivity at the HZP condition in a PWR is managed through fully inserting most of the control rod banks. Hence, a higher control rod worth is expected. Also, the HZP condition typically has the least negative Doppler feedback, which takes a few seconds to be effective (i.e. at higher fuel temperature) and limits the power excursion. During normal operation of a PWR at full power, only one bank of control rods is partially inserted in the core. The reactivity changes under normal operation, e.g. caused by core depletion and Xenon transients, are compensated by changing the soluble boron concentration rather than by control rod movements. Therefore, the amount of reactivity that is added by the ejection of a control rod during normal full power operation is limited (Rudling et al., 2016).

The worst possible REA consequences in the boron-free core are totally different from the ones in Gen-II PWRs. In the boron-free core, excess reactivity at the Hot Full Power (HFP) condition is managed by fully inserting some of the control rod banks, in order to minimize the axial power peaking. Whereas at HZP condition, more control rod banks are fully inserted into the core. As a result, both scenarios (i.e. the HZP and HFP conditions) have to be investigated in order to check that the associated safety parameters do not exceed the REA acceptance criteria highlighted in chapter 2.

## 6.2 Analysis of the REA with PARCS/SCF

The REA-analysis is performed with the coupled code PARCS/SCF using two different modeling approaches based on the fuel-cladding gap heat transfer coefficient ( $h_{\text{gap}}$ ):

- 1<sup>st</sup> Approach: A conservative value of  $h_{\text{gap}} = 10,000 \text{ W}/(\text{m}^2\cdot\text{K})$  is used for all FAs to characterize the heat transfer in the gap between the fuel pellet and cladding as reported in (Kozlowski and Downar, 2007).
- 2<sup>nd</sup> Approach: Modeling the fuel-cladding gap behavior by activating the SCF simplified fuel thermo-mechanics model for a more realistic description of the gap heat transfer coefficient.

The impact of both approaches on key safety parameters for the evaluation of the boron-free core during a REA at the beginning of life (BOL) and HZP condition is discussed in details in the next subsections, whereas the analysis at the HFP condition can be found in (Alzaben et al., 2019b). The details of PARCS and SCF developed models for REA analysis are described under Appendix-A.

### 6.2.1 Initial and boundary conditions

The REA initial condition at the HZP condition is summarized in Table 6.1. The initial control rods configuration leading to a critical condition and the position of the highest control rod worth (to be ejected) at the HZP condition is presented in Fig. 6.1. The SCRAM signal, which occurs due to reaching a high power level, is not considered here since the time for the control rod insertion is much longer than the power excursion itself<sup>†</sup>.

**Table 6.1: Initial conditions for REA scenarios under HZP condition**

Parameters	Value
Initial core power (% of nominal power)	1.0E-4
Highest CR worth (pcm) [\$]	998 [1.45]
Position of the highest CR worth in the core	D2
Ejection duration (s)	0.05*
End of transient simulation (s)	3.0
Fuel irradiation status	BOL

\* Since the core active length almost half of typical PWR, the ejection duration of 0.1 seconds reported in (OECD/NEA, 2010) has been divided by 2.

<sup>†</sup> Normally, the failure of SCRAM assumption is related to Anticipated Transient Without Scram (ATWS) events. The justification of neglecting the SCRAM signal in the REA event is due to the fact that the safety criteria are being challenged at the beginning of the REA transient, where the inherent core features are the only mean to limit REA consequences. The effectiveness of the safety system responsible for the long-term coolability is investigated in the next chapter.

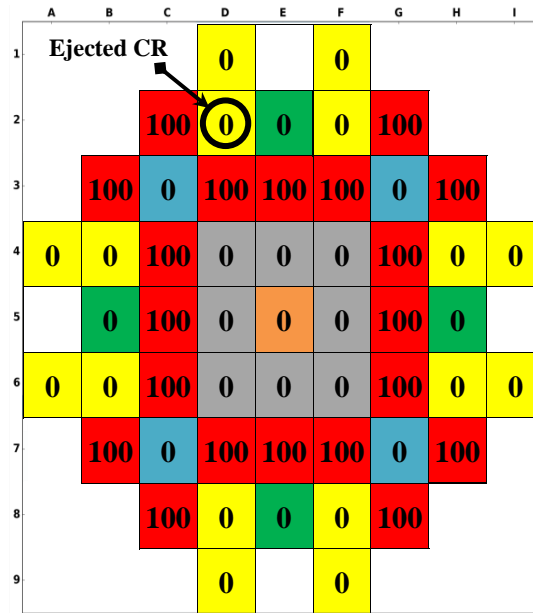


**Fig. 6.1: REA initial CRs configuration and ejected CR position at HZP condition.**

*(Note: “100” means CR is fully extracted and “0” means CR is fully inserted.*

*“Colored-boxes” refer to different CRs types which are explained in Fig. 4.3; whereas “White-boxes” mean there is no CR at that position)*

## 6.2.2 Analysis of a REA at HZP condition - from global perspective

The REA transient is analyzed as a function of time and three space dimensions using the coupled code PARCS/SCF. The total core power evolution following the ejection of the highest CR worth located at D2 (see Fig. 6.1) at the HZP condition is illustrated in Fig. 6.2 together with the ratio of the core power predicted by activating the SCF gap heat transfer model to the power predicted by assigning a constant fuel-cladding gap heat transfer coefficient for all fuel nodes.

Following the REA, the total core power increased exponentially (because the ejected CR has a worth greater than prompt-criticality) reaching to a maximum value of 46.5 times its nominal full power (equivalent to 15.3 GW<sub>th</sub>) in a very short time of about 120 milliseconds after completely ejecting the highest CR worth. Then, the power decreases due to the core inherent features (i.e. Doppler feedback and moderator temperature feedback) till reaching 20% of its nominal value at the end of the transient calculation. This additional 20% is attributed to the decay of delayed neutron precursors and to the fact that the initial CRs critical configuration is changed.

By using a constant fuel-cladding gap heat transfer coefficient, the computed maximum core power depicted in Fig. 6.2 is over predicted by 4% in comparison with the results obtained by activating the SCF gap heat transfer model. At about 0.4 seconds, the core power computed by the constant gap heat transfer coefficient approach under predicts the power obtained with the 2<sup>nd</sup> approach by almost 20% (~37 MW<sub>th</sub> of difference). These findings indicate that using a constant gap heat transfer coefficient is not necessarily yields a conservative estimate. Therefore, a realistic fuel-cladding gap model is recommended to be used when analyzing REA consequences.

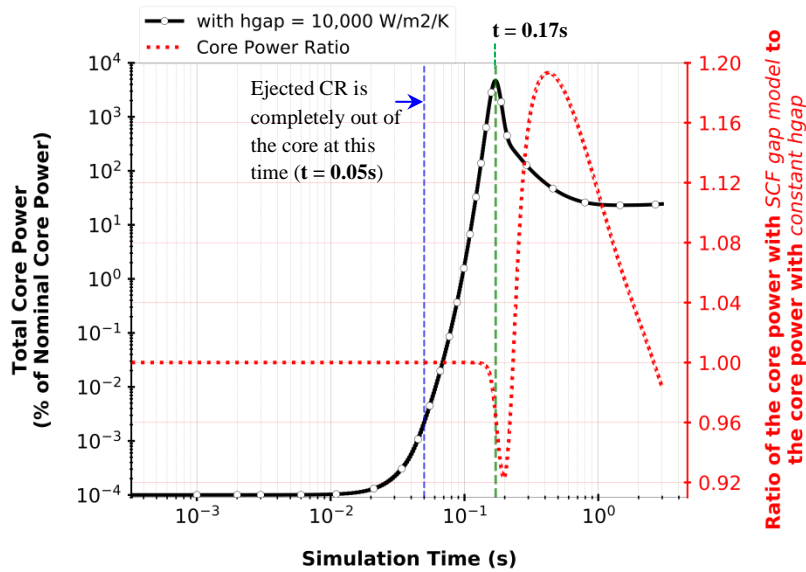


**Fig. 6.2:** Computed total core normalized power evolution following the REA at HZP condition (*left vertical axis*); the ratio of core power calculated using the SCF fuel-cladding gap heat transfer model to the core power calculated using the constant gap heat transfer coefficient (*right vertical axis*), as predicted by the coupled code PARCS/SCF.

To understand the reason for the change in slope of the core power evolution (see Fig. 6.2) at 0.2 seconds, one needs to analyze the total amount of reactivity inserted into the core following the REA. Fig. 6.3 shows the evolution of total core reactivity following the REA at HZP condition. The total reactivity inserted into the core reaches its maximum value of 1.4\$ following the ejection of the highest CR worth, then stays there for about 100 milliseconds. After that, the total core reactivity decreases till reaching its minimum value of -0.8\$ at about 0.8 seconds, then increases towards the end of the transient calculation.

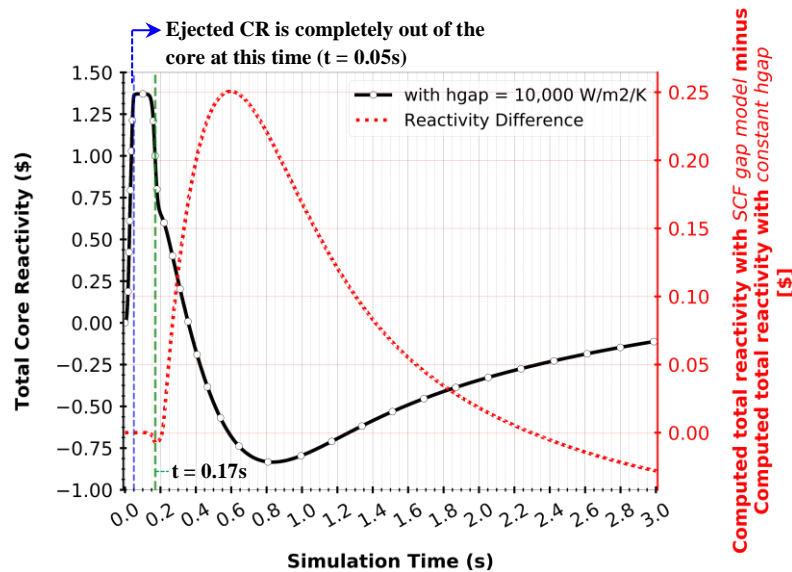


**Fig. 6.3:** Computed total core reactivity evolution following the REA at HZP condition (*left vertical axis*); the difference between the total reactivity calculated using the SCF fuel-cladding gap heat transfer model and the total reactivity calculated using the constant gap heat transfer coefficient (*right vertical axis*), as predicted by the coupled code PARCS/SCF.

The slope change of the total core power evolution observed from Fig. 6.2 at 0.2 seconds is being observed also for the total inserted reactivity into the core at the same time (see Fig. 6.3). By analyzing the temporal behavior of each feedback components (i.e. fuel and moderator temperature feedback), one can reveal such a change in the slope. Fig. 6.4 illustrates the behavior of the fuel and moderator temperature feedback as a function of time. At 0.2 seconds, the fuel temperature reactivity feedback reaches its minimum value of  $-0.65\%$  then increases till the end of the transient calculation. At that time, the moderator temperature reactivity feedback just starts to be effective and decreases till reaching its minimum value of  $-1.42\%$  at about 0.8 seconds. Such a change in the evolution of both the fuel and moderator temperatures reactivity feedback causes the change in slope observed in Fig. 6.2 and Fig. 6.3 at 0.2 seconds.

From Fig. 6.4 one can also observe that the fuel temperature feedback is the one responsible for limiting the power surge following REA due to the Doppler broadening effect, which is an instantaneous response. The moderator temperature feedback has a delayed response that takes about 100 milliseconds to be effective after completely ejecting the highest CR worth. This delayed response depends on the heat flux from the fuel pellet to the coolant. The physical quantities determining the heat flux during REA transient are: (a) fuel thermal conductivity and heat capacity; (b) fuel-cladding gap heat transfer coefficient; and (c) clad thermal conductivity and heat capacity.

As the used cladding material here is made from Zr-4, its thermal conductivity is known to be high and its heat capacity is low compared to the  $\text{UO}_2$  fuel pellet. Therefore, its thermal conductance is much better than the  $\text{UO}_2$  fuel. The fuel-cladding gap heat transfer coefficient depends on many factors, which will be discussed later in subsection 6.2.4. The fuel thermal conductivity, fuel heat capacity and fuel-cladding gap heat transfer coefficient are the central parameters in delaying the actuation of the moderator temperature feedback. From here one can notice the strong interaction between the two physical domains (i.e. thermal-hydraulics and thermo-mechanics) on the reactivity (neutronics) behavior. The moderator temperature reactivity feedback exhibits a much stronger feedback than the Doppler effect, unlike in a typical PWR. This behavior is attributed to the absence of soluble boron in the moderator.

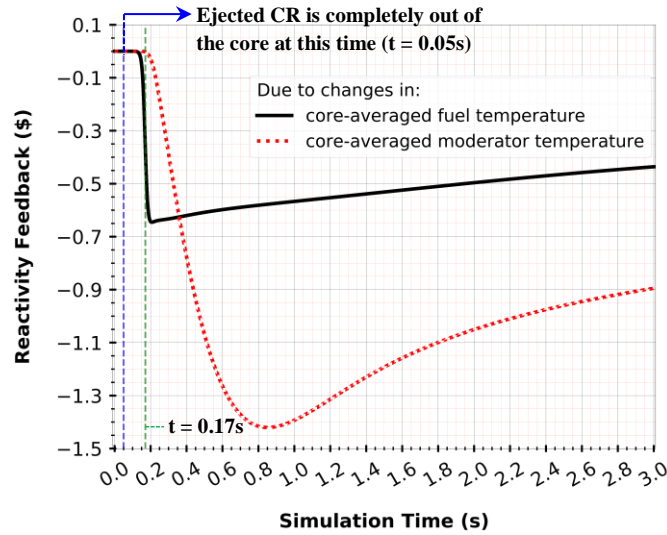


**Fig. 6.4:** Computed fuel and moderator temperature reactivity feedback as a function of time following the REA at HZP condition; as predicted by the coupled code PARCS/SCF with a constant gap heat transfer coefficient.

**6.2.3 Analysis of a REA at HZP condition - from local perspective**

As a consequence of ejecting the highest CR worth (located at D2), a power shift in the core is observed towards FAs located around the ejected CR, as illustrated in Fig. 6.5. The maximum FA power (located at D2) during the REA transients has reached 2.72 times the core average power at 0.17 seconds. Observing Fig. 6.5b, one could notice that the FA located at C2 and E2 have large difference in their normalized radial power although they are neighboring the FA located at D2. This is due to the fact that FA located at E2 has a control rod fully inserted, whereas the C2-FA has a control rod fully extracted throughout the REA transients.

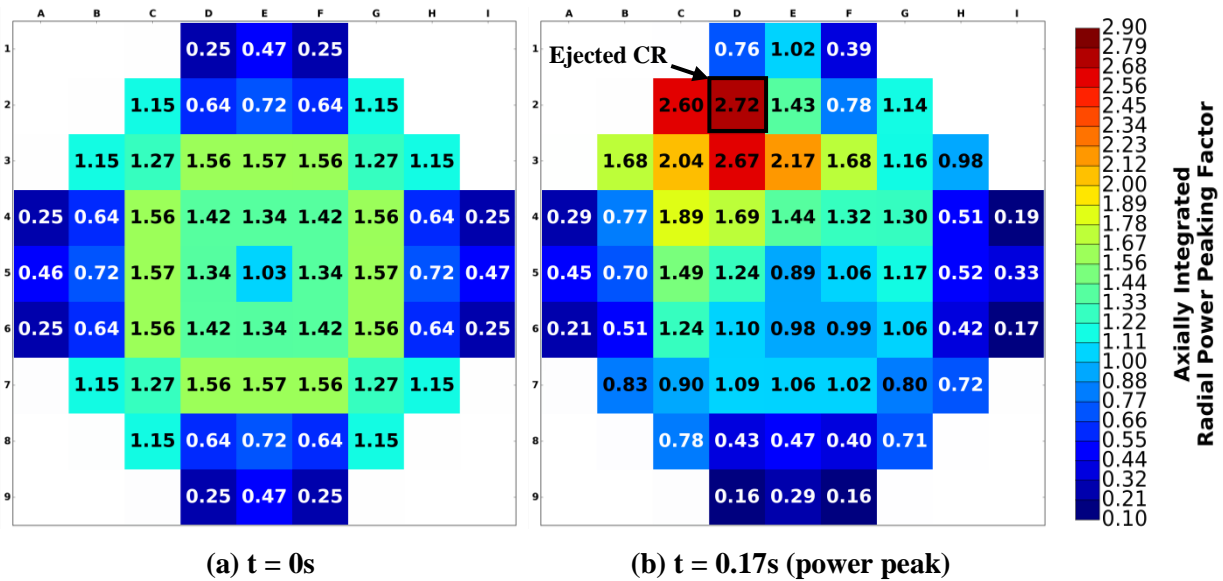


**Fig. 6.5:** Computed axially-integrated radial normalized nodal power distribution (a) initially and (b) at the time where the maximum total core power is attained following the REA at HZP condition as predicted by the coupled code PARCS/SCF with the SCF fuel-cladding gap heat transfer model

From safety perspective, fuel rods (or assemblies) failure might happen following the REA provided that the on-site and off-site dose limit remain within acceptable limits. Therefore, to evaluate the fission products release, if any, one needs to calculate the number of failed fuel rods in the core. Hence, the following safety-related parameters are analyzed: the maximum (i) fuel centerline temperature, (ii) cladding temperature and (iii) fuel enthalpy in the core during the REA transient.

The temporal and spatial behavior of maximum fuel centerline temperature in the core following the REA at HZP condition is illustrated in Fig. 6.6. After the ejection of the highest CR worth, the fuel centerline temperature associated with FA located at D3 in the core (the maximum in the core) has a delayed of about 100 milliseconds to increase, which is attributed to the high heat capacity of  $\text{UO}_2$  fuel pellets. Then, the fuel centerline temperature associated with D3-FA reaches its maximum value of  $886^\circ\text{C}$  at an elevation of 1.05 m from the core bottom and at 1.2 seconds as predicted with PARCS/SCF with the SCF fuel-cladding gap heat transfer model, which is far away from  $\text{UO}_2$  fuel melting temperature of  $2840^\circ\text{C}$ . It is also interesting to observe that using a constant fuel-cladding gap heat transfer coefficient yields an underestimation of the fuel centerline temperature at 1.2 seconds. Therefore, a non-conservative fuel centerline temperature is obtained with what is thought to be a “conservative” fuel-cladding gap heat transfer coefficient.

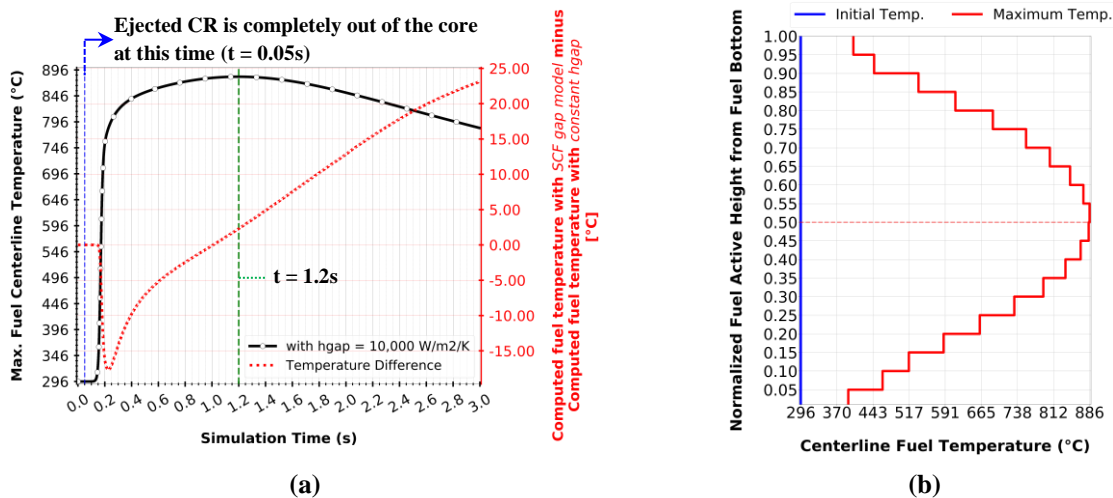


**Fig. 6.6: Computed maximum fuel centerline temperature in the core following the REA at HZP condition, (a) temporal evolution in FA located at D3 and  $Z = 1.05$  m, and (b) axial distribution in FA located at D3 at  $t=0$ s and  $t=1.2$ s as predicted by the coupled code PARCS/SCF with the SCF fuel-cladding gap heat transfer model**

The impact of ejecting the highest CR worth at HZP condition on the cladding temperature is depicted in Fig. 6.7. Following the REA, the cladding temperature associated with FA located at D3 in the core (the maximum in the core) reaches its maximum value of  $374^\circ\text{C}$  at an elevation of 1.05 m from the core bottom and at 0.25 seconds as predicted with PARCS/SCF with the SCF fuel-cladding gap heat transfer model. Therefore, the predicted maximum cladding temperature shows that there is a large margin against Zr-4 cladding allowed peak temperature of  $1200^\circ\text{C}$ .

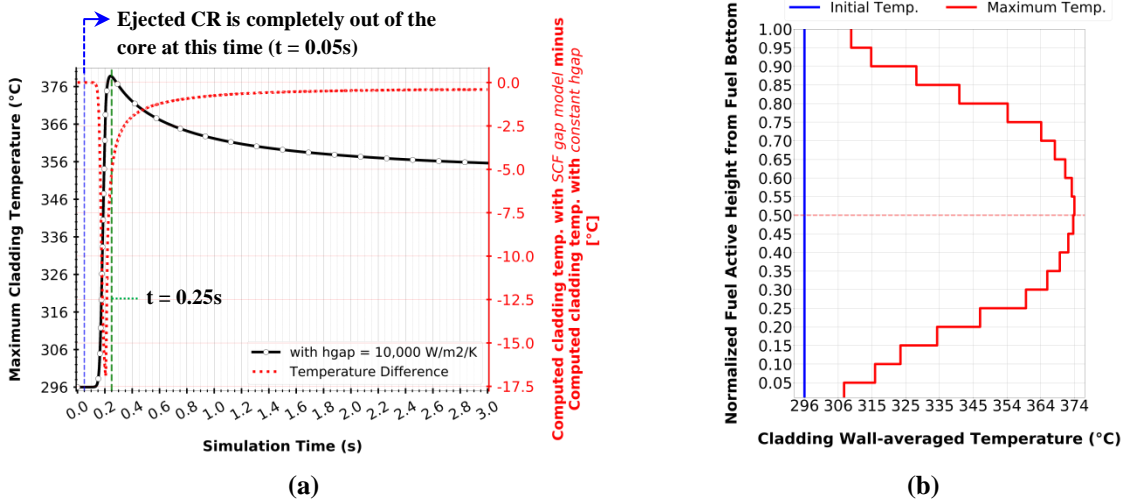


**Fig. 6.7: Computed maximum cladding temperature in the core following the REA at HZP condition, (a) temporal evolution in FA located at D3 and  $Z = 1.05$  m, and (b) axial distribution in FA located at D3 at  $t=0$ s and  $t=0.25$ s as predicted by the coupled code PARCS/SCF with the SCF fuel-cladding gap heat transfer model**

Observing both Fig. 6.6 and Fig. 6.7, one could notice that the maximum cladding temperature reaches before the fuel centerline temperature by about one second. To understand the reason behind such time difference, one needs to analyze the heat flux and moderator temperature evolution for the FA located at D3 and at an axial elevation of 1.05 m from the core bottom, where the maximum fuel centerline and cladding temperatures are located. Fig. 6.8 shows the temporal behavior of the heat flux and moderator temperature as predicted by the coupled code PARCS/SCF with a constant gap heat transfer coefficient.

From Fig. 6.8a, the heat flux for D3-FA at  $Z = 1.05$  m reaches a maximum value of  $1.8 \text{ MW/m}^2$  at 0.25 seconds coinciding in time with the observed maximum cladding temperature (see Fig. 6.7). Afterwards, the heat flux decreases till the end of the transient calculation, which generally exhibits a similar behavior as the total core power evolution (see Fig. 6.2). Interesting to notice here that at 0.25 seconds the heat flux is very high due to the low coolant temperature observed from Fig. 6.8b at that time. With such high heat flux, the cladding temperature reached its maximum value. In addition, it can be observed from Fig. 6.8b that the moderator temperature takes 1.12 seconds to reach its maximum value of  $336^\circ\text{C}$ . Such a long time to heat-up the coolant (water) is attributed to its high heat capacity.

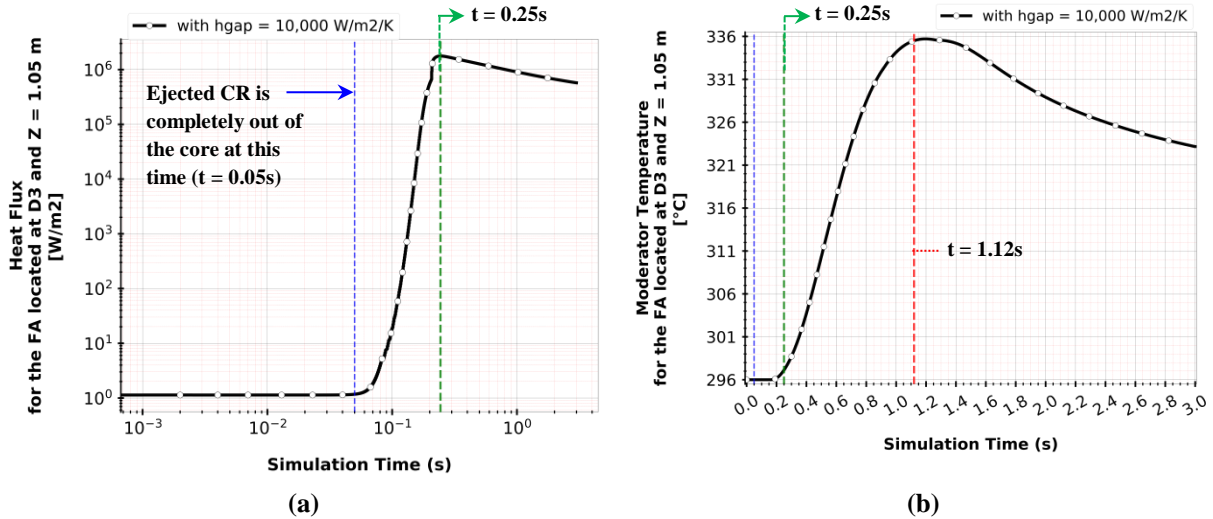


**Fig. 6.8:** Computed evolution in the FA located at D3 and Z = 1.05 m following REA at HZP condition for (a) the heat flux (b) the moderator temperature as predicted by the coupled code PARCS/SCF with a constant gap heat transfer coefficient.

The temporal behavior of fuel enthalpy for the FA located at D3 and an axial elevation of 1.05 m from the core bottom (corresponding to the maximum value in the core) following the REA at HZP condition is illustrated in Fig. 6.9. The highest fuel enthalpy observed in Fig. 6.9 reaches 264 kJ/kg at 0.3 seconds. Therefore, the risk of fuel cladding failure caused by reaching the fuel enthalpy threshold of 400 kJ/kg (i.e. the minimum fuel enthalpy threshold observed in Fig. 2.2) is excluded. A negligible difference is found at 0.3 seconds between the two approaches that are used in describing the fuel-cladding heat transfer coefficient (see Fig. 6.9).

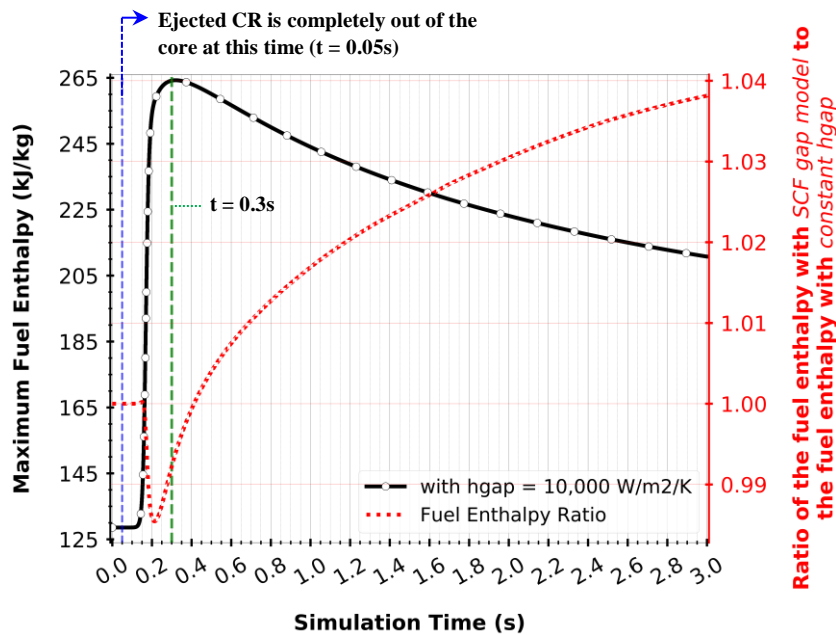


**Fig. 6.9:** Computed fuel enthalpy evolution in the FA located at D3 and Z = 1.05 m following the REA at HZP condition (left vertical axis); the ratio of the fuel enthalpy calculated using the SCF fuel-cladding gap heat transfer model to the fuel enthalpy calculated using the constant gap heat transfer coefficient (right vertical axis), as predicted by the coupled code PARCS/SCF.

#### 6.2.4 Fuel-cladding gap heat transfer coefficient and gap width behavior

So far the fuel-cladding gap heat transfer coefficient behavior itself has not been discussed in depth. The temporal evolution of the fuel-cladding gap heat transfer coefficient for the FA located at D3 and an axial elevation of 1.05 m from the core bottom (corresponding to the maximum value in the core), and the corresponding fuel-cladding gap width after a rapid power increase due to the REA at HZP condition are illustrated in Fig. 6.10 as computed by the coupled code PARCS/SCF with the SCF fuel-cladding gap heat transfer model.

Both graphs in Fig. 6.10 illustrate that the fuel-cladding gap heat transfer coefficient and gap width are not constant in time. Following the REA, the gap heat transfer coefficient reached a maximum value of about 8,050 W/(m<sup>2</sup>.K) at 0.35 seconds. This finding reveals more insight about the obtained maximum fuel centerline temperature (see Fig. 6.6) and maximum cladding temperature (see Fig. 6.7). At t=1.2 seconds (where the fuel centerline temperature reached its maximum value), the gap heat transfer coefficient has a value of about 7,500 W/(m<sup>2</sup>.K), which is less than the assumed conservative value of 10,000 W/(m<sup>2</sup>.K). This simply means a higher thermal resistance is obtained with the SCF fuel-cladding gap heat transfer model; thus, a higher fuel centerline temperature. At t=0.25 seconds (where the cladding temperature reached its maximum value), the gap heat transfer coefficient has a value of about 7,900 W/(m<sup>2</sup>.K) indicating less heat is being transferred to the cladding compared with the gap heat transfer coefficient of 10,000 W/(m<sup>2</sup>.K). Hence, a lower maximum cladding temperature is obtained with the SCF fuel-cladding gap heat transfer model. These findings show the difficulty of choosing just a single conservative value of the gap heat transfer coefficient for a conservative prediction of both the maximum fuel centerline and cladding temperature.

To understand the physical phenomena affecting the gap heat transfer coefficient, one needs to discuss the SCF fuel-cladding gap heat transfer model in more details<sup>‡</sup>. The SCF fuel-cladding gap heat transfer model calculates the gap heat transfer coefficient as a sum of: (a) the conductance due to radiation heat transfer; and (b) the conduction through the filled gas between the fuel pellet and cladding. The former effect is nearly negligible on estimating the gap heat transfer coefficient. The latter effect, on the other hand, plays a significant role in which it depends proportionally on gas thermal conduction and inversely on the gap width. The gas thermal conduction is kept constant during the REA transient because fission gas generation and release is not modeled. This approximation is reasonable for a REA analysis at a BOL. Therefore, the transient behavior of the gap heat transfer coefficient seen in Fig. 6.10a is mainly being affected by the heat conduction through gas in the fuel-cladding gap.

---

<sup>‡</sup> The mathematical expression of the SCF fuel-cladding gap heat transfer model can be found in (Alzaben et al., 2019b).

After the ejection of the highest CR worth in the core at HZP condition, the fuel-cladding gap width for the FA located at D3 and at an elevation of 1.05 m decreases sharply due to the fuel thermal expansion reaching a minimum value of 31  $\mu\text{m}$  at 0.5 seconds. Afterwards, it increases till the end of the transient calculation. This behavior can be understood by analyzing the factors affecting the gap width, according to SCF.

The modeled gap width in SCF depends on: (a) fuel and cladding thermal expansion (reversible deformation); (b) fuel swelling (permanent deformation); and (c) fuel cracking (permanent deformation). Fuel swelling normally happens at high fuel burnup; therefore, its effect is negligible at the BOL. Therefore, the observed behavior of the gap width in Fig. 6.10b indicates that permanent deformation due to fuel pellet cracking is not possible; otherwise, the gap width will not increase after reaching its minimum value. Hence, gap width variation is primarily due to fuel thermal expansion. From a safety perspective, gap closure has not been observed. Therefore, fuel rod failures due to pellet-cladding mechanical interaction (PCMI) can be considered to be unlikely to happen.

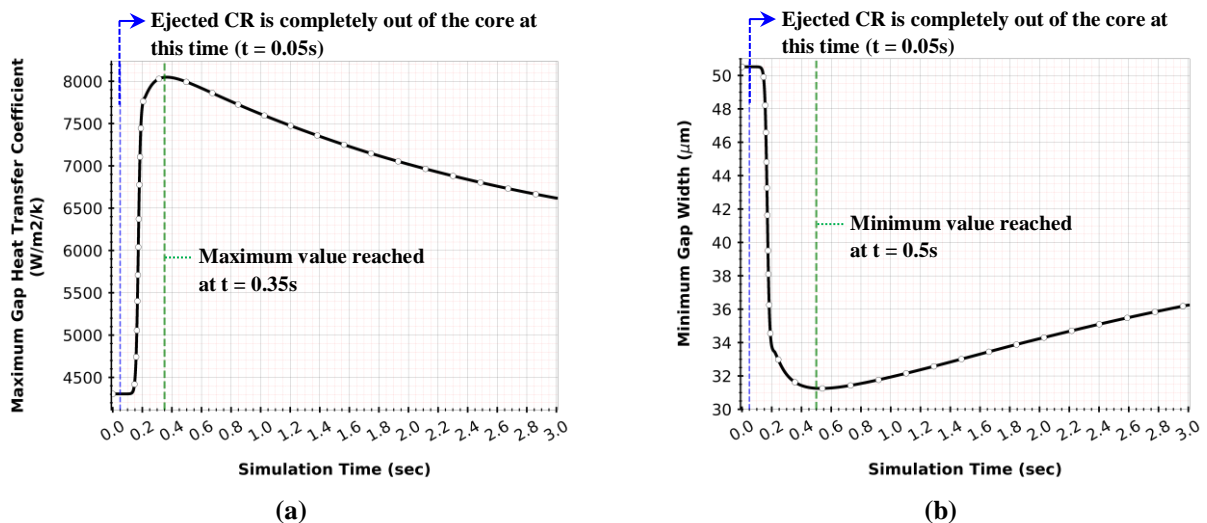


**Fig. 6.10: Computed evolution in the FA located at D3 and Z = 1.05 m following REA at HZP condition for (a) the fuel-cladding gap heat transfer coefficient (b) the fuel-cladding gap width as predicted by the coupled code PARCS/SCF with the SCF fuel-cladding gap heat transfer model.**

### 6.3 Summary and Perspective

The analysis of the potential impact of reactivity-initiated accidents caused by control rod ejection on the boron-free core at BOL and at HZP condition is investigated in this chapter using the coupled code PARCS/SCF. In this investigation, two approaches to predict the fuel-cladding gap heat transfer coefficient are utilized: (a) a fixed value of 10,000 W/(m<sup>2</sup>.K); and (b) an SCF fuel-cladding gap heat transfer model. The impact of using these two approaches on the following key safety parameters: total core power, fuel centerline temperature, cladding temperature, and fuel enthalpy is presented and discussed.

Traditionally, REA consequences for conventional LWRs are analyzed with a constant value for the fuel-cladding gap heat transfer coefficient. In this chapter, it has been demonstrated that using a constant value of the fuel-cladding gap heat transfer coefficient may not result in a conservative estimation for all of the key safety parameters (i.e. fuel centerline temperature, fuel enthalpy and cladding temperature). Thus, the outcome of this investigation suggests the use of a thermo-mechanics code for a more detailed description of the physical phenomena occur in the gap between the fuel pellet and cladding in order to properly study REA consequences, especially at high fuel burnup (e.g. EOC).

It can be concluded that there is no threat to loss fuel-cladding integrity in case of an REA at HZP condition for the boron-free core. Further investigations are needed to predict the local safety parameters by means of pin-by-pin coupled neutronic/thermal-hydraulic and thermo-mechanics simulation; where the fuel rod behavior is described in more details, including the fuel-cladding gap modeling. The accuracy of such an approach is then limited by the accuracy of the generated cross-section data at the pin level calculated by lattice physics codes. In addition, the development of dedicated CHF-correlation for the boron-free core fuel assembly design and its operating condition is needed to demonstrate that DNB is not being experienced following the REA transient.

## **CHAPTER 7: ANALYSIS OF A STEAM LINE BREAK ACCIDENT OF A GENERIC SMART-PLANT WITH THE BORON-FREE CORE**

The steam line break (SLB) accident is a design basis accident that may occur as a result of thermal stresses or cracking in a steam line pipe leading to depressurization of the secondary circuit, and consequently, enhancing heat removal. The enhanced heat removal is then leads to an overcooling of the primary coolant temperature; thus, a positive reactivity is inserted into the core due to the negative moderator temperature coefficient (MTC). The positive reactivity may lead to a core re-criticality; then to a return-to-power even though after a reactor trip. In general, the SLB-accident\* is characterized by an asymmetrical cooling behavior, which is a result of breaking one of the steam lines while others are intact, leading to a strong radial power distortion. In this chapter, the analysis an SLB-accident of the developed boron-free core integrated within the SMART-plant is performed using the coupled codes TRACE/PARCS.

### **7.1 Description of the Accident and Assumptions**

The SLB-accident in the SMART-plant is simulated by double-ended break of one of the steam lines causing a large pressure difference between the broken steam line (5.2 MPa (Sanchez-Espinoza et al., 2018)) and the containment (0.1 MPa (Sanchez-Espinoza et al., 2018)) that accelerates the steam out of the broken line. Such a fast depressurization leads to an accelerated boiling in the steam generator (SG) broken line; thus, enhanced heat removal from the primary to the secondary side. As a result, a rapid cooldown of the primary coolant system occurs. A decrease of the coolant temperature at the core inlet in combination with the high negative MTC of the boron-free core causes an increase of the core power.

In such scenario, the reactor trip could happen as a result of detecting low steam pressure on the secondary side (2 MPa (Kim et al., 2003)) or high core power (115% of the nominal power (Chung et al., 2003)). Therefore, both signals are modeled in this study. When a reactor trip occurs, all control rods are inserted into the core, and the main steam isolation valves (MSIVs) and feedwater isolation valves (FIVs) are closed to isolate the broken line. Also, all coolant pumps begin to coast-down. In order to remove the decay heat from the reactor core, the passive residual heat removal system (PRHRS) is connected to the steam and feedwater lines.

To maximize the consequences of the SLB-accident, the following assumptions are made:

- The break is located upstream the MSIV, which means that the broken SG cannot be isolated, and thus keeps on depressurizing.

---

\* A SLB-accident is improbable to occur in all cooling loops, but rather in one of the coolant circuits.

- The most effective control rod is assumed to be stuck, hence remains out of the core when the SCRAM is actuated. The location of the most effective control rod is selected to be in the core sector that is close to the broken SG. This leads not only to a reduction of the core shutdown margin, but also to a maximization of the strong radial neutron flux distortion.

## 7.2 Analysis of the SLB-Accident with TRACE/PARCS

The SLB-accident is studied using the coupled code TRACE/PARCS at the HFP-BOL condition. The main results of the performed simulations are discussed in the following subsections. The details of PARCS core model are described under Appendix-A, whereas the TRACE full plant model are described under Appendix-B.

### 7.2.1 Initial and boundary conditions

The initial and boundary conditions for the SLB-accident are listed in Table 7.1. It can be observed that a good agreement is obtained between the TRACE/PARCS solution and reference values. The initial control rods position at HFP condition is presented earlier in chapter 4 at Fig. 4.4.

**Table 7.1: Initial and boundary conditions for the analysis of the SLB-accident**

Parameter	Reference Values	TRACE/PARCS Results
<i>Primary-side</i>		
Core nominal power (MW <sub>th</sub> )	330.0* (Kim et al., 2016)	330.0
Pressurizer pressure (MPa)	15.0* (Kim et al., 2016)	15.0
RCS mass flow rate (kg/s)	2090.0* (Kim et al., 2016)	2090.0
Core mass flow rate (kg/s)	2006.4 (Kim et al., 2016)	2002.2
Core inlet temperature (°C)	295.7 (Kim et al., 2016)	295.9
Core outlet temperature (°C)	323.0 (Kim et al., 2016)	324.1
<i>Secondary-side</i>		
Steam pressure (MPa)	5.2 (Kim et al., 2016)	5.2
Feedwater flow rate (kg/s)	160.8* (Kim et al., 2016)	160.8
Feedwater pressure (MPa)	6.03* (Kim et al., 2016)	6.03
SG secondary coolant inlet temperature (°C)	200* (Kim et al., 2016)	200
SG secondary coolant outlet temperature (°C)	>296.4 (Chung et al., 2015)	299.1

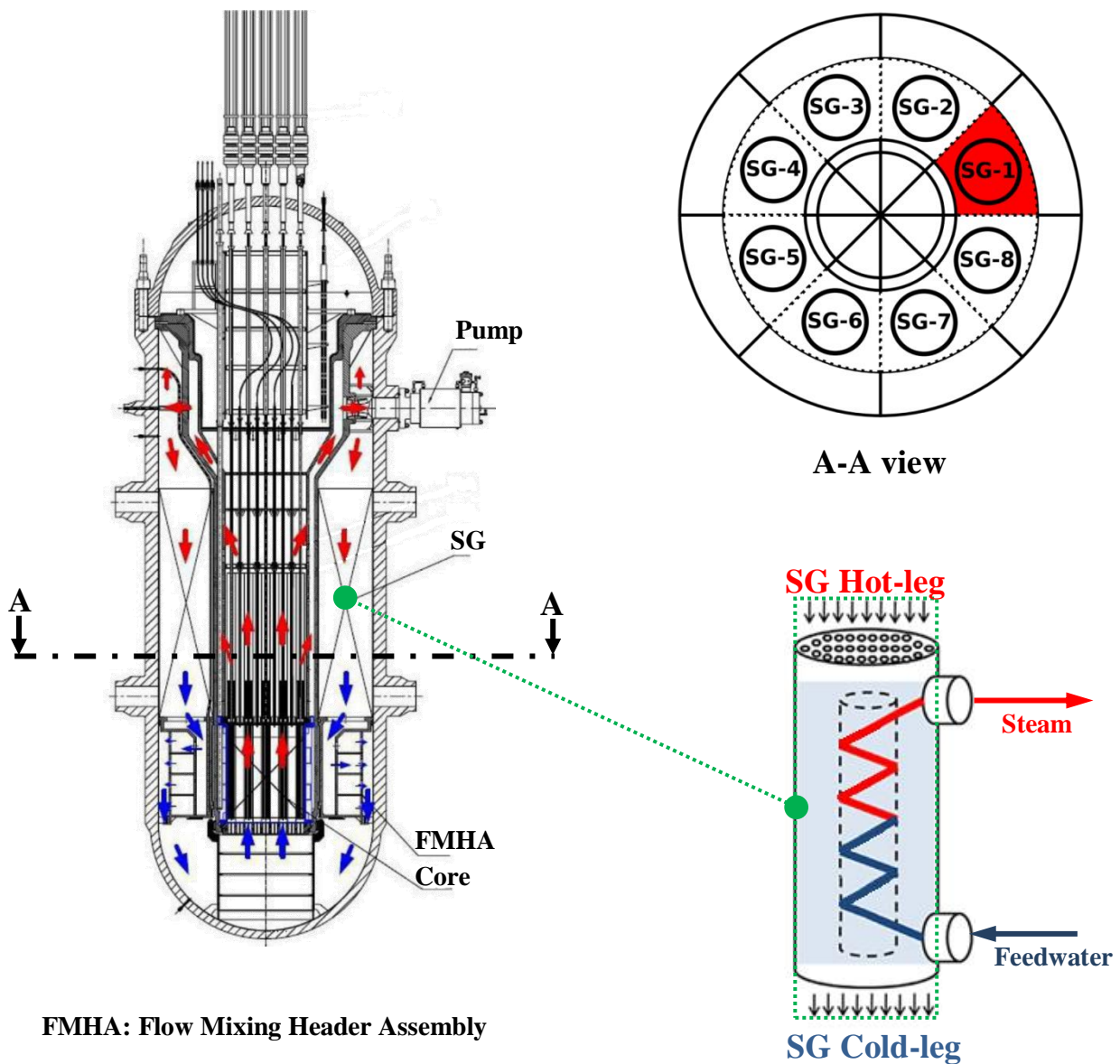
\* Boundary condition

### 7.2.2 Accident progression

The main events following a break of a steam line from one of the eight SGs in the SMART-plant are listed in Table 7.2. The transient starts at time zero followed by breaking the steam line of SG-1 at 50 seconds. The location of SG-1 inside the RPV is depicted in Fig. 7.1 together with the other RPV internal components. The secondary-side of SG-1 and its connection to the PRHRS is illustrated in Fig. 7.2. From that figure, one could also notice that SG-1 and SG-2 are connected to a single heat exchanger of the PRHRS through a single common header.

**Table 7.2: Major events after the SLB-accident**

Sequence of events	Time (s)
SG break initiation	50.00
Reactor trip initiation due to reaching the low steam pressure (2.0 MPa) signal	50.54
Control rods fully inserted	51.48
PRHRS IVs completely open	55.54
Pump rotational speed completely stopped (reaching 0 rpm)	60.10
MSIVs/FIVs completely close	70.54
End of transient calculation	1800.0



FMHA: Flow Mixing Header Assembly

SG: Steam Generator

**Fig. 7.1:** SMART's RPV internal components (Kim et al., 2016) along with a schematic of the RPV discretization (top right) and its connections to the eight SGs.  
 (Note: The steam line of SG-1 is the broken steam line)

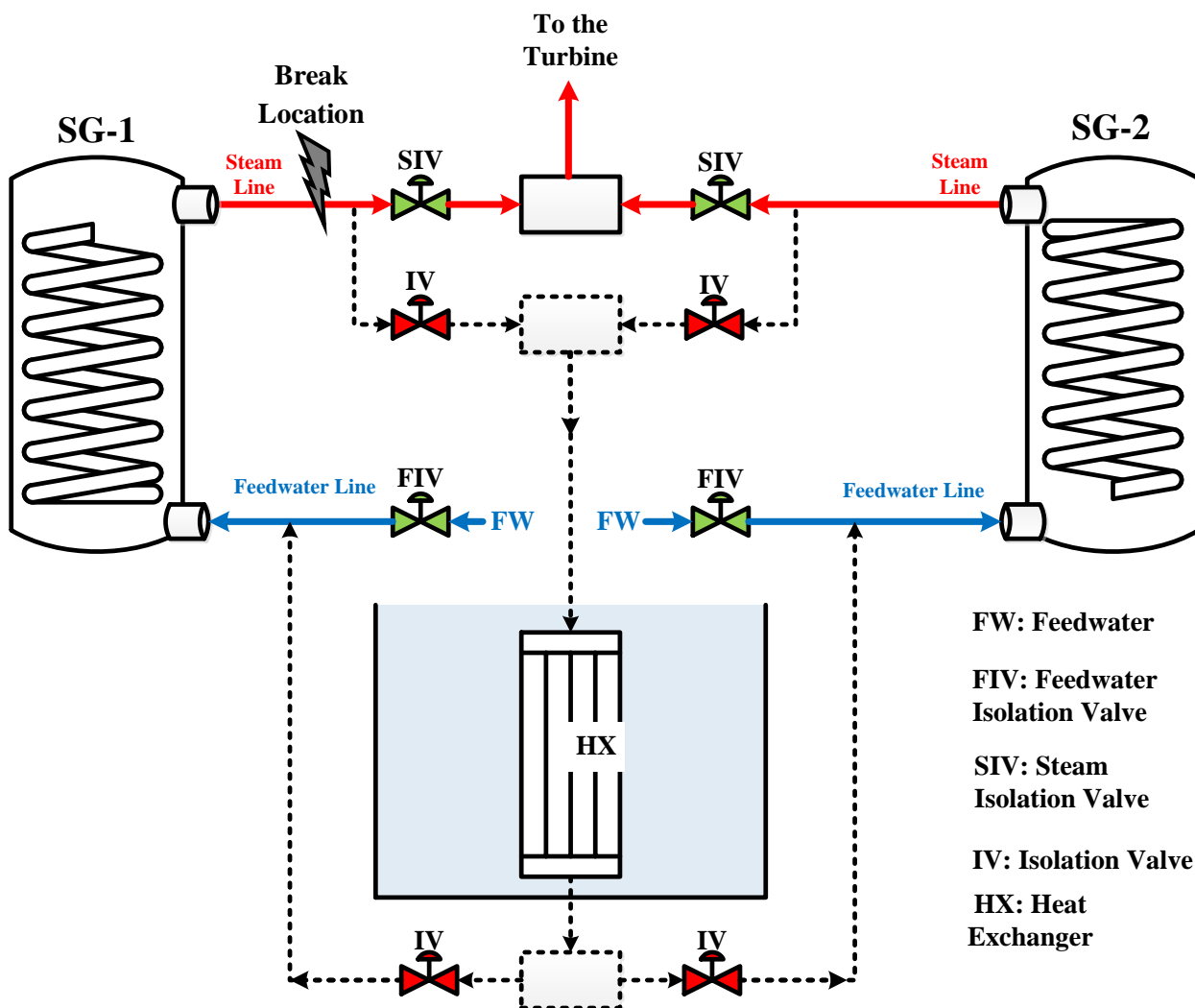


**Fig. 7.2:** A schematic of SMART's secondary-side components and their connections to the passive residual heat removal system (PRHS).

(Note: The steam line of SG-1 is the broken steam line)

The computed temporal evolution of the total core power after the SLB-accident is depicted in Fig. 7.3 along with the overall heat transfer rate from the primary-side of all the SGs to the secondary-side. The spikes-like behavior of the total heat transfer to the secondary-side is due to flow regimes fluctuation between different flow regimes inside the helical tubes of SG-1, which exhibit different heat transfer coefficients, leading to different heat transfer capabilities.

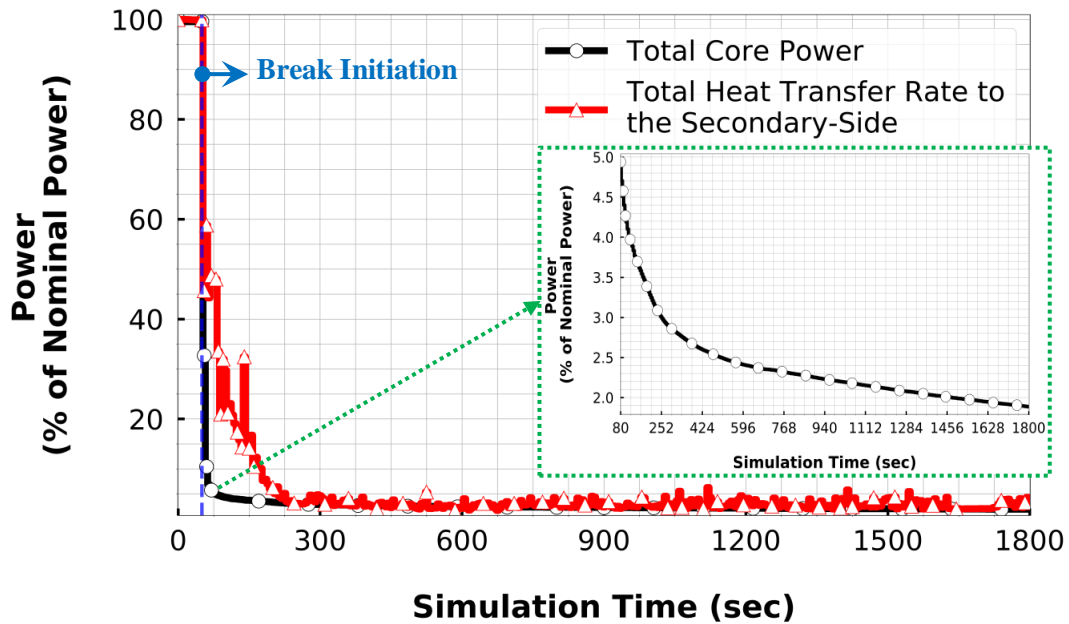


**Fig. 7.3: Computed total core power and heat transfer rate to the secondary-side through all SGs as a function of time after the SLB-accident anticipated at  $t=50s$**

Fig. 7.4 shows the computed temporal behavior of the total heat removal rate through the heat exchangers of the PRHRS. Since both SG-1 and SG-2 are connected into a common header (see Fig. 7.2) and the break location is assumed to be upstream the SIV, then, the steam flow path of both SG-1 and SG-2 is guided through the break (i.e. to the containment of 0.1 MPa). From a different perspective, this can be seen as a loss of one of the PRHRS trains in addition to the steam line break. Hence, the transferred total decay-heat to the PRHRS that is shown in Fig. 7.4 corresponds to only three trains of the PRHRS. Despite that “failure” of one of the PRHRS’s train, one can observe that decay-heat is being effectively removed from the core to the emergency cooldown tank. One can observe also from Fig. 7.4 that the total heat removal rate through the heat exchangers of the PRHRS increased promptly to reach 5% of the nominal core power at about 80 seconds. This prompt increase matches the core decay-heat generated at 80 seconds.

As stated previously that one of the safety concerns of the SLB-accident is the return-to-power after the reactor SCRAM. However, the performed simulation shows that the return-to-power is not a concern for this type of reactor loaded with the designed boron-free core.

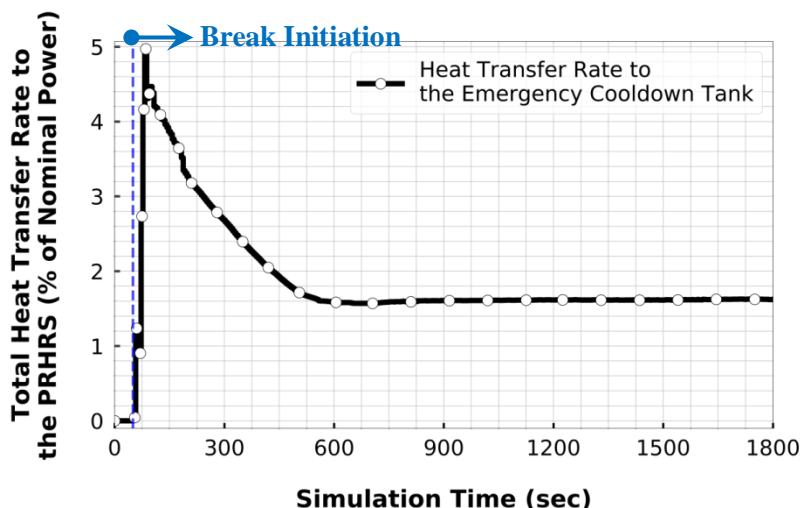


**Fig. 7.4: Computed temporal evolution of the decay-heat removal rate through the PRHRS after the SLB-accident anticipated at t=50s**

After the SLB-initiation, a strong depressurization occurs in the broken steam line causing an overcooling of the primary-side. Since only a single steam line is broken (i.e. the steam line associated with SG-1), a strong temperature variation between different SGs cold-leg is expected as illustrated in Fig. 7.5a. Such an asymmetrical cooling behavior out of SGs cold-leg is terminated at the core inlet thanks to the flow mixing header assembly (see Fig. 7.1) that enhances the flow mixing, and therefore, a homogenous coolant temperature at the core inlet is obtained, as depicted in Fig. 7.5b. Because of the utilization of the 3D cylindrical vessel modeling approach in TRACE for modeling the RPV’s downcomer, the physical phenomena of the coolant mixing behavior is captured.

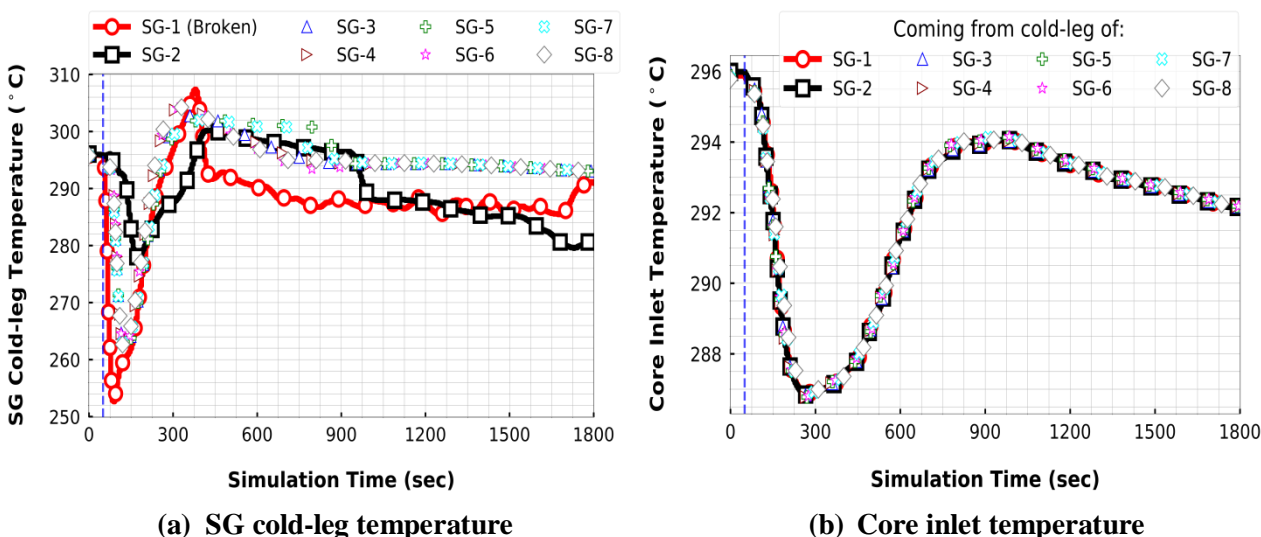


**Fig. 7.5: (a) SG cold-leg and (b) core inlet temperatures behavior as a function of time after the SLB-accident anticipated at t=50s**

Due to the overcooling of the primary-side, a positive reactivity is inserted into the core according to the negative moderator and fuel temperature coefficients. Fig. 7.6 shows the computed total reactivity inserted into the core, which is a sum of control rods (CRs) inserted reactivity, moderator

and fuel temperature reactivity feedbacks, as a function of time following the SLB-accident. A slight increase in the total core reactivity after the SLB-initiation can be observed from Fig. 7.6. This increase is due to the strong positive rise in the moderator temperature reactivity feedback. Although with that increase, the return-to-criticality is not observed; thus, it is not a safety concern for the SMART-plant integrated with the developed boron-free core.

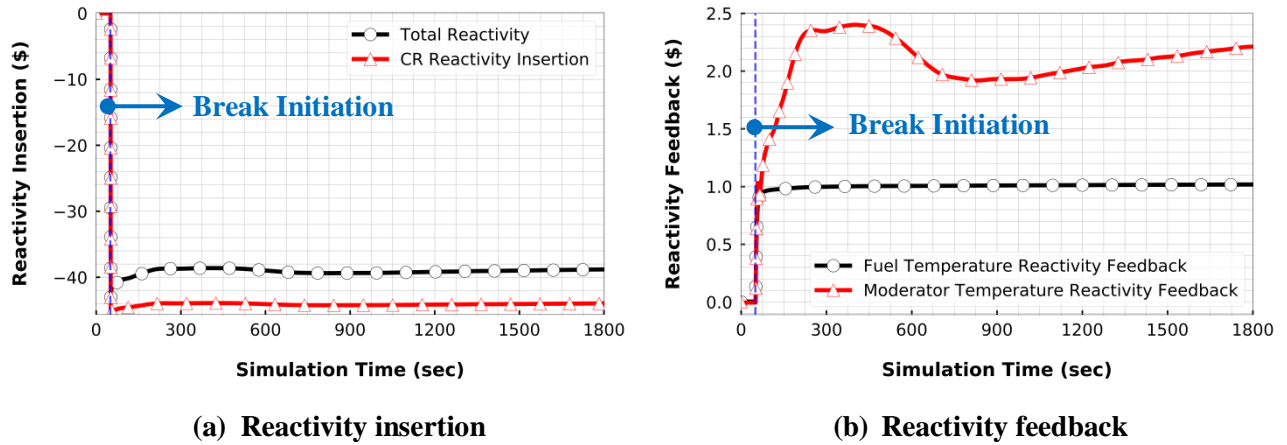


**Fig. 7.6:** (a) Total core reactivity and (b) its three components (i.e. CR reactivity, moderator and fuel temperature reactivity feedbacks) as a function of time following the SLB-accident anticipated at t=50s

To understand the reason for the behavior of the moderator and fuel temperature reactivity feedbacks, one needs to analyze the fuel and moderator temperatures behavior. Fig. 7.7 shows the computed core-averaged fuel and moderator temperatures as a function of time. In that figure, the moderator temperature starts to increase at 525 seconds to reach a maximum temperature after the reactor trip around 900 seconds. Then, it monotonically decreases till the end of the transient calculation. This behavior affects the corresponding moderator reactivity feedback (see Fig. 7.6).

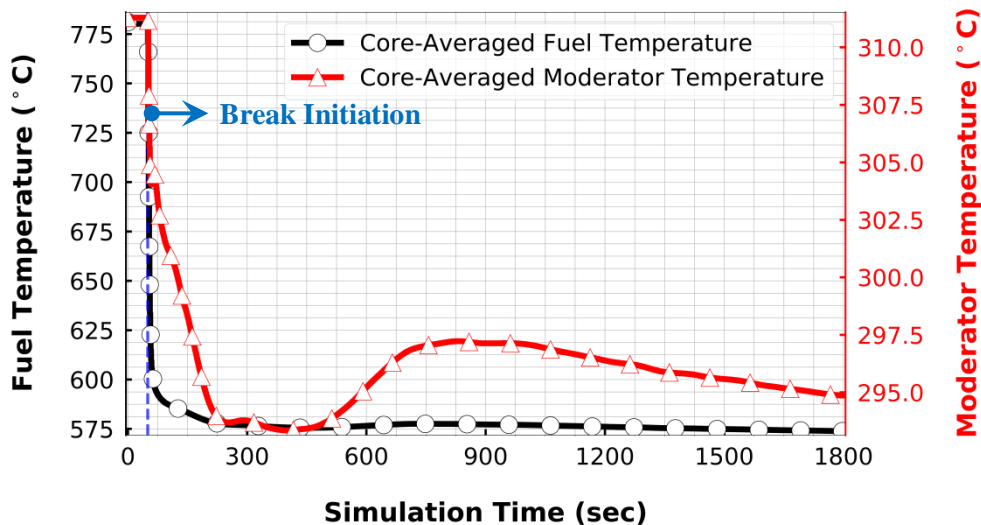


**Fig. 7.7:** Computed core-averaged fuel and moderator temperatures behavior as a function of time following the SLB-accident anticipated at t=50s

This unique behavior of the core-averaged moderator temperature can be explained by analyzing the core inlet mass flow rate following the SLB-accident, which is illustrated in Fig. 7.8. Following the reactor trip at first the reactor coolant pumps coast-down by their inertia, then the core inlet mass flow rate continuously decreases in time. Then at about 265 seconds, natural circulation caused by the coolant density gradient between the core and SGs being located above the core starts to develop. After that at around 1100 seconds, the natural circulation in the primary-side has fully established. From the time the natural circulation starts to develop until being fully established, the coolant stayed a more extended period inside the core which allows the moderator temperature to increase after the SLB-initiation.

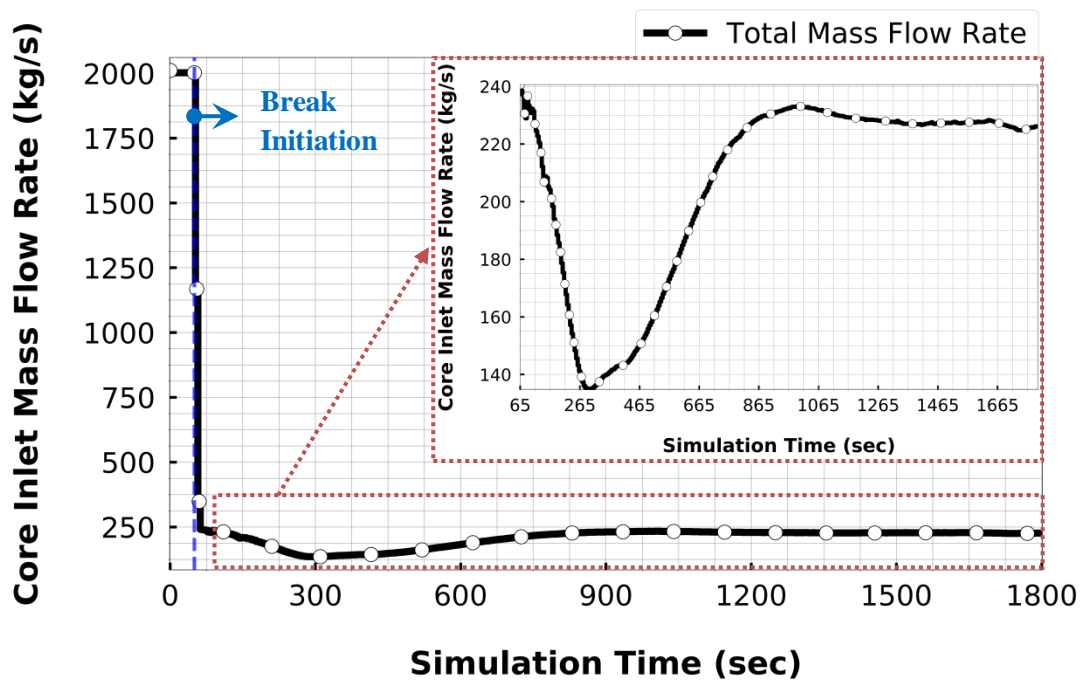


**Fig. 7.8: Computed total core inlet mass flow rate as a function of time after the SLB-accident anticipated at  $t=50s$**

The pressure evolution in the primary and secondary-side is depicted in Fig. 7.9. It can be observed from Fig. 7.9 that the pressure in the primary-side is decreasing due the enhanced heat removal caused by the broken steam line. Furthermore, the pressure in the unbroken steam lines (i.e. connected to SG-3 through SG-8) is increased after closing the steam isolation valves. The steam line pressure increase is caused by the simultaneous opening of the valve connecting the steam line with the PRHRS and the closure of the turbine stop valve. It must be noted that the area of the valve connecting the steam line with the PRHRS is half of the size of the steam line area (see Fig. 7.2). In Fig. 7.9, the pressure in both the broken steam line of SG-1 and the intact steam line of SG-2 go to the containment pressure (i.e. 0.1 MPa) since both steam lines are connected through a common header.

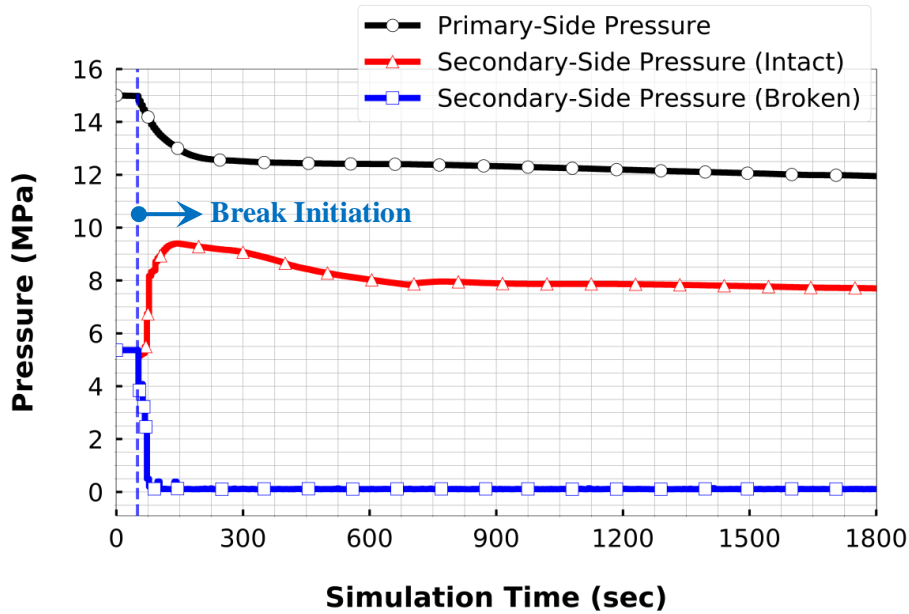


**Fig. 7.9: Computed temporal evolution of primary and secondary-side pressure after the SLB-accident anticipated at t=50s**

The mass flow rate in the secondary-side of the intact steam lines is decreased by closing the feedwater isolation valves as part of the reactor trip actions, as illustrated in Fig. 7.10. It can be observed that two-phase natural circulation is established at around 1200 seconds due to the density gradient between the SGs secondary-side and the PRHRS’s heat exchangers submerged in the emergency coolant tank being located above the SGs.

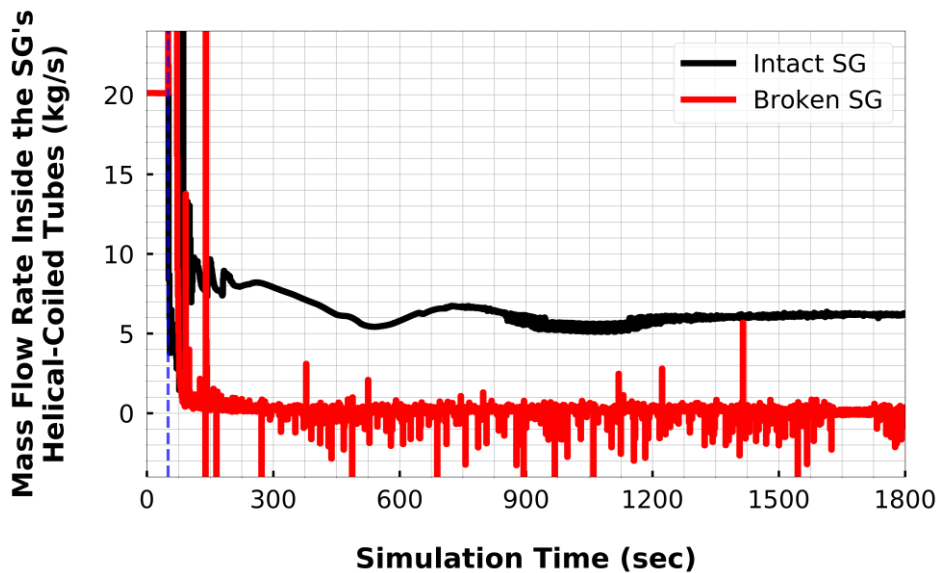


**Fig. 7.10: Computed secondary-side mass flow rate as a function of time after the SLB-accident anticipated at t=50s**

The establishment of an almost constant core inlet mass flow rate caused by natural circulation flow in the primary-side assures a long-term core cooling in the SMART-plant following an SLB-accident without any human intervention and AC-power support as long as the PRHRS is in operation.

### 7.3 Total Loss of the Ultimate Heat Sink Following the SLB-Accident

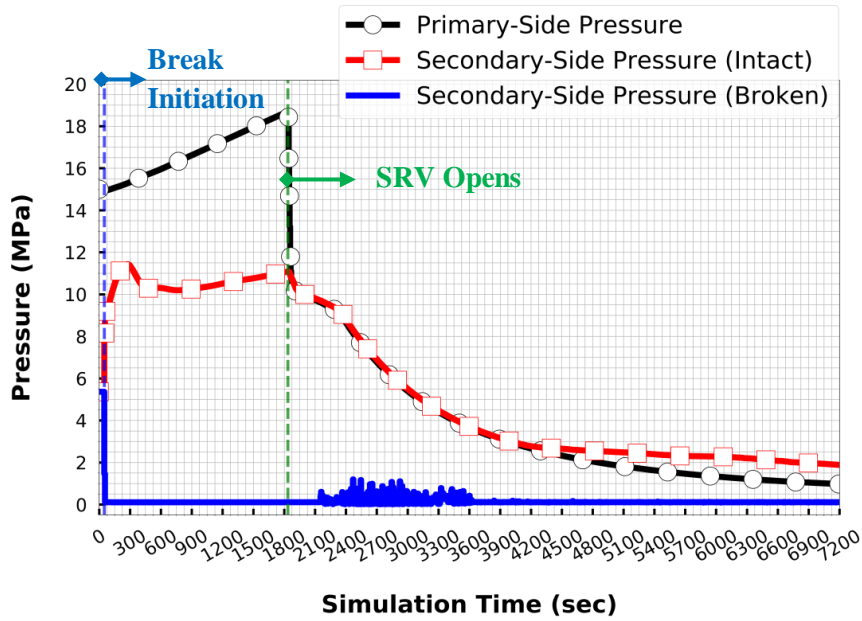
A total loss of the ultimate heat sink following the SLB-accident is categorized as a beyond design basis accident according to (Park et al., 2018) resulting from a hypothetical failure to open the isolation valves connected to the PRHRS following a reactor trip due to an SLB-accident. This scenario is studied to estimate the grace time leading to a potential core uncover without any human intervention and AC-power support. Additionally, a hypothetical failure to operate the passive safety injection system (PSIS) that inject water into the RPV is assumed.

When the total loss of the ultimate heat sink following the SLB-accident occurs, the primary coolant temperature starts to increase due to the inability of removing the generated core decay-heat. With the increase in the coolant temperature, the coolant pressure increases as well till reaching the high-pressure set point of 18.7 MPa (110% of design pressure) (Bae et al., 2001) to open the safety relief valve (SRV). The progression of the main events following the SLB-accident with a complete loss of the PRHRS and PSIS are highlighted in Table 7.3.

**Table 7.3: Major events after a total loss of the ultimate heat sink following the SLB-accident**

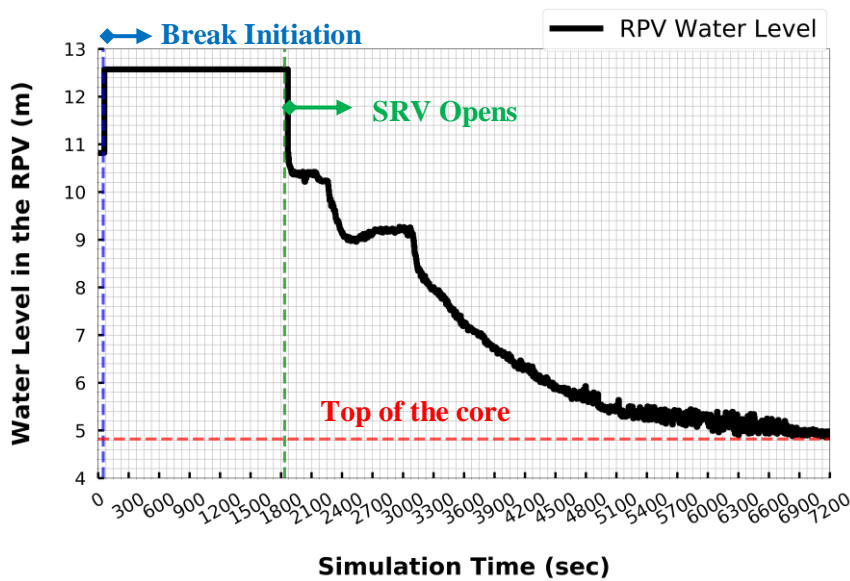
<b>Sequence of events</b>	<b>Time (s)</b>
<b>SG break initiation</b>	50.00
<b>Reactor trip initiation due to reaching the low steam pressure (2.0 MPa) signal</b>	50.54
<b>Control rods fully inserted</b>	51.48
<b>Pump rotational speed completely stopped (reaching 0 rpm)</b>	60.10
<b>MSIVs/FIVs completely close</b>	70.54
<b>The opening of safety relief valve due to reaching high pressurizer pressure (18.7 MPa) set point</b>	1835.0
<b>Core uncover reached</b>	6900.0
<b>End of transient calculation</b>	7200.0

Fig. 7.11 shows the evolution of the primary and secondary pressure following the SLB-accident associated with a complete loss of the PRHRS and PSIS. At first, the primary-side pressure is increasing due to the failure of extracting the decay-heat from the core with a certain time delay attributed to the thermal inertia. The secondary-side pressure of the intact steam lines is increased following the SLB-accident as the MSIVs and FIVs are closed, and the heat is not being removed to the PRHRS. Once the pressure in the primary-side reaches the set point to open the SRV, the pressure in both primary and secondary-sides decreases. In this scenario, it is assumed that the SRV remains stuck at its opening position following its operation.



**Fig. 7.11: Computed temporal evolution of the primary and secondary-side pressure after a total loss of the ultimate heat sink following the SLB-accident anticipated at t=50s**

The main objective of performing this type of hypothetical accident is to evaluate the total grace time available to the reactor operator to take actions in preventing any core degradation. Fig. 7.12 illustrates the variation of the water level inside the RPV as a function of time after a total loss of the ultimate heat sink following the SLB-accident. Fig. 7.12 indicates a grace time available to take actions before reaching core uncover of about two hours. During this time, the operational team has a two hours window to initiate accident management measures to stop the core uncover and avoid core melting. Otherwise, core uncover will start overheating the upper part of fuel rods leading to clad oxidation and start initiating the sever accident early phase phenomena of core degradation.



**Fig. 7.12: Computed water level in the RPV as a function of time after a total loss of the ultimate heat sink following the SLB-accident anticipated at t=50s**

## 7.4 Summary and Perspective

The behavior of the boron-free core integrated into a generic SMART-plant under an SLB-accident at the BOL is studied in this chapter. This investigation revealed that there is a high safety margin against core re-criticality and return-to-power.

The unique design of SMART's steam generator excludes a return-to-power and core re-criticality after a reactor trip. The specific steam generator design has a low secondary-side liquid inventory; thus, the amount of overcooling is limited. Moreover, the SMART-design has eight steam generators in which breaking one of its steam lines represent only a loss of (1/8<sup>th</sup> or 12.5%) of overcooling unlike two-loop PWR designs where SLB-accident results in a 50% of overcooling. In addition, the overcooling amount in the SMART-plant has been reduced due to the existence of the flow mixing header assembly (FMHA) that enhanced the coolant mixing in the downcomer. All these design specific phenomena is captured in this work due to the use of 3D modeling approach to represent the flow inside the SMART's RPV using the TRACE VESSEL component. Because of the FMHA, the core inlet coolant temperature is found uniform even with a break of one of the steam lines.

Following the SLB-accident, the reactor trip signal is initiated to insert all control rods into the core (with an assumption of single failure of the highest control rod worth), reactor coolant pumps start to coast-down, closing of MSIVs and FIVs, opening of IVs connected to the passive residual heat removal system (PRHRS). The objective of the PRHRS is to remove the decay heat without any human actions and AC-power support. In this work, the PRHRS effectiveness is demonstrated and proven to remove core decay heat by means of natural convection establishment in the primary and secondary-sides.

A total loss of the ultimate heat sink following the SLB-accident is then performed with a hypothetical assumption of not being able to open the IVs connected to the PRHRS (i.e. loss of the PRHRS) associated with a failure to operate the passive safety injection system. Thereby, the grace time available to reach core uncover is evaluated. Based on that analysis, about two hours grace time is available for reactor operators to take actions preventing the starts of a core meltdown

## CHAPTER 8: SUMMARY AND CONCLUSIONS

The main objectives of this thesis are the neutronic and thermal-hydraulic development of a boron-free SMR core that can fit into a generic SMART-plant; the demonstration that the developed core and its inherent safety features meet general regulatory requirements; the verification of the core analysis methodology; and the proof that the developed core integrated within the SMART-plant is robust and stable under selected design-basis accidents.

The development of the boron-free SMR core is based on improving core inherent safety features while taking into account many features from the accumulated experience in LWRs such as used material, enrichment, and mechanical structures. Such a development approach pushes for an evolutionary approach where proven technologies from LWRs are used for the core design. However, it limits the degree of innovations in terms of, for instance, having a new type of fuel and cladding material that can further enhance safety, competitiveness, and economics margins (e.g. the accident tolerant fuel concept (IAEA, 2014)).

By removing soluble boron from the moderator, a number of changes on the development of the SMR core are required to fulfill the imposed safety criteria. These changes implied having different enrichment zones radially and axially, the employment of burnable poison rods with different loading schemes, and mixed absorber materials for the control rod design. The developed core has an averaged enrichment of less than 5% with lower enrichment zone in the central core region and higher enrichment in the core periphery. Also, the developed core has two different burnable absorber loading schemes either with 20 or 24 burnable absorber rods per fuel assembly. This variation of loading different burnable absorber rods and with the different enrichment zones minimized the total power peaking factor. In order to (a) reach the required cold zero power shutdown margin (with single failure criteria), (b) reduce the highest control rod worth, and (c) achieve minimum axial offset during normal operation; hybrid (or mixed) absorber materials of the control rods are introduced, and the number of rodded fuel assemblies in the reactor core are increased. All other used materials (e.g. for the fuel pellet and cladding, burnable absorbers, and control rods) corresponds to current LWRs technology. The core development and analysis procedure has been accomplished with a multi-physics framework, including the coupled code PARCS/SUBCHANFLOW. However, it relies on the low order diffusion solver (i.e. PARCS) and the known two-step approximation (i.e. few group cross-section generation, and core simulator).

To verify the predicted core characteristics and safety margins by the used multi-physics framework, a higher order neutron transport solution is provided by the coupled code SERPENT/SUBCHANFLOW. Thereby, the obtained results from the multi-physics framework are found to be within the nuclear cross-section data uncertainties of the higher order solution (i.e. 500 pcm in the core eigenvalue and 5% in nodal power). A potential improvement, to narrow the

discrepancies between the low order approach and the high order solution, exists behind the treatment of the cross-section generation methodology and the modification of the core simulator PARCS. Since the developed core has an axial heterogeneity due to the axial enrichment variations, the generation of nodal neutronics data based on 3D geometries to obtain axial discontinuity factors can preserve the axial leakage between different axial nodes in the core simulator. In addition, PARCS source code modifications are suggested to take these axial discontinuity factors into consideration when solving the diffusion equation. Such a homogenization correction is not needed in modeling typical boron-operated PWRs because they normally have uniform axial fuel composition.

Afterwards, the behavior of the developed core is studied under the following design-basis accidents: control rod ejection, steam line break, and total loss of the ultimate heat sink accidents. This investigation showed that the developed core integrated within a generic SMART-plant has a high safety margin against these types of accidents. Hereafter, a summary of the main outcomes of each accident is presented.

The analysis of core behavior under control rod ejection accident is conducted using two approaches to treat the fuel-clad gap heat transfer coefficient. The first approach follows the legacy methodology of pre-defining the fuel-clad gap heat transfer coefficient as a constant value; while the second one is based on simplified physical models within SUBCHANFLOW describing the phenomena occur inside the fuel-clad gap. By using the first approach to analyze the consequences of control rod ejection accident on the developed core, an underestimation of the maximum fuel centerline temperature is demonstrated in comparison with the more realistic second approach. This outcome emphasizes the need for more advanced thermo-mechanics models to describe fuel behavior during such a transient in a more detailed manner.

The behavior of the developed core integrated within the generic SMART-plant under steam line break accident has also been investigated. That investigation showed a high safety margin against return-to-power and re-criticality following a reactor trip thanks to the control rod design that provided high shutdown margin; and the limited amount of overcooling due to the assumed steam line break of only a single steam generator while the other seven steam generators are unbroken, which represented a loss of 12.5% of cooling. It has also been demonstrated that the core inlet temperature is uniformly distributed following the steam line break accident due to the excellent performance of the flow mixing header assembly, located in the RPV downcomer, which enhanced the coolant mixing.

Last but not the least, an extreme hypothetical accident scenario is studied for the developed core integrated within the generic SMART-plant to simulate a steam line break with an assumed failure of all supporting active and passive safety systems. This accident is considered as a total loss of the ultimate heat sink accidents and it is an initiating event for beyond design basis accidents. The main motivation of studying this extreme accident scenario is to quantify the grace time available to take

preventive actions to preclude core uncovering. That investigation showed a two hour window margin for reactor operators to take preventive actions.



## CHAPTER 9: OUTLOOK

Based on the performed investigations in this dissertation, the key areas for further developments, optimizations and evaluations are listed hereafter; the order of appearance does not reflect any prioritization:

- **Development of a turbulent mixing model in SUBCHANFLOW that can describe the flow mixing phenomena in the presence of spacer grids with mixing vanes.**

Currently, the sub-channel code SUBCHANFLOW can describe the turbulent mixing phenomena using correlations developed during the '70s for spacer grids without mixing vanes. In the case of spacer grids with mixing vanes existence, a user-defined constant value for the two-phase mixing and cross-flow resistance coefficients is the only available option to capture the mass flux lateral exchange between sub-channels and lateral pressure drop. It is well-understood that the heat transfer from the fuel rod surface to the coolant bulk flow is strongly dependent on the local flow conditions. Hence, better physical modeling of the turbulent phenomena would result in improved estimation of local heat fluxes. Therefore, possible improvement of safety margins (i.e. DNBR). Instead of developing a correlation for a specific spacer grids design, (Blyth and Avramova, 2017) suggested a solution to overcome that problem through a method called “*Physics-based Approach for High-to-Low Model Information*” which encourages the use of high-fidelity CFD-informed models for spacer grid-enhanced cross-flow, spacer grid loss coefficient calculations, and spacer grid-enhanced heat transfer models. These modifications were applied to the sub-channel code CTF with the help of the CFD code STAR-CCM+. Such an approach could be improved and applied to SUBCHANFLOW.

- **Development of a dedicated critical heat flux correlation for the developed fuel assembly design which covers the reactor operating conditions during normal and abnormal conditions.**

One of the key safety parameters in evaluating PWR safety is the DNBR which represents the ratio of the critical heat flux over the local heat flux. The critical heat flux is strongly related to the understanding of the boiling crisis phenomena, which is still complicated nowadays, that requires the understanding of bubble formation and diffusion mechanism. The understanding of these two phenomena is needed to explain the mechanism behind the transition from nucleate boiling to film boiling. Instead, nuclear fuel vendors nowadays develop an experimental setup to determine the heat flux value that causes a sudden decrease in the efficiency of the heat transfer from fuel rod surface to the coolant, namely the critical heat flux, at different thermal-hydraulics conditions. Thus, it is suggested out-of-this-work to initiate an experimental investigation to find the critical heat flux correlation for the developed fuel assembly design, and therefore, determine the DNBR using SUBCHANFLOW.

- **Development of advanced optimization algorithms for fuel assembly design, core and control rods arrangements, and fuel reloading pattern optimization.**

Traditionally, nuclear reactor core designs and optimizations are accomplished through iterative trade-off studies between conflict requirements due to the many variables involved (large search space). Alternatively, an approach based on the computational-intelligence field has recently gained popularity in the nuclear area that includes the use of evolutionary algorithms such as the genetic algorithm (GA) to optimize e.g. a gas cooled fast breeder reactor design (Kumar and Tsvetkov, 2015), fuel initial loading and reshuffling of a high-power fast breeder (BN type) reactors (Sobolev et al., 2017) and PWRs (Israeli and Gilad, 2018).

The development of the GA was inspired by Darwin theory of biological evolution that basically finds the most fitted individual (solution) to survive from certain conditions (optimization objectives) after many generations. GA is a global optimization technique based on a stochastic methodology that does not get trapped in local optima, unlike other calculus-based methods which depend on derivatives to find an optimal solution. For that, GA is more suitable for multi-objective problems as in the nuclear reactor core design. However, its drawback is the need for many simulations of each population (i.e. possible solution). A solution to overcome this problem is through the development of a hybrid approach that is based on the concept of fast search tools with approximate models (or reduced-order models) to mimic a reactor simulation code. Other nature-inspired optimization algorithms, e.g. ant-colony (Machado and Schirru, 2002) (Lin and Lin, 2012), artificial bee-colony (Safarzadeh et al., 2011) and particle swarm optimizations (Meneses et al., 2009), have been briefly explored in the nuclear area. Henceforth, it is suggested to study and apply one of these advanced optimization algorithms to further optimize the proposed boron-free core concept.

- **Evaluation of fuel cycle and management options of the developed core.**

Fuel cycle analysis is necessary to demonstrate the cycle length of the developed core. In addition to the safety optimization objective proposed within this dissertation, the fuel cycle analysis requires an additional optimization related to a number of energy-economics factors; including, cycle length, end-of-cycle (EOC) exposure, cycle capacity factor. While the once-through fuel cycle approach, adopted by many boron-free SMR concepts such as B&W mPower (Erighin, 2012) aims to reduce the outages periods, it may result in fuel under-utilization, in contrast to the multi-batch approach. Thus, it is suggested to investigate these two approaches to select the most appropriate one in terms of fulfilling safety and energy-economics objectives. Afterward, it is proposed to study the core behavior at the EOC under selected design-basis accidents, for instance, control rod ejection and steam line break accidents.

- **Uncertainty quantification and sensitivity analysis within a multi-physics framework to quantify their impact on key safety parameters.**

One of the current trends in the nuclear science community is the assessment of uncertainties and their impact on integral (e.g. feedback coefficients) or local (e.g. DNBR) safety parameters. These uncertainties could be originating from nuclear data (e.g. cross-sections, emission spectra, etc.), thermal-hydraulics correlations (e.g. CHF correlations), material composition, and manufacturing process. In that effort, the benchmark for uncertainty analysis in modeling (UAM) for the design, operation and safety analysis of LWRs (OECD/NEA, 2013) has been formulated to tackle the challenges behind that area of study. Therefore, it is proposed to (a) define a framework to propagate uncertainties originating from different sources through coupled codes (e.g. the in-house coupled code PARCS/SUBCHANFLOW/TRANSURANUS) to find key safety parameters with an associated confidence interval; and (b) decide where additional efforts needed to be undertaken to reduce uncertainties.

- **Evaluating the need for the flow mixing header assembly located inside the SMART RPV from a safety perspective.**

From the study of the impact of steam line break accidents on the developed core integrated within SMART-plant, a large margin against the return-to-criticality and power is found to be available. Hence, the following question is formulated: From a safety perspective, is there a need to include the flow mixing header assembly while there is a large safety margin, in which this component requires maintenance, inspection, and strict quality control to be within the RPV?

- **Development of a calculation line for routine nodal data generation at pin level with homogenization correction for a more accurate determination of local safety parameters.**

Key safety parameters such as DNBR, fuel enthalpy rise, linear heat generation rate, etc. are expressed at fuel pin level. Traditionally, core simulators (e.g. PARCS, SIMULATE) employ the pin-power reconstruction method to find local safety information. However, the accuracy of this methodology is limited to typical LWRs design, more details about the shortcoming of the pin-power reconstruction method is highlighted in chapter 3. Therefore, it is proposed to generate the needed nodal data at pin level for the proposed core design to account for local thermal-hydraulics feedback on the cross-sections. To improve the accuracy of the proposed methodology, it is suggested to implement one of the famous homogenization corrections: super-homogenization factors (SPH) (Hébert, 1993) or interface discontinuity factors (IDF) (Smith, 1986).

## REFERENCES

- Alzaben, Y., Sanchez-Espinoza, V.H., Stieglitz, R., 2019a. Core neutronics and safety characteristics of a boron-free core for Small Modular Reactors. *Annals of Nuclear Energy*, vol. 132, pp. 70–81. <https://doi.org/10.1016/j.anucene.2019.04.017>
- Alzaben, Y., Sanchez-Espinoza, V.H., Stieglitz, R., 2019b. Analysis of a control rod ejection accident in a boron-free small modular reactor with coupled neutronics/thermal-hydraulics code. *Annals of Nuclear Energy*, vol. 134, pp. 114–124. <https://doi.org/10.1016/j.anucene.2019.06.009>
- Avramova, M., Ivanov, K., Kozlowski, T., Pasichnyk, I., Zwermann, W., Velkov, K., Royer, E., Yamaji, A., Gulliford, J., 2015. Multi-physics and multi-scale benchmarking and uncertainty quantification within OECD/NEA framework. *Annals of Nuclear Energy*, vol. 84, pp. 178–196. <https://doi.org/10.1016/j.anucene.2014.12.014>
- Bae, K.H., 2018. Safety Analysis for the Major DBAs in Passive PWR SMART [Presentation]. Presented at Nuclear Safety Analysis Symposium of KAERI-KACARE, 28-29 June, Daecheon, South Korea.
- Bae, K.H., Kim, H.C., Chang, M.H., Sim, S.K., 2001. Safety evaluation of the inherent and passive safety features of the smart design. *Annals of Nuclear Energy*, vol. 28, pp. 333–349. [https://doi.org/10.1016/S0306-4549\(00\)00057-8](https://doi.org/10.1016/S0306-4549(00)00057-8)
- Baiocco, G., Petrucci, A., Bznuni, S., Kozlowski, T., 2017. Analysis of a small PWR core with the PARCS/Helios and PARCS/Serpent code systems. *Annals of Nuclear Energy*, vol. 107, pp. 42–48. <https://doi.org/10.1016/j.anucene.2017.04.008>
- Barber, D.A., Downar, T.J., Wang, W., 1998. Final Completion Report for the Coupled RELAP5/PARCS. Technical report of Purdue University, School of Nuclear Engineering, PU/NE-98-31.
- Basualdo, J.R., Sánchez-Espinoza, V.H., Stieglitz, R., Macián-Juan, R., 2017. PARCS-SUBCHANFLOW-TRANSURANUS Multiphysics Coupling for Improved PWR's Simulations, in: *Proceedings of International Congress on Advances in Nuclear Power Plants (ICAPP)*. Fukui and Kyoto, Japan. April 24-28. Paper ID: 17096
- Beam, T.M., Ivanov, K.N., Baratta, A.J., Finnemann, H., 1999. Nodal kinetics model upgrade in the Penn State coupled TRAC/NEM codes. *Annals of Nuclear Energy*, vol. 26, pp. 1205–1219. [https://doi.org/10.1016/S0306-4549\(99\)00006-7](https://doi.org/10.1016/S0306-4549(99)00006-7)
- Bell, G.I., Glasstone, S., 1970. *Nuclear Reactor Theory*. Van Nostrand Reinhold Company, New York, USA. Library of Congress Catalog Card Number 73-122674.
- Berkhan, A., Sánchez, V., Imke, U., 2011. Validation of PWR-Relevant models of SUBCHANFLOW using the NUPEC PSBT data, in: *The 14th International Topical Meeting on Nuclear Reactor Thermalhydraulics (NURETH-14)*. Toronto, Ontario, Canada. Sep. 25-30. Paper ID: 191
- Blyth, T.S., Avramova, M., 2017. Development and Implementation of CFD-Informed Models for the Advanced Subchannel Code CTF. ORNL/TM-2017/191; CASL-U-2017-1308-000. <https://doi.org/10.2172/1355890>
- Calleja, M., Sanchez, V., Jimenez, J., Imke, U., Stieglitz, R., Macián, R., 2014. Coupling of COBAYA3/SUBCHANFLOW inside the NURESIM platform and validation using selected benchmarks. *Annals of Nuclear Energy*, vol. 71, pp. 145–158. <https://doi.org/10.1016/j.anucene.2014.03.036>
- Carbajo, J.J., Yoder, G.L., Popov, S.G., Ivanov, V.K., 2001. A review of the thermophysical

- properties of MOX and UO<sub>2</sub> fuels. *Journal of Nuclear Materials*, vol. 299, pp. 181–198.  
[https://doi.org/10.1016/S0022-3115\(01\)00692-4](https://doi.org/10.1016/S0022-3115(01)00692-4)
- Casal, J., Stamm'ler, R., Villarino, E., Ferri, A., 1991. HELIOS: Geometric Capabilities of a New Fuel-Assembly Program, in: *Proceedings of the International Topical Meeting on Advances in Mathematics, Computation, and Reactor Physics*. Pittsburgh, Pennsylvania, USA. April 28-May 2. Vol. 2, p. 10.2.1:1-13.
- Choi, S., 2015. Small modular reactors (SMRs): the case of the Republic of Korea, in: *Handbook of Small Modular Nuclear Reactors*. Woodhead Publishing in Sawston, Cambridge, UK, pp. 379–407. ISBN 978-0-85709-851-1 <https://doi.org/10.1533/9780857098535.4.379>
- Chung, Y.J., Kim, H.R., Chun, J.H., Kim, S.H., Bae, K.H., 2015. Strength assessment of SMART design against anticipated transient without scram. *Progress of Nuclear Energy*, vol. 85, pp. 617–623. <https://doi.org/10.1016/j.pnucene.2015.08.005>
- Chung, Y.J., Kim, S.H., Kim, H.C., 2003. Thermal hydraulic analysis of SMART for heat removal transients by a secondary system. *Nuclear Engineering and Design*, vol. 225, pp. 257–270. [https://doi.org/10.1016/S0029-5493\(03\)00193-6](https://doi.org/10.1016/S0029-5493(03)00193-6)
- Clifford, P.M., 2015. Technical and Regulatory Basis for the Reactivity-Initiated Accident Acceptance Criteria and Guidance. Office of Nuclear Reactor Regulation, Nuclear Regulatory Commission, USA. Report: ML14188C423
- Daeubler, M., Ivanov, A., Sjenitzer, B.L., Sanchez, V., Stieglitz, R., Macian-Juan, R., 2015. High-fidelity coupled Monte Carlo neutron transport and thermal-hydraulic simulations using Serpent 2/SUBCHANFLOW. *Annals of Nuclear Energy*, vol. 83, pp. 352–375. <https://doi.org/10.1016/j.anucene.2015.03.040>
- Downar, T., Ward, A., Xu, Y., Seker, V., Hudson, N., Barber, D., Larsen, L., Neykov, B., 2017. PARCS v3.3.0 - Volume I: Input Manual. Nuclear Engineering and Radiological Sciences Department, University of Michigan Ann Arbor, MI, USA.
- Ecomatrix, 2009. Investigation of the Environmental Fate of Tritium in the Atmosphere. Canadian Nuclear Safety Commission. Report: INFO-0792. ISBN 978-1-100-13928-9
- Electric Power Research Institute (EPRI), 1989. Elimination of Soluble Boron for a New PWR Design. Report: EPRI-NP-6536, California, USA.
- Erighin, M.A., 2012. A 48-month Extended Fuel Cycle for the B&W mPower™ Small Modular Nuclear Reactor, in: *PHYSOR 2012 - Advances in Reactor Physics - Linking Research, Industry, and Education*. Knoxville, Tennessee, USA. April 15-20. Paper ID: 199
- Franceschini, F., Godfrey, A.T., Stimpson, S., Evans, T., Collins, B., Gehin, J.C., Turner, J., Graham, A., Downar, T., 2015. AP1000® PWR Startup Core Modeling and Simulation with VERA-CS. CASL technical report: CASL-U-2015-0132-000
- Fridman, E., Leppänen, J., 2011. On the use of the Serpent Monte Carlo code for few-group cross section generation. *Annals of Nuclear Energy*, vol. 38, pp. 1399–1405. <https://doi.org/10.1016/J.ANUCENE.2011.01.032>
- García-Herranz, N., Cuervo, D., Sabater, A., Rucabado, G., Sánchez-Cervera, S., Castro, E., 2017. Multiscale neutronics/thermal-hydraulics coupling with COBAYA4 code for pin-by-pin PWR transient analysis. *Nuclear Engineering and Design*, vol. 321, pp. 38–47. <https://doi.org/10.1016/J.NUCENGDES.2017.03.017>
- GE, 2011. General Electric Systems Technology Manual - Chapter 7.4 Standby Liquid Control System [Online]. URL: <https://www.nrc.gov/docs/ML1125/ML11258A347.pdf> (Accessed 28-Mar-2019).

- Godfrey, A., Collins, B., Gentry, C., Stimpson, S., Ritchie, J., 2017. Watts Bar Unit 2 Startup Results with VERA. ORNL/TM-2017/194; CASL-U-2017-1306-000. <https://doi.org/10.2172/1355891>
- Gomez-Torres, A.M., Sanchez-Espinoza, V.H., Ivanov, K., Macian-Juan, R., 2012. DYN SUB: A high fidelity coupled code system for the evaluation of local safety parameters – Part I: Development, implementation and verification. *Annals of Nuclear Energy*, vol. 48, pp. 108–122. <https://doi.org/10.1016/J.ANUCENE.2012.05.011>
- Gómez Torres, A.M., 2011. Further Developments of Multiphysics and Multiscale Methodologies for Coupled Nuclear Reactor Simulations. Dissertation, Faculty of Mechanical Engineering, Technical University of Munich.
- Gonzalez-Vargas, J.A., Sanchez-Espinoza, V.H., Stieglitz, R., Macian-Juan, R., 2018. Development and validation of the new coupled code system TRADYN. *Annals of Nuclear Energy*, vol. 112, pp. 685–692. <https://doi.org/10.1016/J.ANUCENE.2017.07.027>
- Halfinger, J.A., Haggerty, M.D., 2012. The B&W mPower Scalable, Practical Nuclear Reactor Design. *Nuclear Technology*, vol. 178, pp. 164–169. <https://doi.org/10.13182/NT11-65>
- Hébert, A., 1993. A Consistent Technique for the Pin-by-Pin Homogenization of a Pressurized Water Reactor Assembly. *Nuclear Science and Engineering*, vol. 113, pp. 227–238. <https://doi.org/10.13182/NSE92-10>
- Herbert, A., 1980. Développement de la méthode SPH: homogénéisation de cellules dans un réseau non uniforme et calcul des paramètres de réflecteur. Dissertation, University of Paris-Sud. Reactor Design and Development Division, Saclay Nuclear Research Centre. CEA-N-2209.
- IAEA, 2018a. Climate Change and Nuclear Power 2018 [Online]. URL: [https://www-pub.iaea.org/MTCD/Publications/PDF/CCNAP-2018\\_web.pdf](https://www-pub.iaea.org/MTCD/Publications/PDF/CCNAP-2018_web.pdf) (Accessed 28-Mar-2019).
- IAEA, 2018b. Advances in Small Modular Reactor Technology Developments [Online]. URL: [https://aris.iaea.org/publications/smr-book\\_2018.pdf](https://aris.iaea.org/publications/smr-book_2018.pdf) (Accessed 4-Apr-2019).
- IAEA, 2014. Accident Tolerant Fuel Concepts for Light Water Reactors. IAEA TECDOC Series No. 1797. ISBN 978-92-0-105216-2.
- IAEA, 2011. Status report 81- Advanced Passive PWR (AP 1000) [Online]. URL: <https://aris.iaea.org/pdf/ap1000.pdf> (Accessed 4-Apr-2019).
- IAEA, 2006. Fundamental Safety Principles. IAEA Safety Standard Series No. SF-1, Vienna. ISBN 92-0-110706-4.
- IAEA, 2003. Accident Analysis for Nuclear Power Plants with Pressurized Water Reactors. IAEA Safety Reports Series No. 30, Vienna. ISBN 92-0-110603-3.
- IAEA, 1996. Defence in Depth in Nuclear Safety. IAEA INSAG Reports Series No. 10, Vienna. ISBN 92-0-103295-1.
- IAEA, 1981. Handling of Tritium-Bearing Wastes. IAEA Technical Reports Series No. 203, Vienna. ISBN 92-0-125081-9.
- Imke, U., Sanchez, V., Gomez-Torres, A.M., 2010. SUBCHANFLOW: A New Empirical Knowledge Based Subchannel Code, in: Jahrestagung Kerntechnik. Berlin, Germany. May 4-6. Paper ID: 202
- Imke, U., Sanchez, V.H., 2012. Validation of the subchannel code SUBCHANFLOW using the NUPEC PWR tests (PSBT). *Science and Technology of Nuclear Installations*, vol. 2012, Article ID 465059, 12 pages. <https://doi.org/10.1155/2012/465059>
- Israeli, E., Gilad, E., 2018. Novel genetic algorithm for loading pattern optimization based on core

- physics heuristics. *Annals of Nuclear Energy*, vol. 118, pp. 35–48. <https://doi.org/10.1016/J.ANUCENE.2018.03.042>
- Ivanov, A., Sanchez, V., Stieglitz, R., Ivanov, K., 2013. High fidelity simulation of conventional and innovative LWR with the coupled Monte-Carlo thermal-hydraulic system MCNP-SUBCHANFLOW. *Nuclear Engineering and Design*, vol. 262, pp. 264–275. <https://doi.org/10.1016/J.NUCENGDES.2013.05.008>
- Jackson, C.J., Cacuci, D.G., Finnemann, H.B., 1999. Dimensionally Adaptive Neutron Kinetics for Multidimensional Reactor Safety Transients—I: New Features of RELAP5/PANBOX. *Nuclear Science and Engineering*, vol. 131, pp. 143–163. <https://doi.org/10.13182/NSE99-A2025>
- Jaeger, W., Manes, J.P., Imke, U., Escalante, J.J., Espinoza, V.S., 2013. Validation and comparison of two-phase flow modeling capabilities of CFD, sub channel and system codes by means of post-test calculations of BFBT transient tests. *Nuclear Engineering and Design*, vol. 263, pp. 313–326. <https://doi.org/10.1016/J.NUCENGDES.2013.06.002>
- Jessee, M.A., DeHart, M.D., 2017. TRITON: A Multipurpose Transport, Depletion, and Sensitivity and Uncertainty Analysis Module. SCALE Code System Version 6.2.2. Technical Report No. ORNL/TM-2005/39. Oak Ridge National Laboratory, Oak Ridge, Tennessee, USA.
- Jessee, M.A., Wieselquist, W.A., Evans, T.M., Hamilton, S.P., Jarrell, J.J., Kim, K.S., Lefebvre, J.P., Lefebvre, R.A., Merturek, U., Thompson, A.B., Williams, M.L., 2014. Polaris : a New Two-Dimensional Lattice Physics Analysis Capability for the SCALE Code System, in: *PHYSOR 2014 - The Role of Reactor Physics toward a Sustainable Future*. Kyoto, JAPAN. Sep. 28 - Oct. 3. Paper ID: 1127872
- Jiménez Escalante, J., 2010. Desarrollo e implementación de la descomposición en subdominios del acoplamiento neutrónico-termohidráulico mediante disecciones alternadas con un sistema de cálculo multiescala. Dissertation, Escuela Técnica Superior de Ingenieros Industriales, Universidad Politécnica de Madrid.
- Keung Koo Kim, Wonjae Lee, Shun Choi, Hark Rho Kim, Jaejoo Ha, 2014. SMART: The First Licensed Advanced Integral Reactor. *Journal of Energy and Power Engineering*, vol. 8, pp. 94–102. <https://doi.org/10.17265/1934-8975/2014.01.011>
- Kim, H.C., Chung, Y., Bae, K.H., Zee, S.Q., 2003. Safety Analysis of SMART, in: *GENES4/ANP2003: International Conference on Global Environment and Advanced Nuclear Power Plants*. Kyoto, JAPAN. Sep. 15-19. Paper ID: 1050.
- Kim, Y.I., Bae, Y., Chung, Y.J., Kim, K.K., 2015. CFD simulation for thermal mixing of a SMART flow mixing header assembly. *Annals of Nuclear Energy*, vol. 85, pp. 357–370. <https://doi.org/10.1016/j.anucene.2015.05.019>
- Kim, Y.S., Bae, S.W., Cho, S., Kang, K.H., Park, H.S., 2016. Application of direct passive residual heat removal system to the SMART reactor. *Annals of Nuclear Energy*, vol. 89, pp. 56–62. <https://doi.org/10.1016/j.anucene.2015.11.025>
- Koebke, K., Hetzelt, L., 1985. On the Reconstruction of Local Homogeneous Neutron Flux and Current Distributions of Light Water Reactors from Nodal Schemes. *Nuclear Science and Engineering*, vol. 91, pp. 123–131. <https://doi.org/10.13182/NSE85-A27435>
- Kozlowski, T., Downar, T.J., 2007. OECD/NEA and U.S. NRC PWR MOX/ $\text{UO}_2$  Core Transient Benchmark – Final Report. OECD/NEA Report No. 6048. ISBN 92-64-02330-5.
- Kozmenkov, Y., Kliem, S., Rohde, U., 2015. Validation and verification of the coupled neutron kinetic/thermal hydraulic system code DYN3D/ATHLET. *Annals of Nuclear Energy*, vol. 84, pp. 153–165. <https://doi.org/10.1016/j.anucene.2014.12.012>

- KTA, 2012. Design of Reactor Cores of Pressurized Water and Boiling Water Reactors; Part 2: Neutron-Physical Requirements for the Design and Operation of the Reactor Core and Adjacent Systems. Safety Standards Report No. 3101.2 of the Nuclear Safety Standards Commission (KTA), Germany.
- Kumar, A., Tsvetkov, P. V., 2015. A new approach to nuclear reactor design optimization using genetic algorithms and regression analysis. *Annals of Nuclear Energy*, vol. 85, pp. 27–35. <https://doi.org/10.1016/J.ANUCENE.2015.04.028>
- Lamarsh, J.R., Baratta, A.J., 2001. *Introduction to Nuclear Engineering*, 3<sup>rd</sup> Ed. ed. Prentice-Hall Inc. ISBN 0-201-82498-1
- Langenbuch, S., Velkov, K., 2005. Overview on the Development and Application of the Coupled Code System ATHLET-QUABOX/CUBBOX, in: *Mathematics and Computation, Supercomputing, Reactor Physics and Nuclear and Biological Applications*. American Nuclear Society, Palais des Papes, Avignon, France. Sep. 12-15. Paper ID: 163
- Leppänen, J., Mattila, R., 2016. Validation of the Serpent-ARES code sequence using the MIT BEAVRS benchmark – HFP conditions and fuel cycle 1 simulations. *Annals of Nuclear Energy*, vol. 96, pp. 324–331. <https://doi.org/10.1016/J.ANUCENE.2016.06.014>
- Leppänen, J., Mattila, R., Pusa, M., 2014. Validation of the Serpent-ARES code sequence using the MIT BEAVRS benchmark – Initial core at HZP conditions. *Annals of Nuclear Energy*, vol. 69, pp. 212–225. <https://doi.org/10.1016/J.ANUCENE.2014.02.014>
- Leppänen, J., Pusa, M., Viitanen, T., Valtavirta, V., Kaltiainenaho, T., 2015. The Serpent Monte Carlo code: Status, development and applications in 2013. *Annals of Nuclear Energy*, vol. 82, pp. 142–150. <https://doi.org/10.1016/j.anucene.2014.08.024>
- Lin, C., Lin, B.-F., 2012. Automatic pressurized water reactor loading pattern design using ant colony algorithms. *Annals of Nuclear Energy*, vol. 43, pp. 91–98. <https://doi.org/10.1016/J.ANUCENE.2011.12.002>
- Liu, Z., Smith, K., Forget, B., Ortensi, J., 2018. Cumulative migration method for computing rigorous diffusion coefficients and transport cross sections from Monte Carlo. *Annals of Nuclear Energy*, vol. 112, pp. 507–516. <https://doi.org/10.1016/j.anucene.2017.10.039>
- Machado, L., Schirru, R., 2002. The Ant-Q algorithm applied to the nuclear reload problem. *Annals of Nuclear Energy*, vol. 29, pp. 1455–1470. [https://doi.org/10.1016/S0306-4549\(01\)00118-9](https://doi.org/10.1016/S0306-4549(01)00118-9)
- Manno, V.P., Golay, M.W., 1985. Nuclear power plant design innovation through simplification. *Nuclear Engineering and Design*, vol. 85, pp. 315–325. [https://doi.org/10.1016/0029-5493\(85\)90231-6](https://doi.org/10.1016/0029-5493(85)90231-6)
- Meneses, A.A. de M., Machado, M.D., Schirru, R., 2009. Particle Swarm Optimization applied to the nuclear reload problem of a Pressurized Water Reactor. *Progress in Nuclear Energy*, vol. 51, pp. 319–326. <https://doi.org/10.1016/J.PNUCENE.2008.07.002>
- Mignot, G., Royer, E., Rameau, B., Todorova, N., 2004. Computation of a BWR Turbine Trip with CATHARE-CRONOS2-FLICA4 Coupled Codes. *Nuclear Science and Engineering*, vol. 148, pp. 235–246. <https://doi.org/10.13182/NSE04-A2454>
- Miller, R.M., Downar, T.J., 1999. Completion Report for the Coupled TRAC-M/PARCS Code. Technical Report of Purdue University, School of Nuclear Engineering, PU/NE-99-20.
- Morgan, M.G., 1993. What would it take to revitalize Nuclear Power in the United States? *Environment: Science and Policy for Sustainable Development*, vol. 35, pp. 6–32. <https://doi.org/10.1080/00139157.1993.9929072>

- Nikitin, K., Judd, J., Grandi, G.M., Manera, A., Ferroukhi, H., 2010. Peach Bottom 2 Turbine Trip 2 Simulation by TRACE/S3K Coupled Code, in: PHYSOR 2010 – Advances in Reactor Physics to Power the Nuclear Renaissance. Pittsburgh, Pennsylvania, USA. May 9-14. Paper ID: 62
- NuScale Power, 2012. NuScale Plant Design Overview. Technical Report of NuScale Power, LLC, NP-ER-0000-1198.
- Oberkampf, W.L., Roy, C.J., 2010. Verification and Validation in Scientific Computing. Cambridge University Press, New York, USA. <https://doi.org/10.1017/CBO9780511760396>. ISBN 9780511760396.
- OECD/NEA, 2013. Benchmarks for Uncertainty Analysis in Modelling (UAM) for the Design, Operation and Safety Analysis of LWRs. NEA/NSC/DOC(2013)7.
- OECD/NEA, 2010. Nuclear Fuel Behaviour Under Reactivity-initiated Accident (RIA) Conditions. OECD/NEA Report No. 6847. ISBN 978-92-64-99113-2.
- Oneid, P., 2012. SMR-160: Unconditionally Safe & Economical Green Energy Technology for the 21<sup>st</sup> Century. HOLTEC International, Jupiter, Florida, USA [Online]. URL: <https://www.sseb.org/downloads/AssociateMem-2012/PR/oneid.pdf> (Accessed: 28-Mar-2019)
- Park, H.-S., Bae, H., Ryu, S.-U., Yang, J.-H., Jeon, B.-G., Yun, E., Bang, Y.-G., Yi, S.-J., 2018. Safety-Related Integral Effect Tests with the SMART-ITL Facility for the SMART Design, in: 12th International Topical Meeting on Nuclear Reactor Thermal-Hydraulics, Operation and Safety (NUTHOS-12). Qingdao, China. October 14-18. Paper ID: 767.
- Park, K.B., 2011. SMART: An Early Deployable Integral Reactor for Multi-purpose Applications [Presentation], in: INPRO Dialogue Forum on Nuclear Energy Innovations: CUC for Small & Medium-Sized Nuclear Power Reactors. Vienna, Austria. October 10-14.
- Périn, Y., Velkov, K., 2017. CTF/DYN3D multi-scale coupled simulation of a rod ejection transient on the NURESIM platform. Nuclear Engineering and Technology, vol. 49, pp. 1339–1345. <https://doi.org/10.1016/J.NET.2017.07.010>
- Ramos, E., Roman, J.E., Abarca, A., Miró, R., Bermejo, J.A., Ortego, A., Posada, J.M., 2017. Verification of the Parallel Pin-Wise Core Simulator pCTF/PARCSv3.2 in Operational Control Rod Drop Transient Scenarios. Nuclear Science and Engineering, vol. 187, pp. 254–267. <https://doi.org/10.1080/00295639.2017.1320892>
- Rempe, K.R., Smith, K.S., Henry, A.F., 1989. SIMULATE-3 Pin Power Reconstruction: Methodology and Benchmarking. Nuclear Science and Engineering, vol. 103, pp. 334–342. <https://doi.org/10.13182/NSE89-A23686>
- Rhodes, J.D., Ferrer, R.M., Hykes, J., 2013. CASMO5: A Fuel Assembly Burnup Program User's Manual. Studsvik Scandpower Technical Report No. SSP-07/431 Rev 8, Waltham, MA, USA.
- Romano, P.K., Horelik, N.E., Herman, B.R., Nelson, A.G., Forget, B., Smith, K., 2015. OpenMC: A state-of-the-art Monte Carlo code for research and development. Annals of Nuclear Energy, vol. 82, pp. 90–97. <https://doi.org/10.1016/j.anucene.2014.07.048>
- Rudling, P., Jernkvist, L.O., Garzarolli, F., Adamson, R., Mahmood, T., Strasser, A., Patterson, C., 2016. Nuclear Fuel Behaviour under RIA Conditions. ZIRAT21/IZNA16 Special Topic Report, Advanced Nuclear Technology (ANT) International, Mölnlycke, Sweden.
- Safarzadeh, O., Zolfaghari, A., Norouzi, A., Minuchehr, H., 2011. Loading pattern optimization of PWR reactors using Artificial Bee Colony. Annals of Nuclear Energy, vol. 38, pp. 2218–2226. <https://doi.org/10.1016/J.ANUCENE.2011.06.008>
- Sanchez-Espinoza, V.-H., Marin, V.M., Alzaben, Y., Jimenez, G., Stieglitz, R., 2018. Integral

- SMART Plant Model Development using the System Thermal-Hydraulic Code TRACE for Transient Analysis, in: NUTHOS-12: The 12th International Topical Meeting on Nuclear Reactor Thermal Hydraulics, Operation and Safety. Qingdao, China. October 14-18. Paper ID: 574.
- Sánchez, V., Imke, U., Ivanov, A., Gomez, R., 2010. SUBCHANFLOW: A Thermal-Hydraulic Sub-Channel Program to Analyse Fuel Rod Bundles and Reactor Cores, in: 17th Pacific Basin Nuclear Conference. Cancún, Q.R., México. October 24-30. Paper ID: 17021.
- Schneider, M., Froggatt, A., 2018. The World Nuclear Industry Status Report 2018. Annual Report of WNISR, Paris, France.
- Smith, K.S., 2017. Nodal diffusion methods and lattice physics data in LWR analyses: Understanding numerous subtle details. *Progress in Nuclear Energy*, vol. 101, pp. 360–369. <https://doi.org/10.1016/j.pnucene.2017.06.013>
- Smith, K.S., 1986. Assembly homogenization techniques for light water reactor analysis. *Progress in Nuclear Energy*, vol. 17, pp. 303–335. [https://doi.org/10.1016/0149-1970\(86\)90035-1](https://doi.org/10.1016/0149-1970(86)90035-1)
- Sobolev, A.V., Gazetdinov, A.S., Samokhin, D.S., 2017. Genetic algorithms for nuclear reactor fuel load and reload optimization problems. *Nuclear Energy and Technology*, vol. 3, pp. 231–235. <https://doi.org/10.1016/J.NUCET.2017.07.002>
- Stamm'ler, R.J.J., Abbate, M.J., 1983. *Methods of Steady-State Reactor Physics in Nuclear Design*. Academic Press Inc., London, UK. ISBN 0-12-663320-7.
- Strategic Insights, 2015. Small Modular Reactor Outlook [Online]. URL: <https://strategicinsights.ca/reports/2015-small-modular-reactor-outlook/> (Accessed: 16-May-2018)
- Todreas, N.E., Kazimi, M.S., 2001. *Nuclear Systems II: Elements of Thermal Hydraulic Design*, 1st Ed. ed. Taylor & Francis, New York, USA. ISBN 0-89116-936-9.
- Todreas, N.E., Kazimi, M.S., 1993. *Nuclear Systems I: Thermal Hydraulic Fundamentals*, 2nd Ed. ed. Taylor & Francis, New York, USA. ISBN 0-89116-935-0.
- Tong, L.S., Weisman, J., 1996. *Thermal Analysis of Pressurized Water Reactors*, 3rd Ed. ed. American Nuclear Society, La Grange Park, Illinois, USA. ISBN 978-0-89448-038-6.
- U.S. NRC, 2013. TRACE V5.840 Theory Manual. Division of Safety Analysis, Office of Nuclear Regulatory Research, U. S. Nuclear Regulatory Commission, Washington, DC 20555-0001.
- U.S. NRC, 2017. MAPTAB Input Manual and User Guide. Division of Safety Analysis, Office of Nuclear Regulatory Research, U. S. Nuclear Regulatory Commission, Washington, DC 20555-0001.
- Viitanen, T., Leppanen, J., 2016. New Interpolation Capabilities for Thermal Scattering Data in Serpent 2, in: PHYSOR 2016 - Unifying Theory and Experiments in the 21<sup>st</sup> Century. Sun Valley, Idaho, USA. May 1–5. pp. 1556–1567.
- Viitanen, T., Leppanen, J., 2011. New Data Processing Features in the Serpent Monte Carlo Code. *Journal of the Korean Physical Society*, vol. 59, pp. 1365–1368. <https://doi.org/10.3938/jkps.59.1365>
- Wagner, W., Cooper, J.R., Dittmann, A., Kijima, J., Kretschmar, H.-J., Kruse, A., Mareš, R., Oguchi, K., Sato, H., Stöcker, I., Šifner, O., Takaishi, Y., Tanishita, I., Trübenbach, J., Willkommen, T., 2000. The IAPWS Industrial Formulation 1997 for the Thermodynamic Properties of Water and Steam. *Journal of Engineering for Gas Turbines and Power*, vol. 122, pp. 150-184. <https://doi.org/10.1115/1.483186>

- Western European Nuclear Regulators Association, 2013. Safety of New NPP Designs. A Report of the Reactor Harmonization Working Group (RHWG), WENRA [Online]. URL: [http://www.wenra.org/media/filer\\_public/2013/08/23/rhwg\\_safety\\_of\\_new\\_npp\\_designs.pdf](http://www.wenra.org/media/filer_public/2013/08/23/rhwg_safety_of_new_npp_designs.pdf) (Accessed 4-Apr-2019).
- Westinghouse Electric Corporation, 2005. Westinghouse Technology Systems Manual - Section 2.2 Power Distribution Limits [Online]. URL: <https://www.nrc.gov/docs/ML1122/ML11223A208.pdf> (Accessed 28-Mar-2019).
- World Nuclear Association, 2019a. Nuclear Power in the World Today [Online]. URL: <http://www.world-nuclear.org/information-library/current-and-future-generation/nuclear-power-in-the-world-today.aspx> (Accessed 28-Mar-2019).
- World Nuclear Association, 2019b. Small Nuclear Power Reactors [Online]. URL: <http://www.world-nuclear.org/information-library/nuclear-fuel-cycle/nuclear-power-reactors/small-nuclear-power-reactors.aspx> (Accessed 28-Mar-2019).
- Xu, Y., Downar, T., 2006. GenPMAXS Code for Generating the PARCS Cross Section Interface File PMAXS. Technical Report of Purdue University, School of Nuclear Engineering, PU/NE-00-20 (Rev. 8).



## APPENDIX-A: NEUTRONICS AND THERMAL- HYDRAULICS CORE MODELLING

In this appendix, the models developed to carry-out the neutronics and thermal-hydraulics core optimization as well as for the analysis of control rod ejection accidents will be described hereafter.

### A.1. Nodal Neutronics Data Generation For The Core Simulator

Multi-group constants are one of the key elements to determine the accuracy of neutronics core simulators such as PARCS. In this work, Serpent2 was used for this purpose to generate nodal group constants in the core. For each fuel assembly (FA) type in the core, 2D models are developed using Serpent2 and for different material composition along the active core height. These 2D models represent FA slices in a detailed manner i.e. all pins are modeled explicitly. Then, spatial homogenization and energy-group condensation are carried-out for each FA-2D model using a reflective boundary condition and two-group structure with the two-group separation at 0.625 eV. For each model, group constants are generated for 40 branch variations originating from varying fuel and moderator temperatures, and CR position. The moderator density is changed according to its associated moderator temperature and the reactor operating pressure except at the 300 K where the pressure corresponds to the atmospheric value (i.e. 0.1 MPa). The complete branch structure used in the nodal data generation is listed in Table A.1 that represents the core states under normal and abnormal operating conditions. For every branch calculation with Serpent2, a total of 1 billion active neutron histories divided into 2000 active cycles is used with 500 inactive cycles in order to ensure the convergence of fission source. The large number of active neutron histories is used to reduce the statistical noise associated with generating group-wise form functions that are used later to reconstruct pin powers in PARCS.

The axial reflector (top and bottom) group constants are generated by modeling a 3D FA with Serpent2 using radially reflective and axially black boundary conditions. For the spatial homogenization, the bottom reflector water conditions are set to the core inlet temperature, while the top reflector used the average core outlet temperature. The active fuel region used the average core coolant and fuel temperatures. For the energy-group condensation, the same two-group structure is used as in the FAs energy-group condensation.

The group constants of the radial reflector nodes in the traditional methodology are generated through modeling the core central row FAs surrounded from the right and left with the core baffle and then light water; using black boundary condition along the horizontal plane, and with reflective boundary condition in the other directions.

**Table A.1: Branch structure used in the nodal group constants generation**

	CR Position	$T_{\text{fuel}}$ (K)	$T_{\text{cool}}$ (K)
1	Out/In	300	300
2			590
3		569.15	569.15
4			590
5		900	300
6			569.15
7			590
8			615
9		1200	569.15
10			590
11			615
12		1500	569.15
13			590
14			615
15		1800	569.15
16			590
17			615
18		2100	569.15
19			590
20			615

However, the method used in this thesis is quite different in which the group constants are generated by developing a 3D full core model with Serpent2 using radially and axially black boundary conditions. In this model, the radial reflector and fuel regions are set to the average core coolant and fuel temperatures. The radial reflector is divided into different nodes, in which each node is adjacent to a fuel assembly (see Fig. A.1). Each homogenization region has a size of a single FA where the core baffle is homogenized with the surrounding light water. Thus, for the quarter core geometry, nine unique reflector group constants data are generated for each unique position.

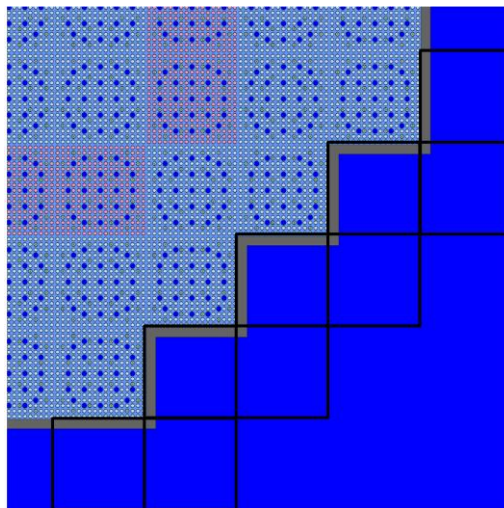


**Fig. A.1: Quarter of a 3D full core model used for the reflector group constants generation. Each box represents a homogenization region. Core baffle is presented in gray color which is surrounded by light water in dark blue color.**

The new developed methodology to generate the radial reflector group constants has an advantage compared to the traditional methodology. This new methodology captures the precise neutron spectrum used in the reflector energy-group condensation process; especially for those reflector nodes that are surrounded by two FAs.

### **A.2. The PARCS Core Model**

The PARCS-neutronic model of the core consists of a radial node per fuel assembly (i.e. in total 57 nodes for the active core) and by 40 nodes representing the radial reflectors, which have the same fuel assembly size. Axially, the core was divided into 22 layers where the top and bottom layers represent the axial reflectors; and the rest 20 axial layers represent the active core. Each 3D node of the core is associated with nodal cross-section sets in dependence of the thermal-hydraulic feedback parameters and the material composition of the different fuel assembly types of the core. A zero-flux boundary condition has been selected for the exterior surfaces (i.e. radially and axially) of the reactor core model.

### **A.3. The SUBCHANFLOW Core Model**

The thermal-hydraulics behavior of the core is modeled by SUBCHANFLOW (SCF) using two approaches: a channel-wise and sub-channel-wise. The channel-wise approach is used for the optimization work with the coupled code PARCS/SCF in which each fuel assembly is represented by a single coolant channel that has an averaged fuel rod divided into 20 equi-spaced axial layers. In each coolant channel: flow area, wetted and heated perimeter, and the number of the heated rods are defined.

Coolant turbulent mixing is a feature being advertised by many sub-channel analysis codes. In this regard, the coolant mixing between sub-channels in the SCF depends on three factors: (i) mixing coefficient; (ii) cross-flow resistance coefficient; and (iii) gap distance between sub-channels. The first two factors are normally empirically determined when spacer grids with mixing vanes exists, as in the optimized core. Whereas, the third factor depends on the geometry of the problem under consideration, in which smaller gap distance is associated when the sub-channel-wise modeling approach is adopted in comparison with channel-wise modeling approach.

Due to the numerical nature of the work performed here, an experimental setup to determine the first two coefficients affecting the coolant mixing is out-of-scope. Instead, the mixing and crossflow resistance coefficients have been determined from validating the SCF using the NUPEC PWR Subchannel and Bundle Tests (PSBT) (Imke and Sanchez, 2012). Therefore, an optimum mixing coefficient between coolant sub-channels of 0.06 is found by fixing the crossflow resistance coefficient at 0.5 and iterating over the mixing coefficient. Based on that finding, one-tenth of that value (i.e. 0.006) is assumed for the mixing coefficient and ten-times increase of the crossflow

resistance coefficient (i.e. 5.0) is adopted for the channel-wise modeling approach. The applied scaling factor to the mixing and crossflow resistance coefficients are simply due to the fact that less turbulent mixing is expected with larger channel volume, as in the case with a single channel represents a single fuel assembly.

In that regard, a sensitivity study has been performed to determine which one of these three factors is mostly contributing to the changes to coolant channel exit temperature at the same thermal-hydraulic boundary conditions. Therein, the gap distance is found to be the largest influential factor on the coolant turbulent mixing. This suggests that the effect of the adopted scaling factor is negligible on the turbulent mixing in the case of channel-wise modeling.

The sub-channel-wise modelling approach is used for predicting local safety parameters using the pin power predicted by the pin-power-reconstruction capability in PARCS. In that model, the mixing and crossflow resistance coefficients have been set to 0.06 and 0.5, respectively, according to the PSBT (Imke and Sanchez, 2012) validation work.

#### A.4. The SERPENT Full Core Model

A detailed 3D full core model is developed with Serpent2 to provide a reference for the PARCS solution. This model included the modelling of the core baffle, barrel, neutron pads, spacer grids, and RPV walls. In that model, the number of neutron histories used is: 700,000 particles per cycle, 1000 active cycles, and 500 inactive cycles to achieve a converged fission source distribution. This resulted in a maximum nodal power statistical uncertainty below 0.1% at  $1\sigma$ . Fig. A.2 shows the Serpent's details full core model.

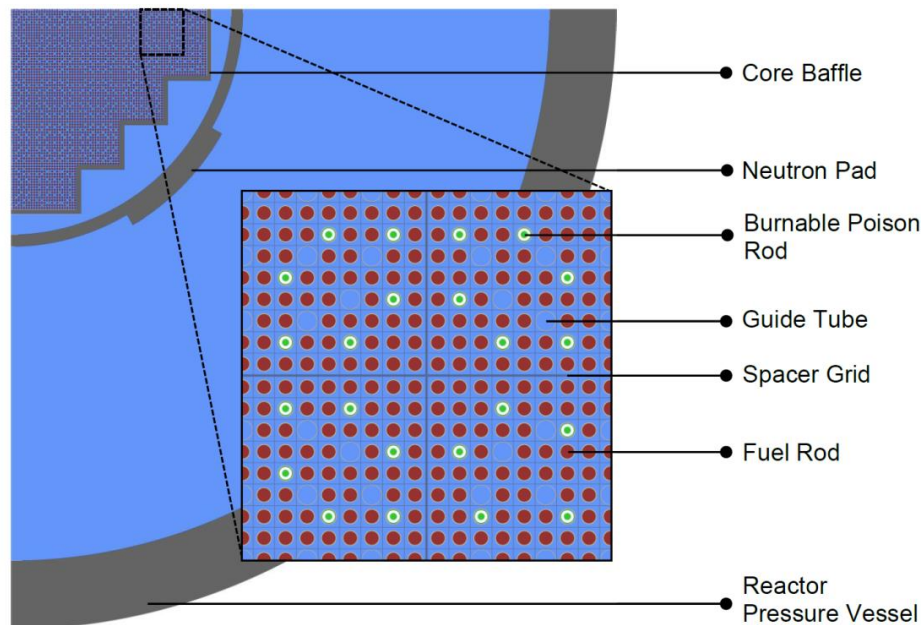


**Fig. A.2: Quarter-core model showing the detailed core structures integrated within SMART RPV (figure was generated from Serpent)**

## APPENDIX-B: SMART SYSTEM THERMAL-HYDRAULICS MODELING USING TRACE

The TRACE system thermal-hydraulics modeling of the SMART-plant consists of the reactor core, steam generators (SGs), pressurizer, reactor pressure vessel (RPV), secondary circuit, and passive residual heat removal system (PRHRS). A brief description of the nodalisations of all these parts is explained in the following sections. A schematic diagram of the TRACE full plant model is shown in Fig. B.1 as generated by the SNAP user interface.

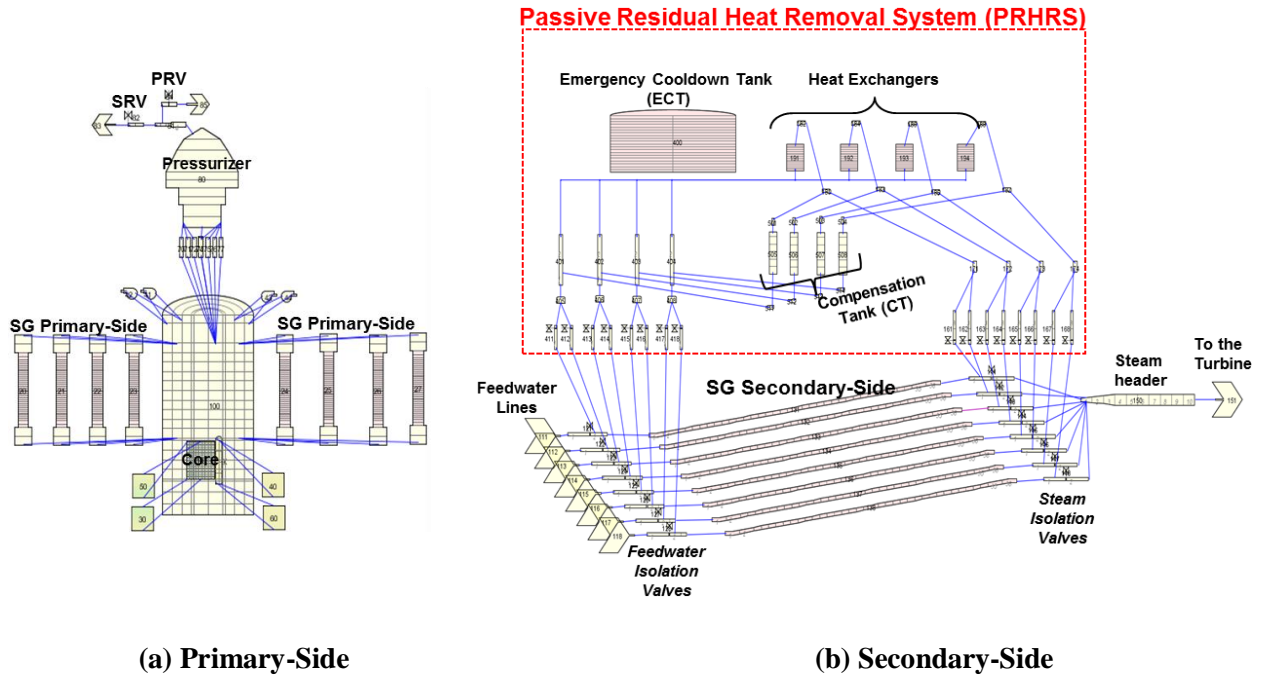


**Fig. B.1: (a) Primary and (b) Secondary Side of the TRACE full plant model and its connections to the PRHRS. (The model is developed through SNAP user interface)**

### B.1. The Core Model in TRACE

The core hydraulics model is described by the 3D CARTESIAN VESSEL component in TRACE. This 3D core model is divided into 57 zones in the radial direction, in which each zone is subdivided into 22 axial meshes (20 meshes are devoted to the active core, and the remaining two meshes are for the bottom and top reflectors) forming a total of 1254 hydraulic cells. In each of these cells, flow area, hydraulic diameter, and form loss coefficients are defined in each x, y, and z-direction allowing for 3D flow path representation.

Each hydraulic cell related to the active core region is connected to a heat structure. Namely, 57 heat structures are modeled to represent the core heat source. Each heat structure is divided into 20 axial meshes where these meshes are one-to-one mapped to the 3D CARTESIAN VESSEL component. This way of modeling the core facilitates a one-to-one data mapping between PARCS and TRACE through defining a proper MAPTAB file. A schematic diagram of the core model and the radial mapping between PARCS and TRACE is presented in Fig. B.2.

Core bypass was modeled in TRACE by a CYLINDRICAL VESSEL, in which flow bypass was controlled by varying flow area.

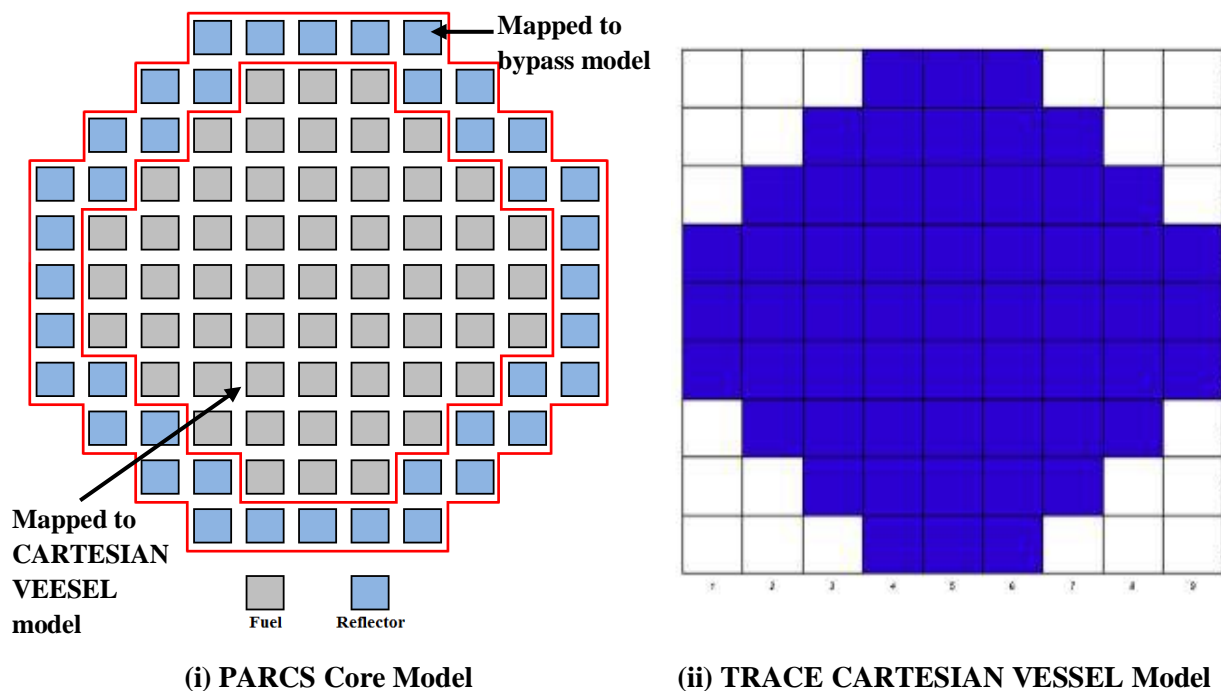


**Fig. B.2: A schematic of the radial mapping of fuel assemblies and reflector nodes from (i) PARCS core model to the (ii) thermal-hydraulic TRACE CARTESIAN VESSEL**

## B.2. Steam Generator Model

The helical-coiled SG model consists of a cassette, helically coiled tubes, and heat structures that thermally connect the upward secondary-coolant that flows inside these tubes with the downward primary-coolant that flows outside the helically coiled tubes. The SG's cassette is divided into 40 axial cells where 36 of these cells are one-to-one connected to the helical-coiled tubes through defining heat structures. Each heat structure is radially subdivided into eight cells to properly calculate the heat transfer through conduction between the tube outer and inner surfaces. Eight SGs is modeled; in which they are symmetrically arranged inside the RPV-model above the core region (see Fig. B.1). To manage the thermal balance between the primary and secondary side during normal operation, the number of helical-coiled tubes were varied to match as much as possible the predicted core inlet coolant temperature with the reference temperature 295.7°C (Kim et al., 2016). From that analysis, it is found that with 327 helical-coiled tubes, a thermal balance between the primary and secondary side can be achieved.

## B.3. Pressurizer Model

The pressurizer model has a pipe of a pressurizer-type component, eight surge lines connected to the RPV model, power-operated relief valve (PRV) and safety relief valve (SRV). These valves are connected to a break component with a pressure of 0.1 MPa representing the containment. The pressurizer pipe is divided into ten axial cells which are partly filled with steam. The pressure during normal operation is set at 15 MPa according to the SMART design (Kim et al., 2016).

## B.4. Reactor Pressure Vessel Model

The RPV-model is represented by a 3D CYLINDRICAL VESSEL component with eight azimuthal, five radial cells and 21 axial cells. Each SG model is connected to an azimuthal sector, which are situated above the reactor core. The connections between the RPV CYLINDRICAL

VESSEL and core CARTESIAN VESSEL are accomplished with vessel junctions though proper flow area consideration. In every cylindrical cell of the RPV model, flow area, hydraulic diameter, and form loss coefficients are defined in each radial, azimuthal, and axial direction. By modeling the RPV and the core as a 3D component, flow mixing in the lower and upper plenums and between fuel assemblies is properly handled.

The flow mixing header assembly (FMHA) has a complex geometry (see Fig. B.3), and is difficult to be precisely modeled with TRACE. The details of the FMHA real geometry can be found in (Kim et al., 2015).

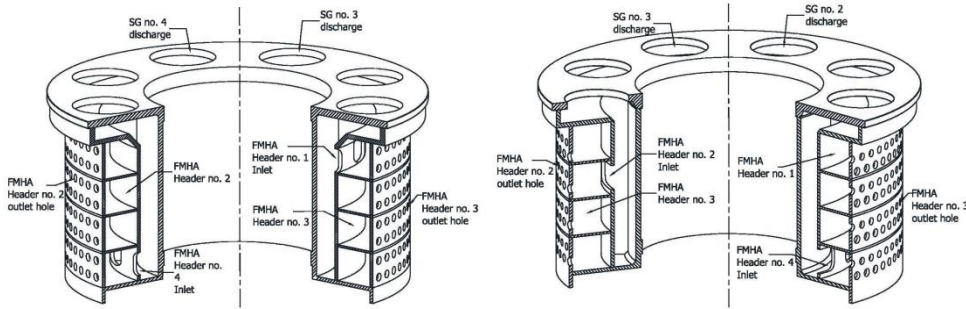


**Fig. B.3: Flow mixing header assembly configuration** (Kim et al., 2015)

To model the FMHA with TRACE and within the RPV model using the 3D CYLINDRICAL VESSEL component, its real geometry was simplified by assuming a symmetrical inner and outer holes distribution. These holes were accounted for by reducing the flow area in the flow direction that passes through these holes, similar to the porous media modeling approach. The FMHA model is located in the annular space below the SGs. The flow path inside the RPV model is shown in Fig. B.4 which was controlled by manipulating with the flow area in each radial, azimuthal, and axial direction to have similar flow path as the one reported within SMART RPV (Kim et al., 2016).

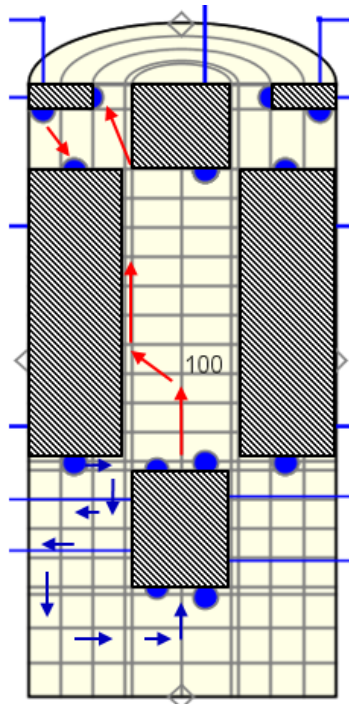


**Fig. B.4: Coolant flow path within the 3D CYLINDRICAL VESSEL component of the RPV model**

Four pumps are connected to the RPV-model to provide a total mass flow rate of 2090 kg/s as specified in (Kim et al., 2016).

### **B.5. Secondary Circuit Model**

The secondary-side model has eight feedwater lines each represented by fill component, feedwater isolation valves (FIVs), eight helical-coiled tubes for the secondary-side of SG, steam isolation valves (SIVs), a steam header connected to a break component that represents turbine boundary condition. In normal operation, the FIVs and SIVs are fully opened whereas in emergency conditions, they are closed, and the coolant flow path is connected to the PRHRS.

### **B.6. Passive Residual Heat Removal System Model**

The PRHRS model consists of four trains thermally connected to an emergency cooldown tank that is represented by a 3D cylindrical vessel component, steam and feedwater cut-off valves, and a compensating tank. Each train is represented by a 1D pipe discretized into 15 cells. During normal operation, the steam and feedwater cut-off valves are closed. The PRHRS is connected to the feedwater and steam pipes through a common header represented by a plenum component. This component is used to connect two SGs secondary-side into one train since there are eight SGs and four trains in the PRHRS.